DESIGN OF WIND TUNNEL CONTRACTIONS

Thesis

Submitted by

JAMES GIRVAN RODGER

for the degree of

DOCTOR OF PHILOSOPHY

University of Edinburgh

April 1976

ABSTRACT

This thesis is concerned with the methods of designing two-dimensional and axisymmetric wind tunnel contractions of finite length.

Previous methods of designing contractions are examined and, in particular, one two-dimensional design is considered in detail. This two-dimensional design results in the production of tables from which wind tunnel contractions of various contraction ratios and adverse pressure gradients can be built to have a known wall velocity profile. An approximate transformation is applied to this two-dimensional solution to obtain the flow through correspond-:ing axisymmetric contractions. It is shown how tables similar to those for the two-dimensional case can be prepared for the axisymmetric case and an example of these tables is given. The results of experimental measurements of the flow through an axisymmetric contraction designed in this way are given and are found to compare well with the theoretically predicted results.

The final part of this thesis is concerned with a method of calculating flows through two-dimensional and axisymmetric contractions. This method uses surface singularity distributions from which the flow is calculated. The results obtained for two-dimensional flows are found to be very good. The results in the axisymmetric case, however, are not as good and an attempt to improve on these results by modifying the method is described.

DECLARATION

I declare that this thesis was composed entirely by myself and that, except where indicated, the work described is my own.

James G. Rodger

CONTENTS

		Page
Preface		i
Acknowledgements		ii
Summary		iii
CHAPTER 1	REVIEW OF DESIGN METHODS	1
CHAPTER 2	TWO-DIMENSIONAL DESIGNS	
2.1	Introduction	13
2.2	Adverse Pressure Gradients	13
2.3	Whitehead, Wu and Waters	14
2.4	Jordinson's Contraction	15
2.5	The Parameters ℓ_1 and ℓ_2 and the Constant Velocities	22
2.6	Infinite Length Contractions	23
CHAPTER 3	APPROXIMATE SOLUTION TO THE AXISYMMETRIC FLOW	
3.1	Introduction Equation for the Stream Function	25
3.2	The Whitehead, Wu and Waters Approximation	26
3.3	Implications of W.W.W.'s Approximation	28
3.4	Application to the Two-Dimensional Contraction	30
3.5	The Singularity	32
3.6	The Numerical Evaluation of $\int y d\beta$	34
3.7	Results	36
CHAPTER 4	EXPERIMENTAL MEASUREMENTS	
4.1	Introduction	40
4.2	Description of Model	40
4.3	Description of Experiment and Apparatus	41
4.4	Results	41
4.5	Conclusions	43

CHAPTER 5 /

C O N T E N T S (contd.)

		Page
CHAPTER 5	THE SURFACE SINGULARITY METHOD	
5.1	Introduction	44
5.2	Theoretical Justification	44
5.3	The Method of Smith and Pierce	48
5.4	The Two-Dimensional Case	50
5.5	The Axisymmetric Case	56
CHAPTER 6	APPLICATION OF THE SURFACE SINGULARITY METHOD TO WIND TUNNEL CONTRACTIONS	
6.1	Introduction	66
6.2	The Parallel Sections	67
6.3	Distribution of Body Elements	68
6.4	Two-Dimensional Ducts	69
6.5	Leakage and the Higher Order Solution	71
6.6	Axisymmetric Ducts	73
6.7	The Calculated Source Distribution	76
6.8	Computing	77
6.9	Conclusions	82
CHAPTER 7	CONCLUSIONS	83
REFERENCES		87
LIST OF SYMBOLS		89

PREFACE

The research topic of this thesis was originally suggested by Dr. R. Jordinson under whose supervision the research was conducted.

ACKNOWLEDGEMENTS

I would like to thank Dr. R. Jordinson for his help and friendly advice while supervising my research. I would also like to record my gratitude to Professor A.G. Mackie and to the staff of the Department of Applied Mathematics for their suggestions throughout the course of this research. I am indebted to Dr. G. Alder of the Department of Engineering for his enthusiasm and help with the experimental work described in Chapter four of this thesis. A major part of this thesis has been concerned with computer programming and I would like to thank Mr. J.C. Adams of the Department of Computer Science for his advice on some programming problems.

Finally, I would like to thank Mrs. J. Hollingdale for her speedy and efficient typing of this thesis.

SUMMARY

The design of low speed wind tunnels has been of interest to scientists and engineers for over half a century. However, even as late as 1964, Pankhurst and Bradshaw wrote that wind tunnel design lies somewhere between an art and a science with occasional excursions into propitiatory magic. It is hoped that this thesis will show that the science involved in the design of wind tunnel contractions is no longer as imprecise.

The principle parts of a wind tunnel are the fan, the diffuser, the settling chamber, the contraction and the working section and it is with the design of contractions that this thesis is concerned. The contraction is situated between the settling chamber and the working section, and its purpose is to produce a uniform stream of fast moving air in the working section from the uniformly slowly moving air in the settling chamber within as short a distance as possible. There are two main classifications of contractions - those of finite length and those of infinite length - and it is important to distinguish between them. The beginning and end of a contraction of either type will be defined as the points at which the tangents to the wall make angles of zero degrees with the centre line. In a contraction of finite length there will be a finite distance between these points. That is, in a contraction of finite length, points exist at which the walls become straight and parallel to the axis. However in a contraction of infinite length, the points at which the tangents become parallel to the axis lie infinitely far apart. It will be shown that in a contraction of finite /

finite length, adverse pressure gradients exist at the beginning and end of the contraction which, if severe enough, could cause the boundary layer to separate. Infinite length contractions do not suffer from these adverse pressure gradients but, in a practical design, points, a finite distance apart, and at which the tangential wall angle may differ from zero by only a small amount, are chosen as the beginning and end of the contraction. In making the contraction finite in length, adverse pressure gradients which have not been catered for in the design of the contraction are introduced. This is one of the major drawbacks in designing and using contractions of infinite length.

An important point in any design is the overall length of the contraction which, from a practical point of view, should not be longer than necessary to satisfy the flow conditions in the working section. A factor of at least equal importance is the rapidity with which the flow becomes uniform downstream of the contraction. In theory, uniform flow is only obtained at ∞ but normally the flow can be described as uniform to within prescribed limits a finite distance downstream of the contraction. Discussing relative lengths of different contractions is therefore of limited value since this second consideration also decides whether or not one contraction is better than another.

In calculations involving finite length contractions, the settling chamber and working section are treated as infinitely long parallel sided sections joined to the beginning and end of the contraction respectively. This combination of contraction plus parallel sections will henceforth be referred to as a duct.

Methods /

Methods of designing two-dimensional contractions with a specified wall velocity are available and some are discussed in Chapter 1. It was hoped that a similar method could be developed for the design of axisymmetric contractions since, by specifying a suitable wall velocity distribution, the danger of boundary layer separation could be eliminated. The choice of wall velocity is still a matter of experience and guesswork but once a velocity distribution has been specified, numerical methods are now available to determine the approximate boundary layer growth. Thus a design can be tested theoretically without building a model. The axisymmetric problem proved too difficult but it will be shown that a two-dimensional design can be used even more successfully as an axisymmetric design.

Chapter 2 is concerned with two-dimensional designs and, in particular, an approximate design method due to Jordinson (1961). This design is later used as a basis for an axisymmetric contract-:ion a model of which was built and tested.

An approximate method of calculating the flow through an axisymmetric contraction is obtained by applying a transformation to the solution to the flow through the two-dimensional contraction with the same profile as the axisymmetric one. This is given in Chapter 3 and the results compared with those of experiment are given in the following Chapter. The remainder of the thesis is concerned with a method of calculating the flows through two-dimensional and axisymmetric ducts by treating the duct as a thin shell over which there is a distribution of singularities. It was hoped that using this method and employing an iterative scheme, /

scheme, axisymmetric contractions with a specified wall velocity could be designed. However, because of the amount of computing time required and errors inherent in the axisymmetric solution, this was not possible.

Finally a design is presented which allows easy construction of contractions of finite or infinite length for various contraction ratios.

CHAPTER 1

REVIEW OF DESIGN METHODS

1.1 INTRODUCTION

A considerable amount of research has gone into the design of wind tunnel contractions and the methods used are not uncommon in the field of fluid dynamics. In this Chapter some of the more important methods are examined.

1.2.1

Lighthill A.R.C. R. & M. 2112 (1945) uses a conformal mapping to transform the contraction shape onto the unit circle. The flow problem is then solved in this circle plane where the velocity distribution is specified as a function of the azimuth angle on the circle. Using this method, contractions of finite and infinite length can be designed. Because the wall velocity is specified as a function of the azimuth angle, the relationship between the wall velocity and position along the contraction cannot be obtained until after transformation. The only condition on the velocity applicable in the circle plane is that it should not decrease as the angle increases from zero to π . Thus the choice of a suitable velocity distribution in the circle plane is critical if a successful contraction is to be designed.

1.2.2

Several methods of designing two-dimensional and axisymmetric contractions have been developed by specifying the velocity on the centre line as a monotonic increasing function of the distance along /

along the contraction.

Hsue-Shen Tsien, Journ. Aero. Sci, 1943, uses this method to design a large axisymmetric contraction. The wall shape is taken to be the streamline farthest from the centre line along which the velocity still increases monotonically and on which the asymptotic velocity takes the required value. To calculate this streamline and the flow inside the contraction he uses the symmetry of the problem to express the axial component of velocity as an even function of the radial coordinate R and the radial component of velocity as an odd function of R. Therefore, if $f_0(x)$ is the specified axial velocity distribution, V and U can be expressed as

$$U = \sum_{n=0}^{\infty} R^{2n} f_{2n}(x) \tag{1.1}$$

$$V = \sum_{n=0}^{\infty} R^{2n+1} g_{2n+1}(x) \tag{1.2}$$

where the $f_i(x)$ $(i > 0)$ and $g_i(x)$ are functions to be determined. Substituting (1.1) and (1.2) into the equation of continuity

$$\frac{\partial(RU)}{\partial x} + \frac{\partial(RV)}{\partial R} = 0 \ ,$$

and using the condition for irrotational flow

$$\frac{\partial V}{\partial x} - \frac{\partial(U)}{\partial R} = 0 \ ,$$

and then equating equal powers of R, yields the following relations between the functions f_i and g_i

g /

$$g'_{2n-1}(x) = 2nf_{2n}(x) \tag{1.3}$$

$$g_{2n-1}(x) = -\frac{1}{2n} f'_{2n-2}(x) \quad . \tag{1.4}$$

Equations (1.3) and (1.4) give the following recurrence relations between the functions f_i

$$f_{2n}(x) = -\frac{1}{(2n)^2} f''_{2n-2}(x)$$

Therefore

$$f_{2n}(x) = \frac{(-1)^n}{2^{2n}(n!)^2} f_0^{(2n)}(x)$$

Using this recurrence relationship in (1.1) gives

$$U = \sum_{n=0}^{\infty} \frac{(-1)^n R^{2n}}{2^{2n}(n!)^2} f_0^{(2n)}(x) \tag{1.5}$$

Similarly he obtains

$$V = \sum_{n=1}^{\infty} \frac{(-1)^n \, 2n \, R^{2n-1}}{2^{2n}(n!)^2} f_0^{(2n-1)}(x) \tag{1.6}$$

The resultant velocity q and the streamlines can easily be found from the following equations

$$q = \sqrt{U^2 + V^2}$$

$$\psi = \int_0^R RU(x,R)dR$$

Obviously this method requires careful choice of the centre line velocity since pressure gradients are invariably more severe on the wall than on the centre line and there is no way of knowing the /

the wall velocity until the calculation is complete. Tsien chooses the function

$$f_0(x) = 0{\cdot}55 + \frac{0{\cdot}90}{\sqrt{2\pi}} \int_0^x e^{-x^2/2}\, dx$$

which gives an acceptable centre line velocity and also has the advantage that the derivatives of $f_0(x)$ can, by a simple transformation, be related to the Hermite polynomials. The higher derivatives of $f_0(x)$ can then be obtained by using the recurrence relation between the Hermite polynomials, so simplifying the evaluation of (1.5) and (1.6) in which ten terms are used.

Tsien states that since the wall velocity is increasing monotonically along the contraction the pressure must be decreasing monotonically and therefore the danger of boundary layer separation is avoided. However, since the wall shape is taken to be the streamline defined above, the contraction will be infinite in length. In practice, when the contraction is made finite by the addition of parallel sections, adverse pressure gradients will be introduced. Tsien does not mention this and it is not possible to say how the introduction of parallel sections will affect the flow in the contraction.

The length over which the cross sectional area varies significantly is determined to a certain extent by the choice of the centre line velocity. Unfortunately the distance between the points at which this infinite contraction can be considered to begin and end cannot be predetermined.

Thwaites /

Thwaites A.R.C. R. & M. 2278 (1946) uses a similar method to design axisymmetric contractions of finite length by specifying a centre line velocity of the form

$$U(x,0) = a_0 + \sum_{n=1}^{\infty} a_n \cos(nx)$$

where $x = 0$ is the end of the contraction. Only a few of the coefficients a_n are used. They are chosen to make the bounding streamline pass through two given points and to make the velocity on this streamline increase monotonically. Unfortunately this method has the disadvantage that although the contraction is finite, the solution is periodic in x.

1.2.3

Many two-dimensional, inviscid, incompressible flow problems can be solved most easily in the hodograph plane. Whitehead, Wu and Waters (1951) use the hodograph plane to calculate two-dimensional contraction shapes by first specifying a boundary shape in the hodograph plane from which the contraction shape can then be calculated. More will be said of their method in Chapter two. In many cases the logarithmic hodograph plane defined by

$$\zeta = \log\left(\frac{dW}{dZ}\right) = \log(q) - i\theta$$

proves a more convenient plane in which to solve the problem. Gibbings and Dixon (1956) examine a method of designing a two-dimensional contraction of finite length with a specified wall velocity by using a relaxation method in this logarithmic hodograph plane /

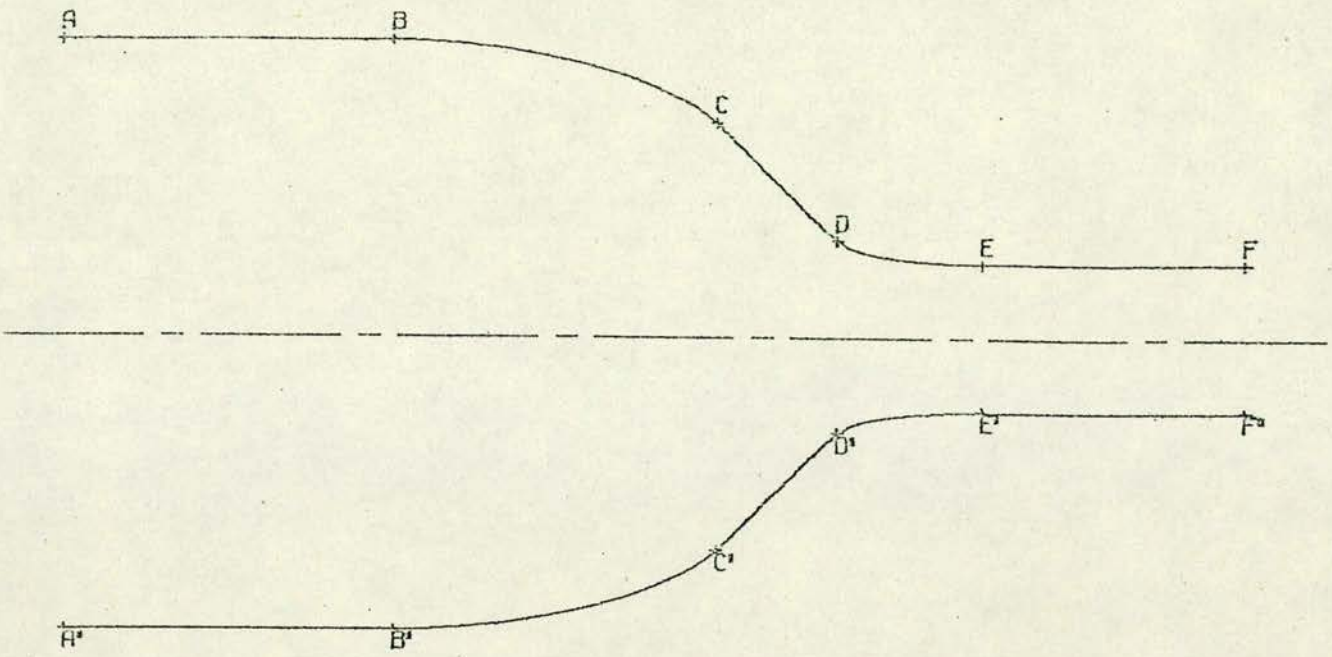

FIGURE (1.1)

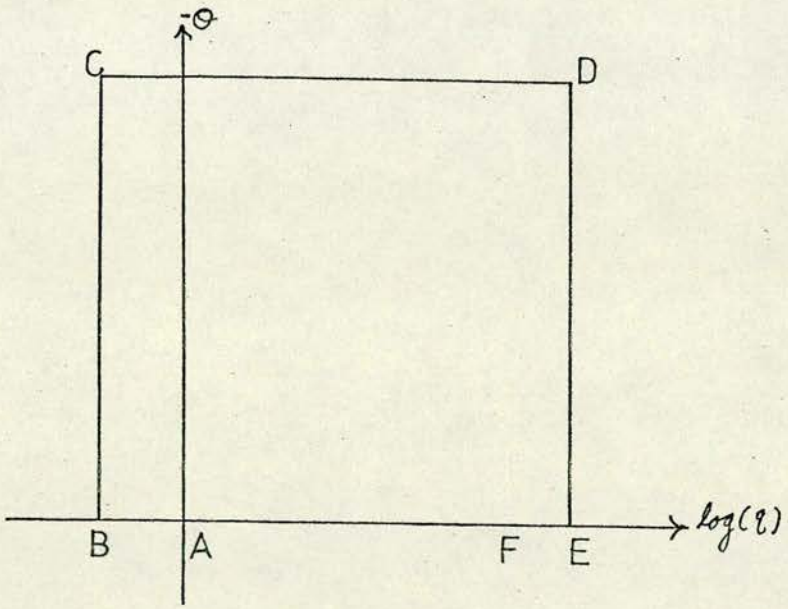

FIGURE (1 2)

plane to solve Laplace's equation for the stream function. The particular example they consider has also been examined by Mooljee (1971) and will be considered in more detail later. Basically, the contraction (figure 1.1) was designed to produce the following velocity distribution on the wall:

(i) The velocity has a constant specified velocity on the curved walls BC and DE

(ii) The velocity increases monotonically on the straight wall from C to D .

In addition the walls AB and EF are straight and parallel to the axis.

In the logarithmic hodograph plane the problem reduces to that of calculating the flow inside a rectangular boundary due to a source at A and a sink of equal strength at F (figure 1.2) . This problem can be solved exactly as has been done by Gibbings and Dixon and by Mooljee by transforming the region inside the rectangle onto the interior of the unit circle. An approximate solution due to Jordinson will be considered in more detail later. However, in designing the contraction Gibbings and Dixon prefer to use a relaxation method which, although requiring more computation than the exact solution was the only way of solving a subsequent problem with a modified boundary in the hodograph plane.

Gibbings and Dixon demonstrate that at points in the physical Z plane, which correspond to stagnation points in the hodograph plane, the velocity gradient is infinite except when

d /

$$\frac{dU'}{dV'} = 0$$

whilst the wall curvature is infinite except when

$$\frac{dV'}{dU'} = 0$$

where U' and V' are defined by

$$\frac{dW}{d\zeta} = U' - iV' \quad .$$

Thus, the adverse pressure gradients along AB and EF become infinite at B and E. Gibbings and Dixon aimed at designing a contraction with the properties given above, but without the infinite adverse velocity gradients, by using as a first approximation the shape calculated from the rectangular boundary in the hodograph plane. The boundary shape at B and E in the hodograph plane was then modified so that the adverse velocity gradients on the corresponding portions of the wall in the physical plane had a constant specified value. This modification, in effect, removed the stagnation points at B and E in figure (1.2) by replacing the 90' corners (ABC and FED) with smooth curves. The new wall shape was then calculated. The modification meant a slight increase in length of the contraction of the order H/10 and a slight change in the velocity distribution near B and E .

Choosing a constant value for the adverse velocity gradient near B and E so that the boundary layer will not separate in a real flow presents added difficulties which are probably unnecessary. Several /

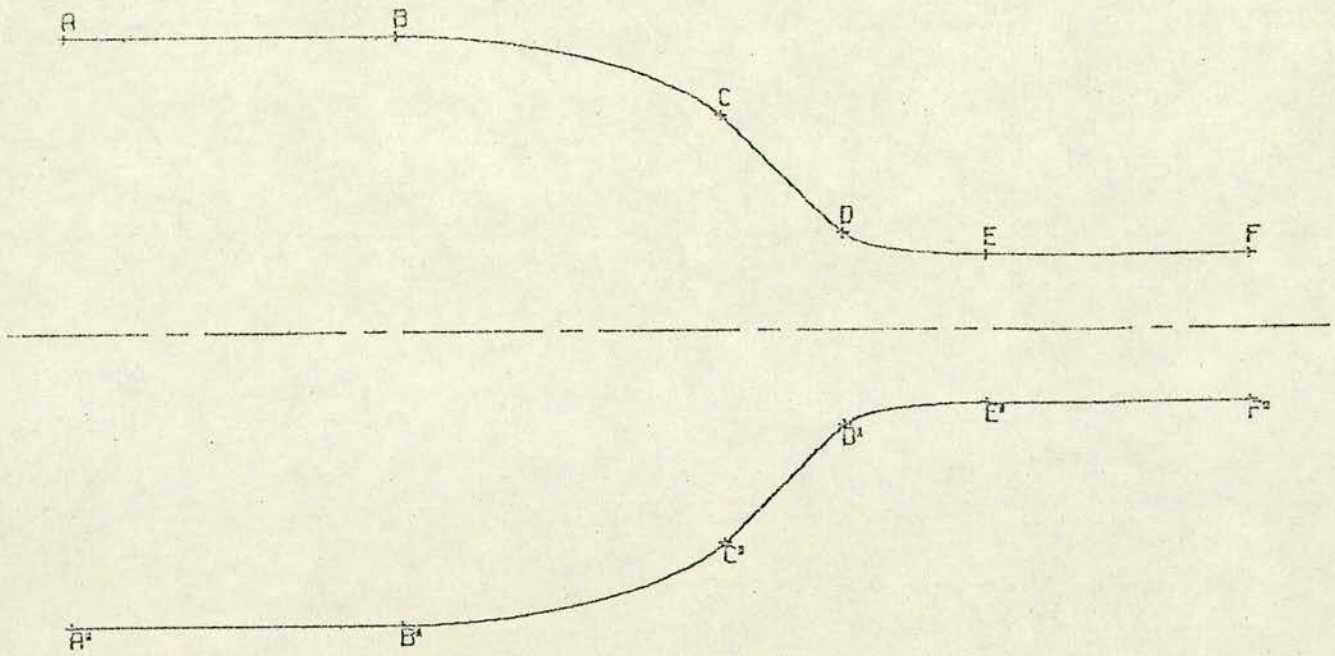

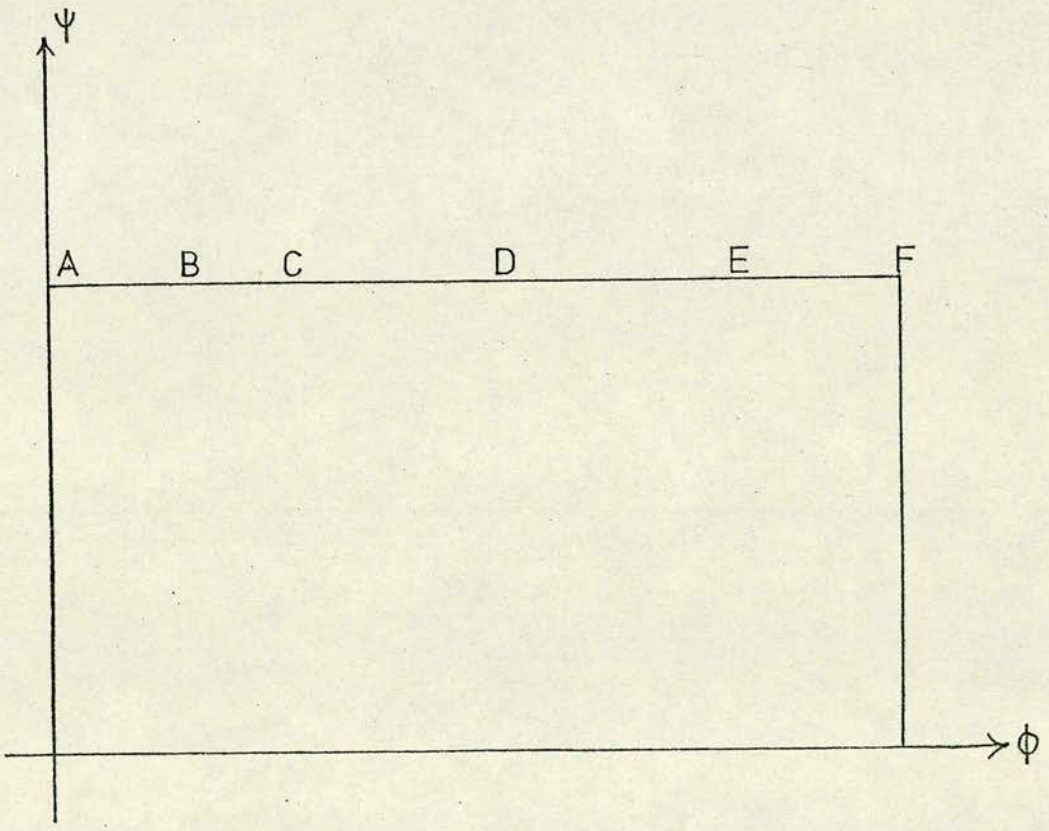

FIGURE (1.3)

Several contractions of finite length have been successfully designed and built by, for example, Jordinson and W.W.W. where the fact that the velocity gradient becomes infinite at one point has been ignored. The success of these designs may be either because in a real flow the boundary layer itself eliminates these singularities or because small inaccuracies inevitable in the construction of these contractions are sufficient to effectively modify the boundary at B and E .

1.2.4

Finite difference methods are often used to solve the differential equations arising in fluid dynamics and the ease of application of these methods depends not only on the boundary conditions imposed but also on the shape of the boundaries on which these conditions are to be applied. A rectangular boundary as obtained by Gibbings and Dixon is particularly convenient for the application of finite difference methods. Jeppson (1969) also uses finite difference methods on a rectangular region to obtain the boundary shape of an axisymmetric nozzle required to produce a specified flow. Jeppson obtains the rectangular region by solving the problem in the plane of the scalar potential function ϕ and the stream function ψ . The quantities to be determined were then the axial and radial coordinates $Z(\phi,\psi)$ and $R(\phi,\psi)$ considered as the dependent variables. Referring to figure (1.3) it can be seen that for a wind tunnel /

tunnel contraction of the type discussed by Gibbings and Dixon the region in the (ϕ,ψ) plane is also a rectangle. The equations to be solved for R and Z in this inverse formulation become

$$\frac{\partial^2 R}{\partial \psi^2} + \frac{1}{R^2}\frac{\partial^2 R}{\partial \phi^2} - \frac{1}{R^3}\left(\frac{\partial R}{\partial \phi}\right)^2 + \frac{1}{R}\left(\frac{\partial R}{\partial \psi}\right)^2 = 0 \qquad (1.7)$$

and

$$R^2\frac{\partial^2 Z}{\partial \psi^2} + \frac{\partial^2 Z}{\partial \phi^2} + 2\frac{\partial Z}{\partial \phi}\frac{\partial Z}{\partial \psi} = 0 \qquad (1.8)$$

Both these equations are nonlinear, but the nonlinearity in (1.7) involves only one of the dependent variables and can be used to begin the solution. The finite difference operator used to solve (1.7) is of the five point star type and is a fourth order polynomial in the value of R at the centre of the star.

$$R(i,j)^4 - \tfrac{1}{2}\{R(i,j+1)+R(i,j-1)\}R(i,j)^3 - \{[R(i,j+1)-R(i,j-1)]^2/8 - 1\}R(i,j)^2 -$$

$$\{R(i+1,j)+R(i-1,j)\}R(i,j)/2 + \{R(i+1,j)-R(i-1,j)\}^2/8 = 0$$

This equation must be solved explicitly for $R(i,j)$ and, since the equation can be shown to have two real positive roots, a certain degree of accuracy is required in assigning initial values to the $R(i,j)$.

Although the method may be able to design nozzles of a certain type, the problem of applying it to contractions is much more difficult. For a contraction, the type of boundary condition varies several times on the same boundary in the (ϕ,ψ) plane and the relative /

relative positions of the points at which the boundary conditions change are unknown - for example B, C, D and E in figure (1.3) .

1.2.5

Some methods are available to calculate approximate solutions to intractible axisymmetric flow problems by using the solution to the corresponding two-dimensional problem. One such method is that described by Wooding (1964) who uses the transformation

$$y = R^2/R_*$$

where R_* is a constant and y and R denote respectively the usual two-dimensional and axisymmetric coordinates. This transformation when applied to the two-dimensional Laplace equation

$$\frac{\partial^2\psi}{\partial x^2} + \frac{\partial^2\psi}{\partial y^2} = 0$$

yields

$$\frac{\partial^2\psi}{\partial R^2} - \frac{1}{R}\frac{\partial\psi}{\partial R} + \frac{4R^2}{R_*^2}\frac{\partial^2\psi}{\partial x^2} = 0 \qquad (1.9)$$

It is proposed that this transformation be used in the solution to the two-dimensional Laplace equation as an alternative to solving the axisymmetric Laplace equation:

$$\frac{\partial^2\psi}{\partial R^2} - \frac{1}{R}\frac{\partial\psi}{\partial R} + \frac{\partial^2\psi}{\partial x^2} = 0 \qquad (1.10)$$

It can be seen that the solutions to (1.9) and (1.10) would be nearly /

nearly equivalent provided that $R \simeq R_*/2$ when $\frac{\partial^2\psi}{\partial x^2}$ is large and that $\frac{\partial^2\psi}{\partial x^2}$ is small over the remainder of the flow field.

The approximate solution obtained using this transformation does not satisfy the condition of irrotationality and R_* is chosen to minimise the vorticity. In this way it is hoped to minimise the departure of the approximate solution from the exact solution. The method, however, requires an analytic solution to the two-dimensional problem and so is not always applicable to contraction problems where often only a numerical solution is available.

Whitehead, Wu and Waters (1951) on the other hand use an entirely different transformation which does not require an analytic solution to the two-dimensional problem. They assume - in the case of duct flow - that the streamlines in the two-dimensional and axisymmetric cases do not differ greatly in shape and make the velocity on the streamlines satisfy the axisymmetric equation of continuity. This method is considered in greater detail in Chapter 3.

1.2.6

The use of singularity distributions is becoming more widely used to calculate flows in two or three dimensions. Moran (1962) has calculated flow fields external to bodies of revolution by using a source distribution along the axis of the body. Necessarily the source distribution must not lie in the flow field and so this method /

method of using an axial source distribution is unsuitable for the calculation of flows in ducts. A method which is suitable for the calculation of duct flows in two or three dimensions is that of Smith and Pierce (1959). This method uses a surface singularity distribution from which the flow field can be calculated. A more detailed account of this method with its application to flows in ducts is given in Chapters 5 and 6 .

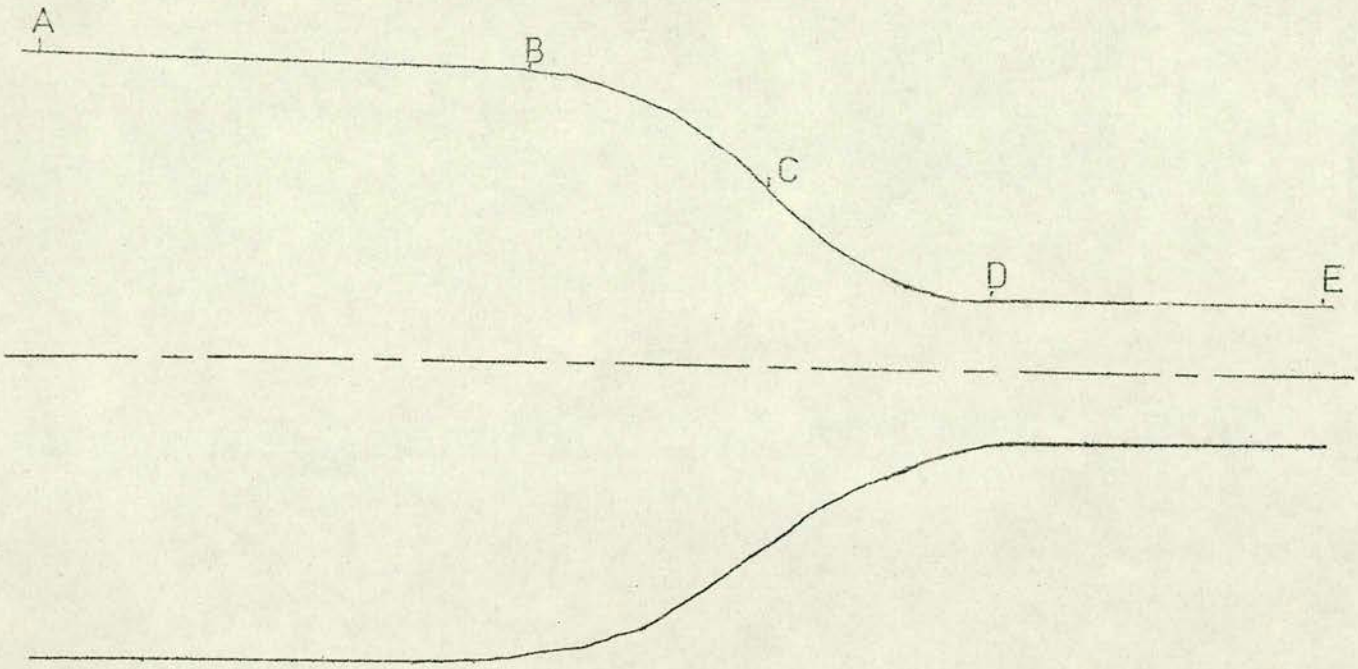

FIGURE (2.1)

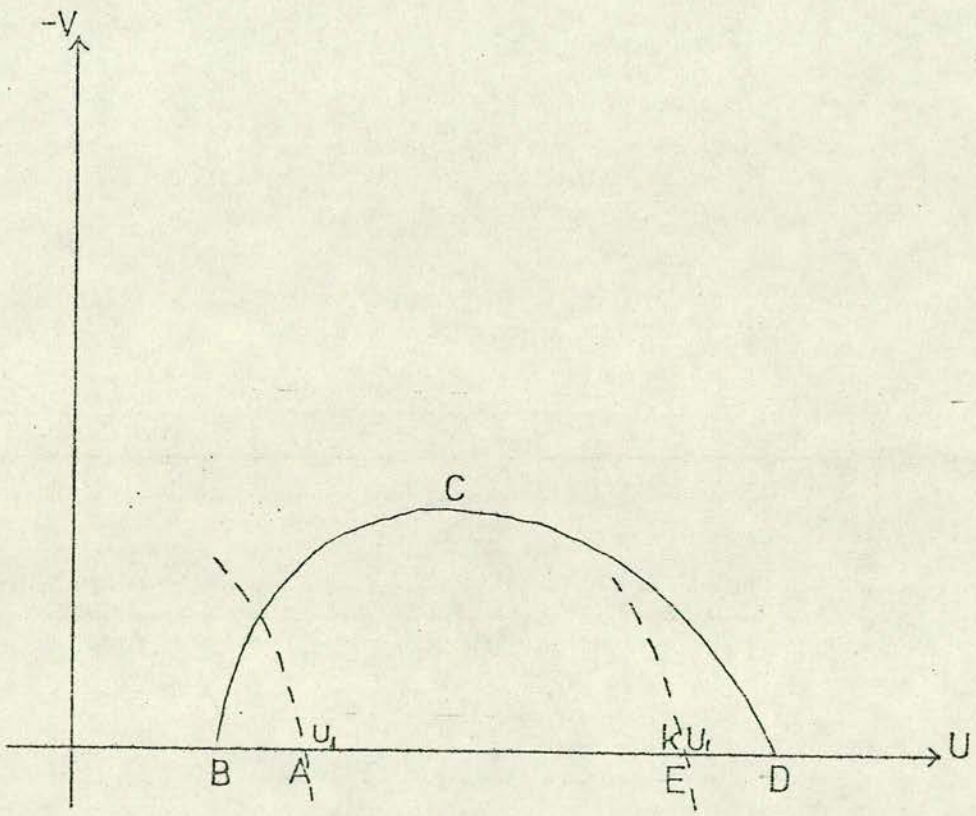

FIGURE (2.2)

CHAPTER 2

TWO-DIMENSIONAL DESIGNS

2.1 INTRODUCTION

A well known method of treating two-dimensional, incompressible, inviscid flow problems is to solve the corresponding flow problem in one of the hodograph planes. When applied to flows in ducts, this method has the advantage that the flow in the hodograph plane can be considered as being generated by a source and a sink of equal strength. This latter problem can often be solved by a standard method (images, conformal transformation) depending on the boundaries in the hodograph plane.

2.2 Adverse Pressure Gradients

For a contraction with parallel sections as shown in figure (2.1) where the wall velocity increases monotonically from B to D, the corresponding boundary in the hodograph (U, -V) plane is shown in figure (2.2) . In addition, the region between the contraction wall ABCDE and the centre line maps onto the region inside the boundary ABCDEA in the hodograph plane. The problem of calculating the flow inside the contraction now reduces to that of calculating the flow generated by a source at A and a sink at E inside the boundary in the hodograph plane where the strengths of both source and sink must equal the total fluid flux $U_1 H$.

It can be seen from the hodograph plane that adverse velocity gradients exist along AB and DE . This is unavoidable in a contraction of finite length. It is stated in W.W.W. that /

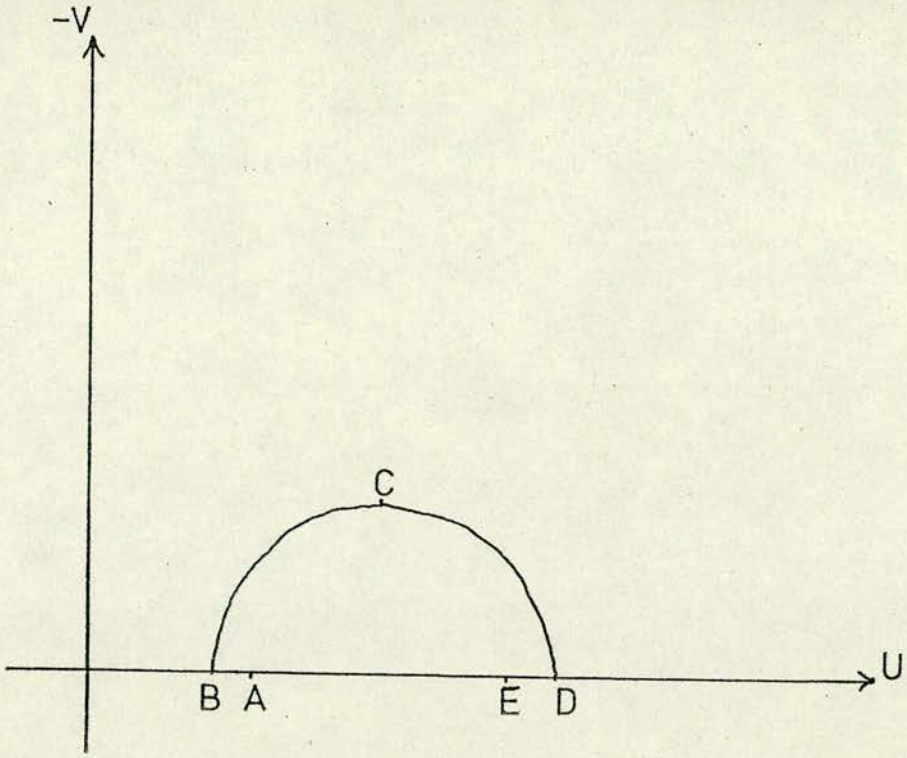

FIGURE (2.3)

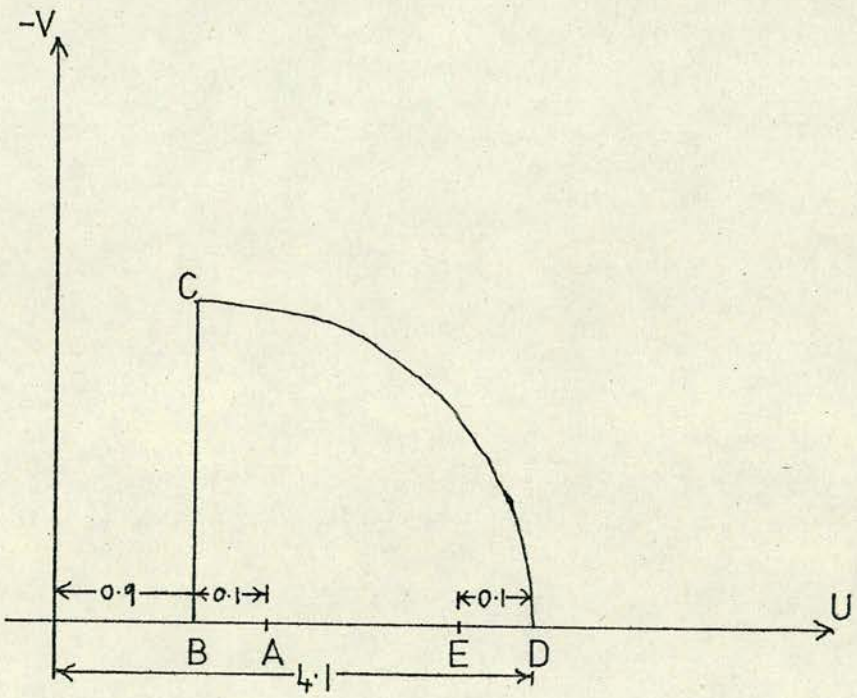

FIGURE (2.4)

that if these adverse velocity gradients are to be eliminated, the boundary in the hodograph plane must lie entirely between two circular arcs of radii U_1 and KU_1 centred at the origin. To satisfy this condition both A and B, and D and E must coincide thus eliminating the sections AB and DE. The implications of this in the physical plane are that B and D now lie at $+\infty$ and $-\infty$ respectively so that the contraction is now infinite in length.

2.3 Whitehead, Wu and Waters

In general, the exact boundary shape in the hodograph plane may be unknown or, if known, not very convenient for calculating the flow. W.W.W. chose to design a contraction by specifying a boundary in the hodograph plane. The choice of the shape of this boundary would depend on its producing a contraction of reasonable shape and, at the same time, being such as to make any calculations reasonably simple. The choice of a semicircle for the hodograph boundary, for example (figure 2.3), would achieve the latter condition but, W.W.W. argue, would not give a satisfactory contraction since BCD must be such as to give a rapid contraction. This implies a large wall slope at C in the physical plane. This in turn would mean a large vertical component of velocity and the choice of a semicircular boundary in the hodograph plane does not result in such a velocity. However, making the boundary BCD a quadrant of a circle (figure 2.4) doubles the maximum vertical wall velocity component and gives a rapid contraction where the pressure falls continuously from B to D. /

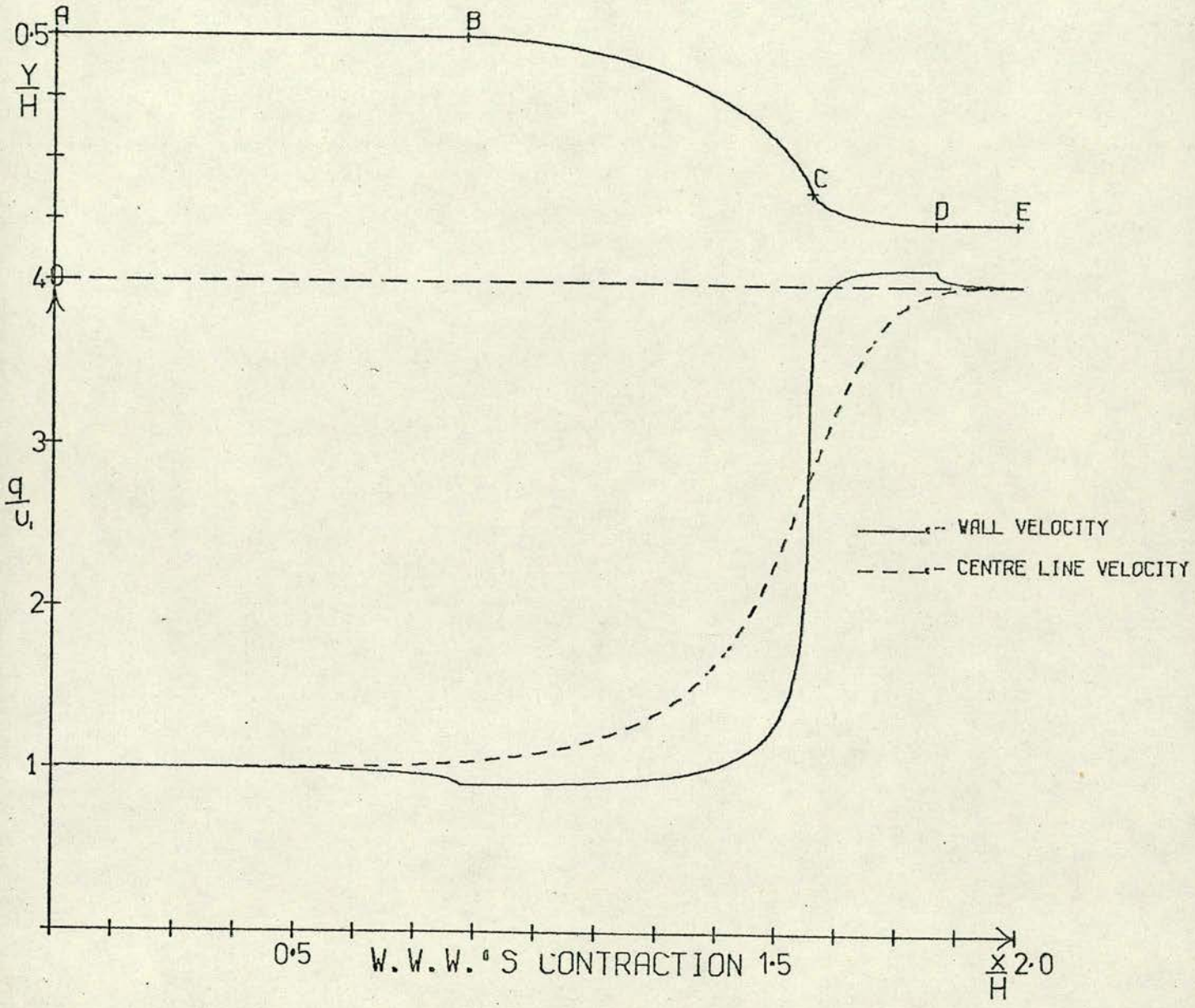
A
B
C
D
E
0·5
Y/H
4·0
3
2
1
q/U₁
WALL VELOCITY
CENTRE LINE VELOCITY
0·5
W.W.W.'S CONTRACTION
1·5
X/H
2·0

FIGURE (2.5)

D. Having chosen this hodograph boundary, W.W.W. use the method of images to solve the flow problem for the complex velocity potential W as a function of the complex velocity q. Now, since the complex velocity is defined as

$$q = \frac{dW}{dZ}$$

the boundary in the physical plane can be obtained by integrating the relation between $\frac{dZ}{dq}$ and q. A contraction shape designed in this way with the corresponding wall and centre line velocity distributions is shown in figure (2.5) for the hodograph boundary of figure (2.4).

W.W.W. calculated contractions of infinite length by the same method by eliminating the sections AB and DE and considering the source and sink to lie at B and D respectively in the hodograph plane. In comparing these infinite contractions with similar ones calculated by Lighthill, they find their method gives a greater maximum wall gradient. However, the designs of both Lighthill and W.W.W. approach the limiting values upstream and downstream slowly.

2.4 Jordinson's Contraction

In contrast Jordinson and Gibbings and Dixon specify the desired wall velocity in the physical plane which determines the boundary in the hodograph plane and from which the contraction shape corresponding to this velocity distribution can be determined.

The specific contraction considered by Gibbings and Dixon together /

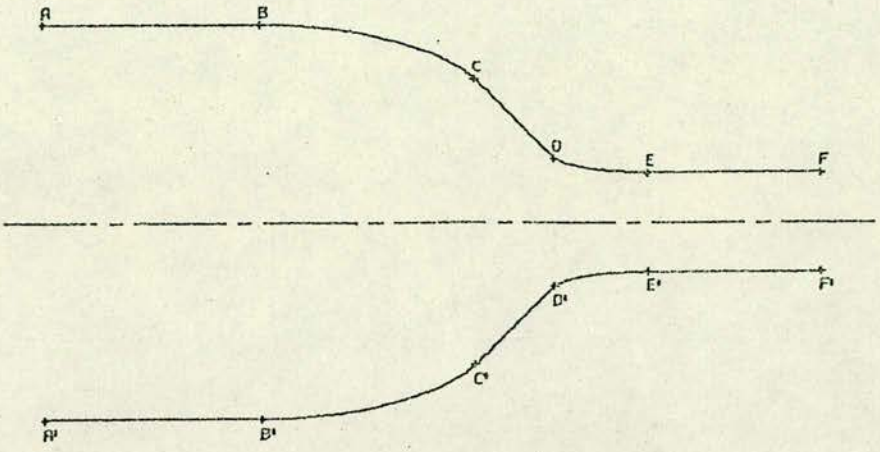

FIGURE (2.6a)

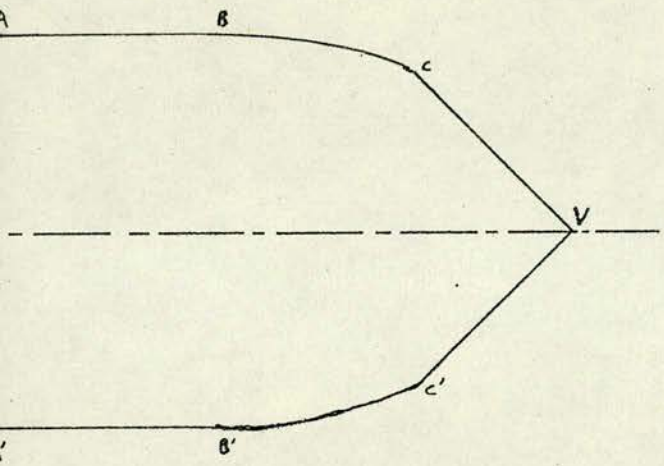

FIGURE (2.6b)

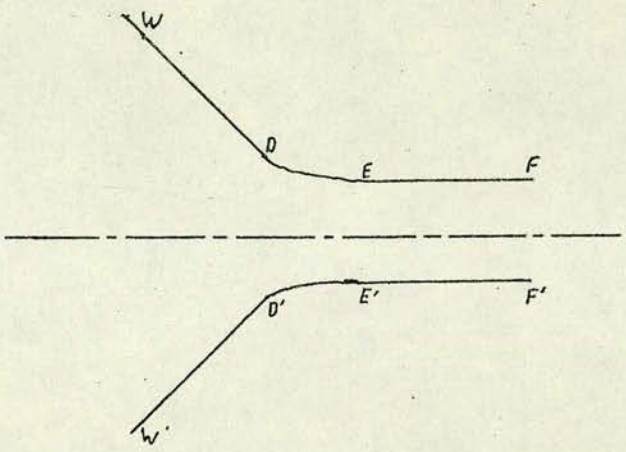

FIGURE (2.6c)

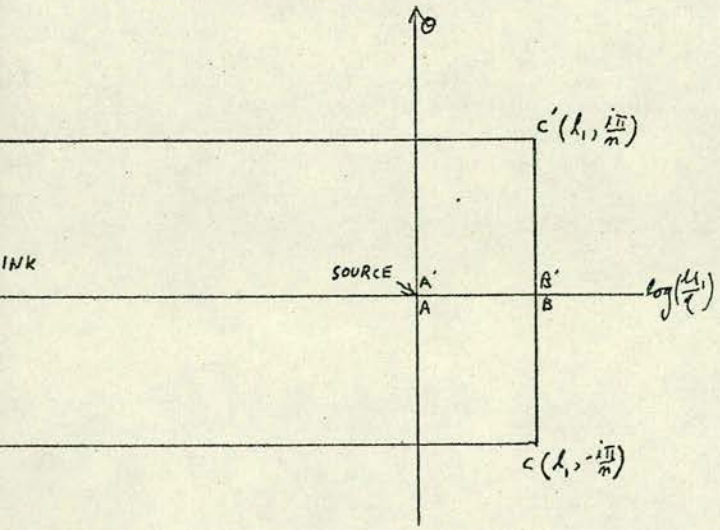

FIGURE (2.6d)

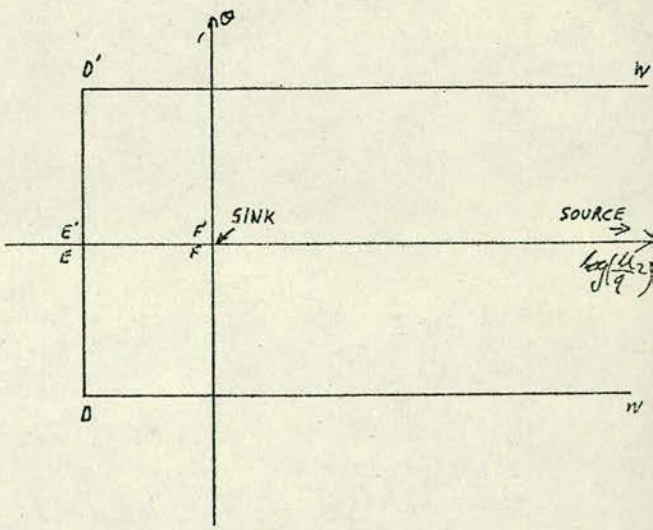

FIGURE (2.6e)

together with their treatment of the problem has already been discussed in section 1.2.3 where the boundary obtained in the hodograph plane was a rectangle. Jordinson's treatment of the same problem involved an approximation. He assumed that the contraction could be split into two parts (figure 2.6a, b, c):

(i) The upstream part where the flow is due to a source at A and a sink at V

(ii) The downstream part where the flow is due to a sink and a source at $+\infty$ and $-\infty$ respectively

and that the solution of the complete problem could be obtained by combining the solutions to both these half problems. In making this approximation, he assumed that the effect of one end of the contraction on the other could be represented by a source or a sink. The accuracy of Jordinson's approximation was found to be extremely good when compared with Mooljee's exact solution and some experimental results. The approximate solution was easier to handle than the exact one and was subsequently used to predict the flow in an axisymmetric contraction with the same profile curve as the two-dimensional shape. This approximate method is now considered in more detail.

The velocity is constant on the curved walls BC and DE and, since the problem is to be solved in the logarithmic hodograph plane defined as

$$\zeta = -\log\left(\frac{dW}{dZ}\right) = \log\left(\frac{U_1}{q}\right) + i\theta$$

for /

for the upstream part and

$$\zeta = -\log\left(\frac{dW}{dZ}\right) = \log\left(\frac{U_2}{q}\right) + i\theta$$

for the downstream part, these constant velocities were expressed as $q = U_1 e^{-\ell_1}$ on BC and $q = U_2 e^{\ell_2}$ on DE (ℓ_1 and ℓ_2 are both positive constants and their values are discussed in more detail later). The straight wall CD is assumed to make an angle of π/n radians with the centre line. Referring to figure (2.6), the two parts of the contraction are shown with their corresponding boundaries in the hodograph planes. For the upstream part it can be seen that the source at $-\infty$ in the physical plane transforms to the origin in the hodograph plane. Similarly, the sink at V in the physical plane transforms to $-\infty$ in the ζ plane. The boundaries in the physical plane map onto the boundaries in the hodograph plane as indicated in the diagram. Thus, the problem of calculating the flow in the upstream part of the contraction reduces to that of calculating the flow inside the semi-infinite strip bounded by VCBB'C'V' in the hodograph plane. Equivalently, for the downstream part, the problem reduces to calculating the flow inside the semi-infinite strip WDEE'D'W' in the hodograph plane due to a sink at the origin and a source at infinity.

Both of these hodograph problems can be solved exactly by using the Schwartz-Christoffel transformation to map the interior of the semi-infinite strips onto the upper half of a new plane (t). Considering the hodograph problem for the upstream part, if the points C' and C' are allowed to map onto the points $t = 1$ and $t = -1$ /

$t = -1$ respectively, the transformation is

$$t = i\sinh\left(n(\ell_1 - \zeta)/2\right) \tag{2.1}$$

The source at the origin in the ζ plane transforms to the point $t = i\sinh(n\ell_1/2)$. The complex potential in the 't' plane can now be obtained directly as

$$W = \alpha + i\beta = m\log\left(t^2 + \sinh^2(n\ell_1/2)\right)$$

or

$$e^{\frac{\alpha+i\beta}{m}} = t^2 + \sinh^2(n\ell_1/2)$$

where m is the source strength. Using (2.1) then gives

$$e^{\frac{\alpha+i\beta}{m}} = \sinh^2(n\ell_1/2) - \sinh^2\left(n(\ell_1 - \zeta)/2\right) \tag{2.2}$$

The shape of the curved wall $B'C'$ can now be found using the fact that on this wall

$$q = U_1 e^{-\ell_1}$$

so that

$$\zeta = \ell_1 + i\theta$$

Therefore, from (2.2) after some manipulation

$$e^{\frac{\alpha+i\beta}{m}} = \left(\cosh(n\ell_1) - \cos(n\theta)\right)/2 \tag{2.3}$$

The right hand side of (2.3) is real and so let $\beta/m = 0$ - the value of the stream function on the wall - giving

$$e^{\frac{\alpha}{m}} = \left(\cosh(n\ell_1) - \cos(n\theta)\right)/2 \tag{2.4}$$

Taking cartesian coordinates parallel and perpendicular to the tunnel axis, origin at B' and measuring the distance s along the wall from the origin yields the following relations:

d/

$$\frac{dx}{ds} = \cos(\theta) \quad ; \quad \frac{dy}{ds} = \sin(\theta) \quad ; \quad \frac{d\alpha}{ds} = q = U_1 e^{-\ell_1}$$

Therefore

$$\frac{dx}{d\theta} = \frac{dx}{ds} \cdot \frac{ds}{d\alpha} \cdot \frac{d\alpha}{d\theta}$$

$$= \cos(\theta) \cdot \frac{1}{U_1 e^{-\ell_1}} \cdot \frac{d\alpha}{d\theta} \qquad (2.5)$$

Also by differentiating (2.4) with respect to θ

$$\frac{d\alpha}{d\theta} = \frac{mn \sin(n\theta)}{\cosh(n\ell_1)-\cos(n\theta)} \qquad (2.6)$$

As already mentioned, the output of the source must be equal to the total flux through the duct. The source strength is therefore given by

$$2\pi m = U_1 H$$

or

$$m = U_1 H/2\pi$$

Using this result and (2.5) and (2.6) gives

$$\frac{dx}{d\theta} = \frac{n\, e^{\ell_1} H}{2\pi} \cdot \frac{\sin(n\theta)\cos(\theta)}{\cosh(n\ell_1)-\cos(n\theta)}$$

The wall coordinates are then found by integrating

$$\frac{1}{H}\int_0^x dx = \frac{n\, e^{\ell_1}}{2\pi}\int_0^\theta \frac{\sin(n\theta)\cos(\theta)}{\cosh(n\ell_1)-\cos(n\theta)}\, d\theta \qquad (2.7)$$

Similarly

$$\frac{1}{H}\int_0^y dy = \frac{n\, e^{\ell_1}}{2\pi}\int_0^\theta \frac{\sin(n\theta)\sin\theta}{\cosh(n\ell_1)-\cos(n\theta)}\, d\theta \qquad (2.8)$$

Both /

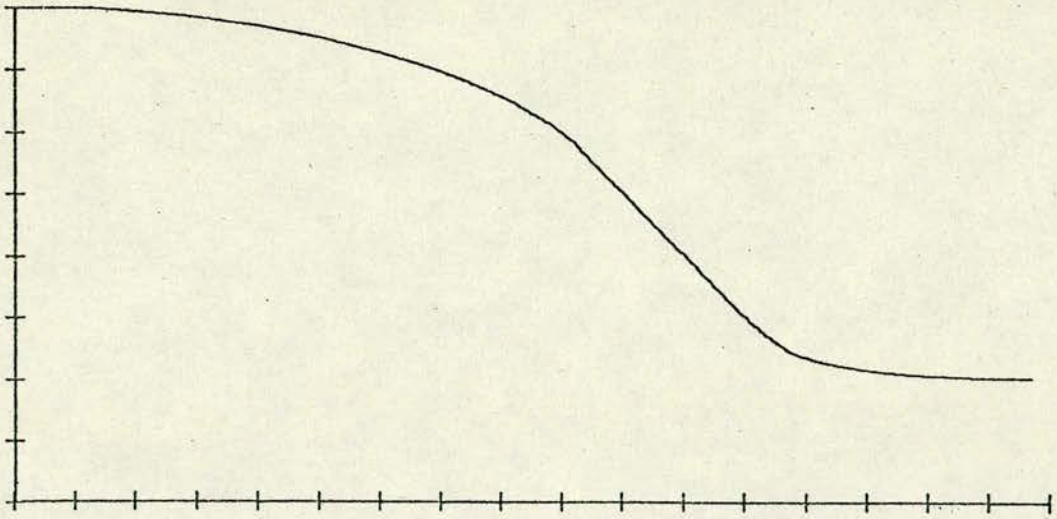

JORDINSON'S CONTRACTION

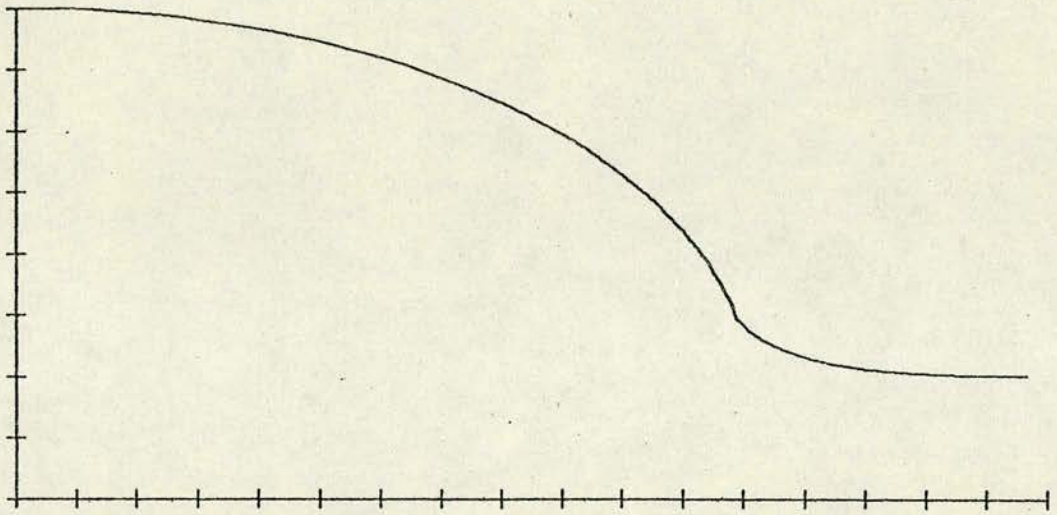

W.W.W.'S CONTRACTION

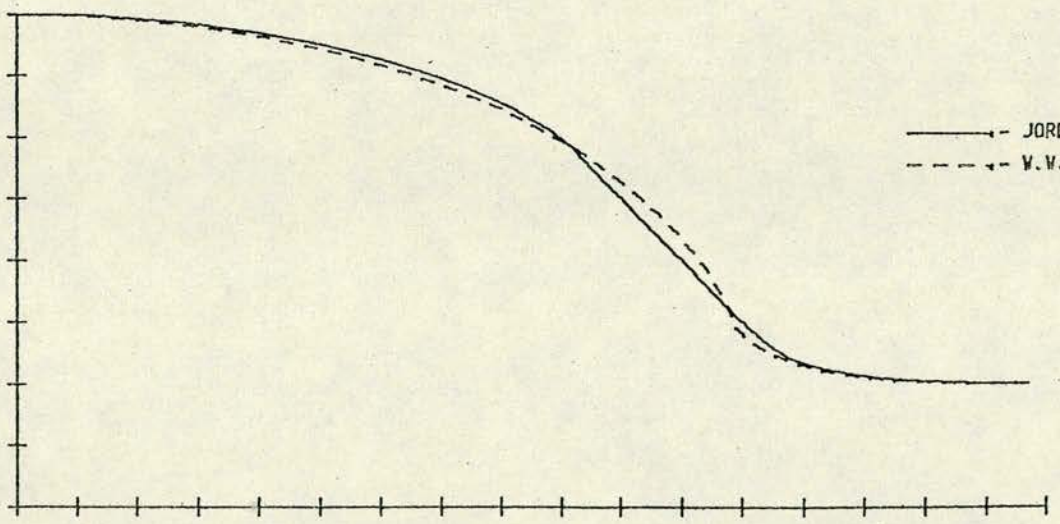

FIGURE (2.7)

Both integrals in (2.7) and (2.8) are valid in the range $0 \leq \theta \leq \pi$ and were evaluated numerically. The calculation for the curved walls at the downstream end is similar to the above where the Schwartz-Christoffel transformation in this case is

$$t = i\sinh\left(n(\ell_2+\zeta)/2\right)$$

The corresponding relations for the downstream wall coordinates are

$$\frac{1}{h}\int_0^x dx = \frac{n\, e^{-\ell_2}}{2\pi} \int_0^\theta \frac{\sin(n\theta)\cos\theta}{\cosh(n\ell_2)-\cos(n\theta)}\, d\theta$$

and

$$\frac{1}{h}\int_0^y dy = \frac{n\, e^{-\ell_2}}{2\pi} \int_0^\theta \frac{\sin(n\theta)\sin\theta}{\cosh(n\ell_2)-\cos(n\theta)}\, d\theta$$

The complete contraction is then obtained by joining both curved sections by a straight wall at an angle π/n to the axis.

The contraction shape calculated in this way for a contraction ratio of 4:1 and factors $n = 4$; $e^{-\ell_1} = 0{\cdot}9$; $e^{+\ell_2} = 1{\cdot}025$ is shown in figure (2.7) where it is compared with a contraction designed using W.W.W.'s method with approximately equal adverse pressure gradients at each end. The contractions differ in length by approximately H/100. However, Jordinson's contraction has a smaller maximum wall angle with a more gentle approach to the downstream parallel section.

The velocity distribution on any of the straight walls CD, AB or DE - figure (2.6a) - can be obtained with relative ease. For example, on the wall CV - figure (2.6b) - using the upstream approximation /

approximation where $\theta = \pi/n$

$$\zeta = \log(U_1/q)+i\pi/n$$

Equation (2.2) yields after some manipulation

$$e^{\frac{\alpha+i\beta}{m}} = \tfrac{1}{2}\cosh(n\ell_1)-\tfrac{1}{4}\{e^{n\ell_1}\left(\frac{q}{U_1}\right)^n e^{-i\pi}+e^{-n\ell_1}\left(\frac{q}{U_1}\right)^{-n} e^{i\pi}\} \qquad (2.9)$$

Again taking $\beta/m = 0$ on the wall gives from (2.9)

$$e^{\frac{\alpha}{m}} = \tfrac{1}{2}\cosh(n\ell_1)+\tfrac{1}{4}\{e^{n\ell_1}\left(\frac{q}{U_1}\right)^n+e^{-n\ell_1}\left(\frac{q}{U_1}\right)^{-n}\} \qquad (2.10)$$

Differentiating (2.10) with respect to s - the distance along the wall measured from C′ - then gives

$$\frac{1}{m} e^{\frac{\alpha}{m}} \frac{d\alpha}{ds} = \frac{n}{4q}\left\{\left(\frac{qe^{\ell_1}}{U_1}\right)^n - \left(\frac{qe^{\ell_1}}{U_1}\right)^{-n}\right\} \frac{dq}{ds} \qquad (2.11)$$

Using $\frac{d\alpha}{ds} = q$ and integrating (2.11) with respect to s results in

$$S = mn \int_{U_1 e^{-\ell_1}}^{q} \frac{\left(\frac{qe^{\ell_1}}{U_1}\right)^{2n} - 1}{\left[\left(\frac{qe^{\ell_1}}{U_1}\right)^{2n}+2\left(\frac{qe^{\ell_1}}{U_1}\right)^n \cosh(n\ell_1)+1\right]q^2} dq$$

Hence the velocity distribution on the wall CV′ can be found. A similar calculation using the downstream approximation gives the velocity distribution on the wall DW′. By combining these results, an approximation to the velocity distribution on the contraction /

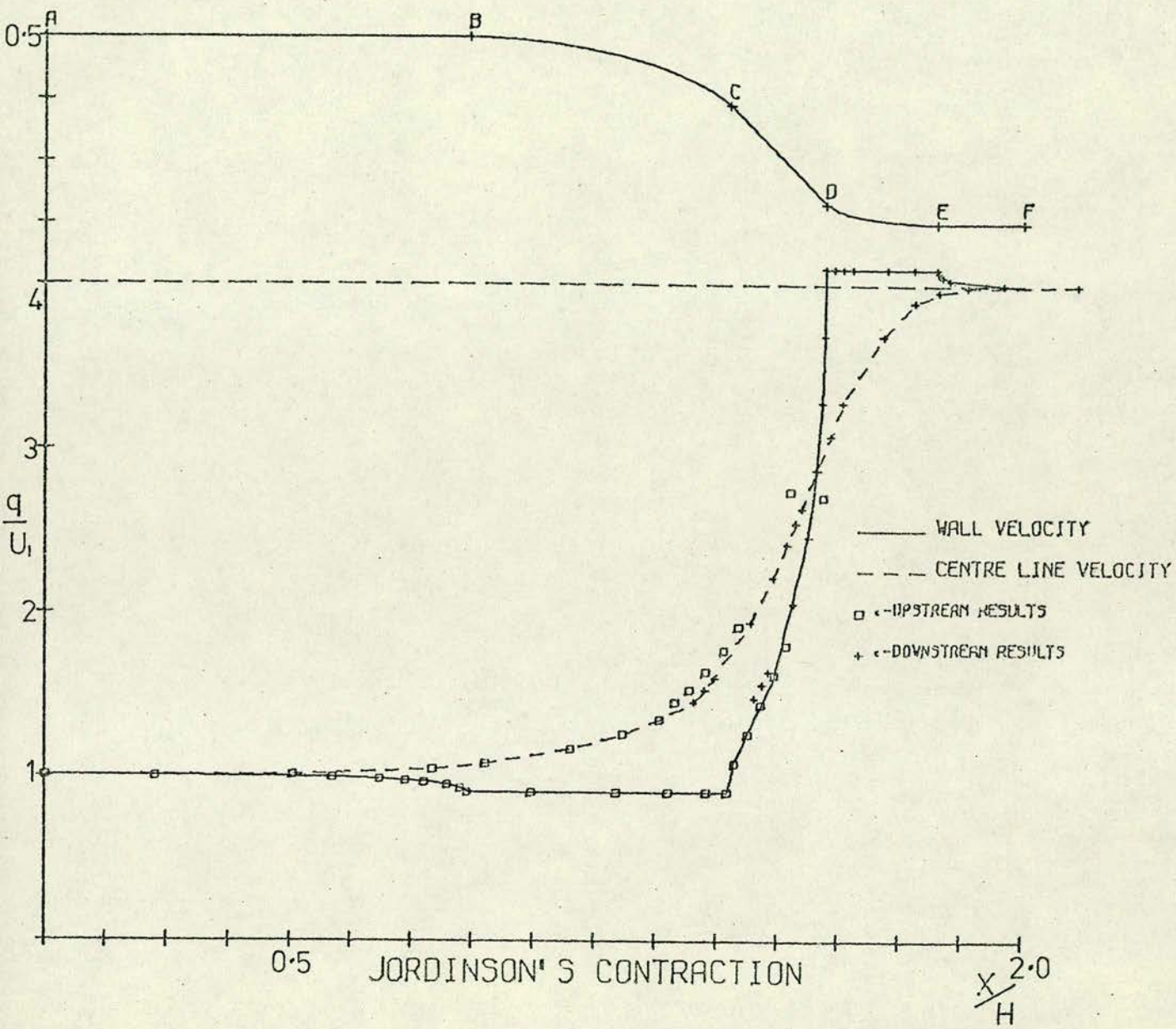
A
B
C
D
E
F
0·5
4
3
2
1
q/U₁
WALL VELOCITY
CENTRE LINE VELOCITY
□ <-UPSTREAM RESULTS
+ <-DOWNSTREAM RESULTS
0·5
JORDINSON'S CONTRACTION
2·0
X/H

FIGURE (2.8)

$\frac{x}{H}$	$\frac{y}{H}$
0.0000	0.5000
0.8654	0.5000
0.9954	0.4908
1.0697	0.4808
1.1434	0.4668
1.2161	0.4483
1.2879	0.4239
1.3529	0.3933
1.3963	0.3636
1.5965	0.1634
1.6207	0.1503
1.6945	0.1327
1.7429	0.1280
1.7928	0.1257
1.8178	0.1251
1.8239	0.1250
2.0000	0.1250

WALL COORDINATES

$\frac{x}{H}$	WALL VELOCITY $\frac{q}{U_1}$
0.0000	1.0000
0.2258	0.9990
0.6835	0.9810
0.7391	0.9720
0.7768	0.9630
0.8247	0.9450
0.8514	0.9270
0.8654	0.9000
0.9954	0.9000
1.1688	0.9000
1.2760	0.9000
1.3518	0.9000
1.3963	0.9000
1.4102	1.0800
1.4373	1.2600
1.4662	1.4400
1.4929	1.6200
1.5164	1.8000
1.5941	2.7000

$\frac{x}{H}$	CENTRE LINE VELOCITY $\frac{q}{U_1}$
0.0000	1.0000
0.5063	1.0080
0.7943	1.0440
0.9025	1.0800
1.0760	1.1700
1.1831	1.2600
1.2589	1.3500
1.2897	1.4517
1.3199	1.5296
1.3548	1.6381
1.3887	1.7678
1.4196	1.9121
1.5260	2.7356

UPSTREAM RESULTS

$\frac{x}{H}$	WALL VELOCITY $\frac{q}{U_1}$
1.4516	1.4760
1.4670	1.5580
1.4808	1.6400
1.5314	2.0500
1.5619	2.4600
1.5802	2.8700
1.5904	3.2800
1.5952	3.6900
1.5965	4.1000
1.6135	4.1000
1.6309	4.1000
1.6520	4.1000
1.7230	4.1000
1.7769	4.1000
1.8239	4.1000
1.8255	4.0795
1.8346	4.0508
1.8497	4.0303
1.9601	4.0016

$\frac{x}{H}$	CENTRE LINE VELOCITY $\frac{q}{U_1}$
1.3484	1.4897
1.3684	1.6003
1.4427	1.9380
1.4893	2.2130
1.5188	2.4150
1.5366	2.5460
1.5484	2.6360
1.5782	2.8700
1.6079	3.0750
1.6323	3.2800
1.7148	3.6900
1.7779	3.8950
1.8280	3.9606
1.8856	3.9893
2.1102	4.0000

DOWNSTREAM RESULTS

TABLE 2.1

contraction wall $C'D'$ can be found. By performing another two similar calculations the centre line velocity distribution can be found. Figure (2.8) shows the wall and centre line velocity distributions relative to the contraction wall as a result of combining the upstream and downstream solutions for the case $n = 4$; $e^{-\ell_1} = 0{\cdot}9$; $e^{\ell_2} = 1{\cdot}025$ and contraction ratio of 4:1 . The corresponding results are shown in table (2.1) .

2.5 The Parameters ℓ_1 and ℓ_2 and the Constant Velocities

Having the velocity constant on the curved walls has the advantage that in addition to the flow behaving as if the walls were free surfaces, the danger of separation along the length of the curved walls is reduced. This suggests that if the contraction could be designed so that the wall velocity was constant along the total length of the contraction, the danger of separation could be considerably reduced. This design is, however, impossible for a contraction of finite length since, from the previous discussion of adverse pressure gradients, the constant velocity would need to be less than the upstream velocity U_1 and, at the same time, greater than the downstream velocity U_2 . This condition obviously cannot be satisfied since $U_1 < U_2$.

Expressing the constant velocities as $U_1 e^{-\ell_1}$ and $U_2 e^{\ell_2}$ is convenient when working in the logarithmic hodograph plane. Since /

Since it is known that adverse pressure gradients exist at each end of the contraction, the parameters ℓ_1 and ℓ_2 must both be positive. The magnitude of the adverse pressure gradient can be adjusted by simply varying the values of ℓ_1 and ℓ_2 . For example, increasing ℓ_1 will increase the adverse pressure gradient along AB (figure 2.6a) and will decrease the length of BC . Similarly, increasing ℓ_2 will increase the adverse pressure gradient along EF and decrease the length of DE. As mentioned in W.W.W., it is not always advantageous to have a low adverse pressure gradient at the downstream end since this would mean a longer curved section DE. This in turn would delay the final rise in the centre line velocity and so slow down the approach to uniform flow. Conversely, too short a curved section is not permissible because of the danger of boundary layer separation. In the following work, values of ℓ_1 and ℓ_2 have been chosen to give a compromise in length of contraction and magnitude of adverse pressure gradients which have already been found to be satisfactory in two-dimensions. (cf. W.W.W., Gibbings and Dixon, Jordinson).

2.6 Infinite Length Contractions

It can be seen from figure (2.6d) that if $\ell_1 = 0$ then CC' lies on the θ axis and A, A', B and B' coincide on the origin. In the physical plane, this means that B lies at $-\infty$ and the velocity on BC is constant at U_1 . Similarly, if $\ell_2 = 0$, DE becomes infinite in length (figure 2.6e) . /

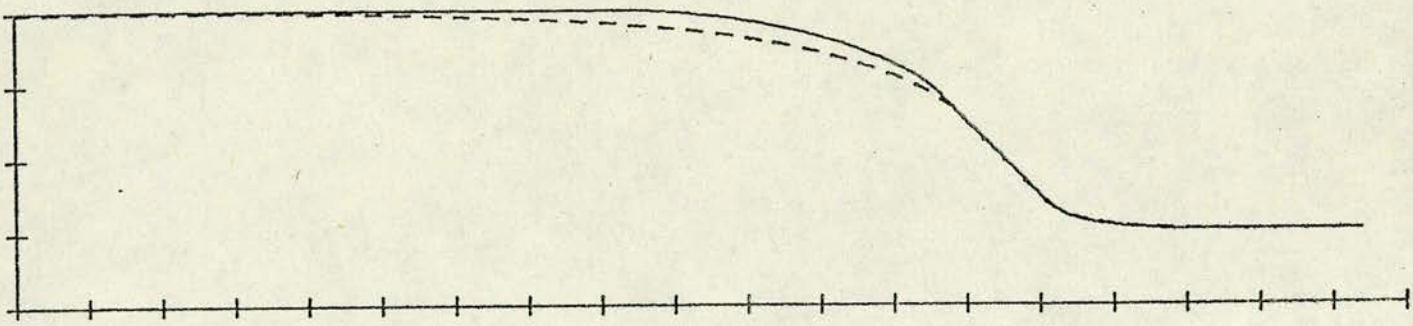

FIGURE (2·9)

2.6e). Hence the case $\ell_1 = \ell_2 = 0$ corresponds to a contraction of infinite length.

When $\ell_1 = 0$ the integral in (2.7) must be treated differently because there is a singularity at $\theta = 0$. In order to obtain the boundary coordinates, the direction of integration should be reversed. That is, $\theta = \pi/n$ should be taken as the origin of coordinates and the integral evaluated as $\theta \to 0$ (that is as $X \to -\infty$). The calculation of the downstream wall when $\ell_2 = 0$ should be treated similarly. An infinite length contraction (contraction ratio 4:1, and n = 4) designed in this way is shown in figure (2.9) where it is compared with the previously described finite length contraction ($n = 4$, $e^{-\ell_1} = 0{\cdot}9$, $e^{\ell_2} = 1{\cdot}025$).

The case $\ell_1 < 0$ or $\ell_2 < 0$ leads to an impossible flow situation in the hodograph plane and could correspond to an expansion rather than a contraction.

Because of the ease with which this approximate solution can be handled, it is used in the next chapter to predict the flow of an axisymmetric contraction with the same profile as the above finite length two-dimensional contraction.

CHAPTER 3

APPROXIMATE SOLUTION TO THE AXISYMMETRIC FLOW

3.1 INTRODUCTION. Equations for the Stream Function ψ

The use of the solution to a two-dimensional problem to predict the solution to the corresponding axisymmetric problem has already been mentioned. In this chapter, a transformation described by W.W.W. is used to obtain an approximate solution to the flow in an axisymmetric contraction from the solution to the flow in the two-dimensional contraction with the same profile.

For incompressible axisymmetric flow where there exists a stream function ψ, the condition that the flow should be irrotational can be written in the form

$$\frac{\partial}{\partial x}\left(\frac{1}{y}\frac{\partial \psi}{\partial x}\right) + \frac{\partial}{\partial y}\left(\frac{1}{y}\frac{\partial \psi}{\partial y}\right) = 0 \qquad (3.1)$$

Equation (3.1) is equivalent to the vanishing of the real part of

$$\frac{\partial}{\partial Z}\left(\frac{1}{y}\frac{\partial \psi}{\partial \overline{Z}}\right) = 0 \qquad (3.2)$$

Now since Z can be considered to be an analytic function of the two-dimensional velocity potential $W = \alpha+i\beta$, (3.2) is equivalent to

$$\frac{\partial}{\partial Z}\left(\frac{1}{y}\frac{\partial \psi}{\partial \overline{Z}}\right) = \frac{\partial}{\partial Z}\left(\frac{1}{y}\frac{\partial \overline{W}}{\partial \overline{Z}}\frac{\partial \psi}{\partial \overline{W}}\right) = \frac{\partial \overline{W}}{\partial \overline{Z}}\frac{\partial W}{\partial Z}\frac{\partial}{\partial W}\left(\frac{1}{y}\frac{\partial \psi}{\partial \overline{W}}\right) = 0 \qquad (3.3)$$

If the real part of the left hand side of (3.3) is zero, then the /

the real part of the right hand side must also be zero. Then, since $\frac{\partial \overline{W}}{\partial \overline{Z}} \frac{\partial W}{\partial Z}$ is real, this means

$$R\left\{\frac{\partial}{\partial W}\left(\frac{1}{y}\frac{\partial \psi}{\partial \overline{W}}\right)\right\} = 0$$

That is

$$\frac{\partial}{\partial \alpha}\left(\frac{1}{y}\frac{\partial \psi}{\partial \alpha}\right) + \frac{\partial}{\partial \beta}\left(\frac{1}{y}\frac{\partial \psi}{\partial \beta}\right) = 0 \qquad (3.4)$$

Equation (3.4) forms the starting point for W.W.W.'s approximation. (cf. Milne-Thomson (1949), second edition: 15.50)

3.2 The W.W.W. Approximation

Equation (3.4) is more convenient for a numerical solution when α and β are known since the boundary conditions become ψ = constant for the two values of β corresponding to the wall and the centre line. In addition it is argued that since the wall and centre line are streamlines of both the two-dimensional and axisymmetric flows, the intermediate streamlines should not differ greatly in shape. The derivatives of ψ with respect to α therefore should be small and smaller than those with respect to β . So, to a first approximation, if the derivatives with respect to α are ignored, equation (3.4) reduces to

$$\frac{\partial}{\partial \beta}\left(\frac{1}{y}\frac{\partial \psi}{\partial \beta}\right) = 0 \qquad (3.5)$$

Similarly, if V_A is the resultant axisymmetric velocity and V_T the resultant two-dimensional velocity, then

$$V_A^2 = /$$

$$V_A^2 = \frac{1}{y^2} \left[\left(\frac{\partial \psi}{\partial y} \right)^2 + \left(\frac{\partial \psi}{\partial x} \right)^2 \right]$$

and

$$V_T^2 = \left[\left(\frac{\partial \beta}{\partial y} \right)^2 + \left(\frac{\partial \beta}{\partial x} \right)^2 \right]$$

Then, as in the derivation of (3.4), it follows that

$$V_A^2 = \frac{V_T^2}{y^2} \left[\left(\frac{\partial \psi}{\partial \beta} \right)^2 + \left(\frac{\partial \psi}{\partial \alpha} \right)^2 \right] \tag{3.6}$$

Again, neglecting the derivatives with respect to α equation (3.6) reduces to

$$V_A = \frac{V_T}{y} \frac{\partial \psi}{\partial \beta} \tag{3.7}$$

Where the positive square root has been taken.

Comparing (3.5) and (3.7) it can be seen that

$$\frac{\partial}{\partial \beta} \left(\frac{V_A}{V_T} \right) = 0 \tag{3.8}$$

It can be deduced from (3.8) that V_A/V_T is a function of α only. That is from (3.7) and (3.8)

$$\frac{V_A}{V_T} = f(\alpha) = \frac{1}{y} \frac{\partial \psi}{\partial \beta} \tag{3.9}$$

In effect, equation (3.9) implies that to this approximation, on an equipotential line the axisymmetric velocity at each point on the line is the same constant multiple of the two-dimensional velocity at the same points. Thus if the two-dimensional velocity distribution is known, the axisymmetric velocity distribution can /

can be calculated if $f(\alpha)$ can be found. From (3.9), integrating along an equipotential line yields

$$\int d\psi = f(\alpha) \int y \, d\beta$$

For flow in a duct with an upstream width H, if ψ is taken as zero on the wall, its value on the centre line will be $-U_1H^2/8$. Integrating across the stream from centre line to wall gives $f(\alpha)$ in the form

$$\frac{U_1H^2}{8} = f(\alpha) \int_{-U_1H/2}^{0} y \, d\beta \qquad (3.10)$$

where $\beta = -U_1H/2$ on the centre line and $\beta = 0$ on the wall. Hence, if the integral in (3.10) is evaluated, the function $f(\alpha)$ can be found and the transformation from the two-dimensional case to the axisymmetric case completed.

3.3 Implications of W.W.W.'s Approximation

It can be seen that far upstream or downstream of the contraction where the flow is simply that in a channel of width H or h respectively, the transformation becomes exact. For example, far upstream of the contraction, for flow in a channel of width H with the previously defined values of ψ and β on the wall and centre line

$$\psi = U_1y^2/2 - U_1H^2/8 \quad ; \quad \beta = U_1y - U_1H/2 \quad ; \quad \alpha = U_1x + \text{constant}$$

so that

$$\frac{\partial \psi}{\partial \alpha} = 0 = \frac{\partial}{\partial \beta}\left(\frac{1}{y}\frac{\partial \psi}{\partial \beta}\right)$$

and /

and

$$\int_{-U_1H/2}^{0} y \, d\beta = U_1H^2/8$$

Therefore from (3.10), $f(\alpha) = 1$. That is, far upstream of the contraction the velocity in an axisymmetric duct is the same as in the two-dimensional duct. Downstream of the contraction, the values of ψ and β on the wall and centre line remain unchanged. However, β can be written equivalently as

$$\beta = U_2y - U_2h/2$$

Using this expression for β, the integral in (3.10) becomes

$$\int_{-U_2h/2}^{0} y \, d\beta = U_2h^2/8 \qquad (3.11)$$

Using (3.11) and (3.10) gives

$$f(\alpha) = \frac{U_1H^2}{U_2h^2} \qquad (3.12)$$

For uniform flow far from the contraction, the equation of conservation of mass gives

$$U_1H = U_2h$$

Therefore (3.12) can be written as

$$f(\alpha) = H/h = K$$

so that the velocity downstream of the axisymmetric contraction is K times greater than in the two-dimensional duct as expected.

It is important to note that since from (3.9)

$$f(\alpha) = \frac{1}{y}\frac{\partial\psi}{\partial\beta}$$

then /

then

$$\frac{\partial f}{\partial x} = \frac{\partial f}{\partial \alpha}\frac{\partial \alpha}{\partial x} = -\frac{1}{y^2}\frac{\partial \psi}{\partial \beta}\frac{\partial y}{\partial \alpha}\frac{\partial \alpha}{\partial x}$$

where derivatives of ψ with respect to α have been neglected as in the original approximation. Now since $\frac{\partial \alpha}{\partial x} > 0$; $\frac{\partial \psi}{\partial \beta} > 0$; and, for a contraction $\frac{\partial y}{\partial \alpha} < 0$, $f(\alpha)$ must be a monotonic increasing function of α increasing from 1 far upstream of the contraction to K far downstream of the contraction. Hence any adverse pressure gradients in the axisymmetric contraction must be less than those in the corresponding two-dimensional case. Similarly, any favourable pressure gradients will be enhanced in the axisymmetric contraction.

3.4 Application to the Two-dimensional Contraction

To calculate $f(\alpha)$ from (3.10) for a given value of α means that the integral must be evaluated numerically. To do this, several values of y must be found with the corresponding values of β on the line α = constant. Using Jordinson's approximate solution described in the previous chapter, the equation governing the flow in the upstream part is

$$e^{\frac{\alpha+i\beta}{m}} = \sinh^2(n\ell_1/2) - \sinh^2\left(n(\ell_1-\zeta)/2\right) \qquad (3.13)$$

Writing $T = (q/U_1)e^{+\ell_1}$ and substituting $\zeta = \log(U_1/q)+i\theta$ in (3.13) gives after equating real and imaginary parts

$$e^{\frac{\alpha}{m}} /$$

$$e^{\frac{\alpha}{m}}\cos(\beta/m) = \cosh(n\ell_1)/2 - (T^n+T^{-n})\cos(n\theta)/4 \qquad (3.14)$$

$$e^{\frac{\alpha}{m}}\sin(\beta/m) = (T^n-T^{-n})\sin(n\theta)/4 \qquad (3.15)$$

For a given value of T on an equipotential line, the corresponding values of β/m and θ can be found from (3.14) and (3.15) .

To tabulate y as a function of β it is now only necessary to find y as a function of T . This is done by differentiating (3.14) and (3.15) with respect to s - the distance measured along an equipotential line - giving two equations involving the derivatives $\frac{\partial\theta}{\partial s}$, $\frac{\partial\beta}{\partial s}$ and $\frac{\partial T}{\partial s}$:

$$\frac{1}{m}e^{\frac{\alpha}{m}}\cos\left(\frac{\beta}{m}\right)\frac{d\alpha}{ds} - \frac{1}{m}e^{\frac{\alpha}{m}}\sin\left(\frac{\beta}{m}\right)\frac{d\beta}{ds} = -\frac{n}{4T}\{T^n-T^{-n}\}\cos(n\theta)\frac{dT}{ds} + \frac{n}{4}\{T^n+T^{-n}\}\sin(n\theta)\frac{d\theta}{ds}$$

$\times \cos n\theta \times (T^n - T^{-n})$

and

$$\frac{1}{m}e^{\frac{\alpha}{m}}\sin\left(\frac{\beta}{m}\right)\frac{d\alpha}{ds} + \frac{1}{m}e^{\frac{\alpha}{m}}\cos\left(\frac{\beta}{m}\right)\frac{d\beta}{ds} = \frac{n}{4T}\{T^n+T^{-n}\}\sin(n\theta)\frac{dT}{ds} + \frac{n}{4}\{T^n-T^{-n}\}\cos(n\theta)\frac{d\theta}{ds}$$

$\times \sin n\theta \,(T^n + T^{-n})$

Using the results $\frac{dy}{ds} = \cos(\theta)$ and $\frac{d\beta}{ds} = q = U_1 T e^{-\ell_1}$, and then eliminating $\frac{d\theta}{ds}$ from these two equations gives

$$\frac{1}{H}\int_0^y dy = \frac{U_1}{2\pi e^{\frac{\alpha}{m}}}\int_{T_0}^{T} \frac{\{T^{2n}+T^{-2n} - 2\cos(2n\theta)\}\cos(\theta)}{T^2\{T^n\sin(n\theta+\frac{\beta}{m})+T^{-n}\sin(n\theta-\frac{\beta}{m})\}}\,dT \qquad (3.16)$$

Knowing β/m and θ as functions of T , this integral can be evaluated numerically giving y as a function of T . The integral /

integral of y with respect to β in (3.10) can now be evaluated giving a value for the function $f(\alpha)$.

3.5 The Singularity

The integrand in (3.16) has a singularity on the centre line where $\theta = 0$ and $\beta/m = -\pi$. This might have been anticipated because, from the symmetry of the problem, $\frac{\partial T}{\partial y}$ should be zero on the centre line. It is possible to show, however, that the integral exists since the singularity can be proved to be of the form $(T-T_0)^{-\frac{1}{2}}$ as $T \to T_0$ where T_0 is the value of T on the centre line on a given equipotential line. The proof of this is as follows.

From (3.14) and (3.15), by squaring and adding

$$\left.\begin{aligned} e^{\frac{2\alpha}{m}} &= \tfrac{1}{4}\cosh^2(n\ell_1) + \frac{1}{16}\{T^{2n}+T^{-2n}\} + \frac{1}{8}\{\cos^2(n\theta)-\sin^2(n\theta)\} - \\ &\quad \tfrac{1}{4}\cosh(n\ell_1)\{T^{n}+T^{-n}\}\cos(n\theta) \\ &= \tfrac{1}{4}\cosh^2(n\ell_1) + \frac{1}{16}\{T^{2n}+T^{-2n}\} + \frac{1}{8}\cos(2n\theta) - \tfrac{1}{4}\cosh(n\ell_1)\{T^{n}+T^{-n}\}\cos(n\theta) \end{aligned}\right\} \quad (3.17)$$

From (3.14) for $\beta/m \simeq -\pi$

$$(T^{n}+T^{-n})\cos(n\theta)/4 = \cosh(n\ell_1)/2 + e^{\frac{\alpha}{m}} \qquad (3.18)$$

Using (3.18) in (3.17) and substituting for θ small

$$\cos(2n\theta) = 1 - 2n^2\theta^2 \quad .....$$

gives

e /

$$e^{\frac{2\alpha}{m}} = \tfrac{1}{4}\cosh^2(n\ell_1) + \frac{1}{16}\{T^{2n}+T^{-2n}\} + \frac{1}{8}\{1-2n^2\theta^2+\ldots\} - \cosh(n\ell_1)\{\tfrac{1}{2}\cosh(n\ell_1)+e^{\frac{\alpha}{m}}\}$$

Therefore

$$n^2\theta^2 = \tfrac{1}{4}\{T^{2n}+T^{-2n}\} - 4e^{\frac{\alpha}{m}}\cosh(n\ell_1) - 4e^{\frac{2\alpha}{m}} + \tfrac{1}{2} - \cosh^2(n\ell_1)$$

$$= H(T)$$

If $T = T_0$ on the centre line, then $H(T_0) = 0$. Expanding $H(T)$ in a series in $(T-T_0)$ for θ small results in

$$n^2\theta^2 = H(T_0) + (T-T_0)H'(T_0) + \ldots$$

Therefore since $H(T_0) = 0$ and

$$H'(T_0) = n(T_0^{2n}-T_0^{-2n})/2T_0 \neq 0$$

then

$$n\theta \simeq (T-T_0)^{\frac{1}{2}}\left(H'(T_0)\right)^{\frac{1}{2}} \qquad (3.19)$$

where the positive square root has been taken. If the integrand in (3.16) is called $G(T)$, then

$$G(T) = \frac{\{T^{2n}+T^{-2n}-2\cos(2n\theta)\}\cos\theta}{T^2\{T^n\sin(n\theta+\frac{\beta}{m})+T^{-n}\sin(n\theta-\frac{\beta}{m})\}}$$

Then on the centre line, when $\beta/m = -\pi$ and using the result that for θ small

$$\sin(n\theta) \simeq n\theta$$

$$G(T) \simeq -\frac{\{T^{2n}+T^{-2n}-2\cos(2n\theta)\}\cos\theta}{n\theta\{T^n+T^{-n}\}T^2} = \frac{\tilde{G}(T)}{n\theta}$$

where $\tilde{G}(T_0)$ is finite

Then, using (3.19), in the region of the centre line,

$G(T)$ /

$$G(T) = \frac{\tilde{G}(T)}{(T-T_0)^{\frac{1}{2}}\sqrt{H'(T_0)}}$$

The singularity in (3.16) is therefore integrable being of the form $(T-T_0)^{-\frac{1}{2}}$ as $T \to T_0$.

3.6 The Numerical Evaluation of $\int y d\beta$

In order to calculate the integral of y with respect to β occurring in (3.10), it is necessary first to tabulate y as a function of T by evaluating the integral in (3.16). A computer programme was written to evaluate (3.16) numerically giving y as a function of T (and therefore of β/m) and also to calculate $\int y d\beta$ by the trapezium rule. Because of the singularity in (3.16) at the centre line, the programme evaluated the integral in the direction from the wall to the centre line using a limiting procedure as the singularity was approached. The integral in (3.16) was calculated using Gaussian quadrature tabulating y as a function of β for several values of T on an equipotential line from the value of T on the wall to a point T' just before the centre line. The limiting procedure used as the centre line was approached consisted of integrating between the limits T_i and T_{i+1} where the T_i are given by

$$T_i = T_0 - \frac{T_0 - T'}{10^i}$$

and summing the contributions from each interval. This process was continued until the contributions to the integral from any interval could be considered negligible. The programme also evaluated the ordinate of the point on the wall which provided a useful check on the accuracy of the limiting process. Hence, for a given equipotential /

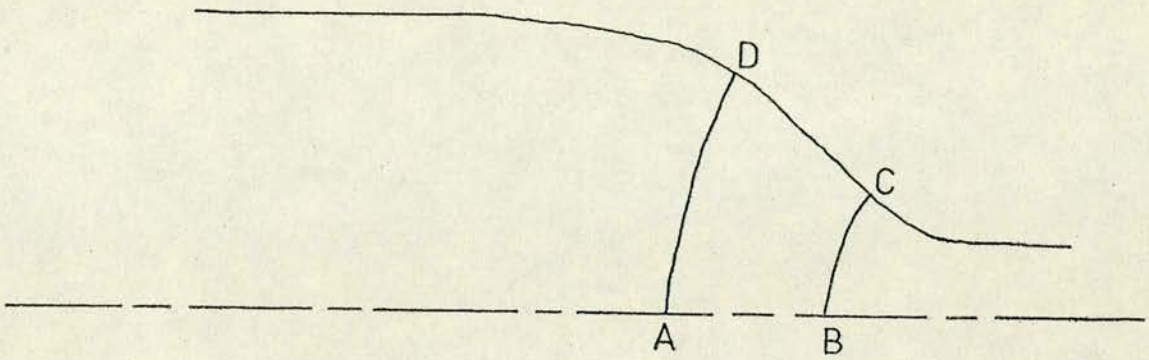

FIGURE (3.1)

equipotential line, the value of $f(\alpha)$ could be found from (3.10).

It is suggested by W.W.W. that it may be more convenient to express the integral $\int y d\beta$ in terms of the integral $\int x d\alpha$ on the wall and the centre line. This can be done by considering the line integral

$$\oint Z dW = \oint (x+iy)(d\alpha+id\beta) \tag{3.20}$$

around the closed contour ABCD in figure (3.1). Since Z is an analytic function of W and there are no singularities of Z within the region bounded by this contour, the integral must be zero. Equating the real part of (3.20) to zero gives

$$\oint x d\alpha - y d\beta = 0 \tag{3.21}$$

Therefore, since α is constant on BC and DA and β is constant on CD and AB, (3.21) can be written as

$$\int_B^C y d\beta = \int_A^B x d\alpha + \int_C^D x d\alpha + \int_A^D y d\beta$$

Therefore, to find the integral $\int y d\beta$ for various values of α, it is only necessary to integrate across the stream once. The other integrals - on the wall and centre line - with respect to α can be found relatively easily from (3.14) and (3.15). For example, on the centre line $\beta/m = -\pi$ and $\theta = 0$. (3.14) becomes, for the upstream approximation

$$e^{\frac{\alpha}{m}} = (T^n+T^{-n})/4 - \cosh(n\ell)/2 \tag{3.22}$$

Differentiating this equation with respect to x and using the relation

$$\frac{d\alpha}{dx} = q = U_1 T e^{-\ell_1}$$

gives /

T ON THE CENTRE LINE	$\int y d\beta$ DIRECT	$\int y d\beta$ CONTOUR	ERROR
1.2000	0.11915	0.11913	0.00002
1.3000	0.11075	0.11082	0.00007
1.5000	0.09502	0.09502	0.00000
3.0000	0.04411	0.04419	0.00008
4.0000	0.03284	0.03289	0.00005
6.0000	0.02173	0.02197	0.00024
8.0000	0.01566	0.01649	0.00083

TABLE (3.1)

gives

$$\frac{1}{H}\int_{x_1}^{x_2} dx = \frac{ne^{+\ell_1}}{2\pi}\int_{T_1}^{T_2} \frac{T^n - T^{-n}}{\{T^n+T^{-n} -2\cosh(n\ell_1)\}T^2}\,dT \qquad (3.23)$$

The integrand in (3.23) is finite for all T under consideration and the integral can be evaluated easily. Similarly, the integral on the wall can also be found. In the following work, the integral $\int y d\beta$ was evaluated directly and also by using this alternative method. Although the integrals with respect to α are the easier ones to determine, the method of integrating round the contour presented difficulties in the programming. For example, since the equipotential lines AD and BC are not straight and perpendicular to the axis and if the origins are taken at A and D for the purpose of integrating along the centre line and wall, then the value of x on the wall must be increased by the horizontal distance between A and D to refer both integrals to the same origin. In fact, it was found that despite the difficulty in integrating directly across the stream, once the programme had been written it was easier and more convenient to evaluate the integral $\int y d\beta$ directly. However, using both methods provided a useful check on the results, some of which are shown in table (3.1) for the upstream approximation.

3.7 Results

Jordinson's approximation implies that each end of the contraction is independent of the other and can be considered separately. Thus, using one upstream part, several downstream parts could be matched to give different contraction ratios or different adverse pressure gradients /

gradients at the downstream end or vice versa. Assuming that the factors $e^{-\ell_1}$ and e^{ℓ_2} and the design of the upstream part remains fixed, then using the W.W.W. method the values of $f(\alpha)$ at the downstream end can be calculated in the form $f(\alpha)h/H$. At the downstream end of the contraction the non-dimensional velocity is $T = q/(U_2 e^{\ell_2})$. Knowing e^{ℓ_2}, the value of T is known as a function of x/h at any point with respect to an origin at E (figure 3.2). The two-dimensional velocity is given as

$$q = U_2 T e^{\ell_2}$$

Therefore using the equation of continuity

$$U_1 H = U_2 h$$

gives the following expression for the two-dimensional velocity

$$\left(\frac{q}{U_1}\right)\left(\frac{h}{H}\right) = T e^{\ell_2} \qquad (3.24)$$

Thus the predicted axisymmetric velocity at the downstream end is given using (3.9), (3.24) and the new expression for the function $f(\alpha)$ as

$$V_A = f(\alpha)\left(\frac{q}{U_1}\right)\left(\frac{h}{H}\right)^2$$

Therefore just one application of W.W.W. method can give the predicted axisymmetric velocity distribution in several contractions for different contraction ratios provided they share a common upstream or downstream part. The only additional calculation required for each contraction is to refer both sets of results - those from the upstream part and those from the different downstream part - to the same origin. This is easily done once the total length of the contraction has been found from section (2.4) .

Tables /

x/H	T	q/U_1	$f(\alpha)$	axisymmetric q/U_1
-0.6396	1.1100	0.9990	1.0005	0.9995
-0.0016	1.0100	0.9090	1.0216	0.9287
0.0059	1.0000	0.9000	1.0221	0.9199
0.0117	1.0000	0.9000	1.0227	0.9204
0.0234	1.0000	0.9000	1.0253	0.9228
0.1300	1.0000	0.9000	1.0491	0.9442
0.3034	1.0000	0.9000	1.1286	1.0157
0.4106	1.0000	0.9000	1.2173	1.0956
0.4864	1.0000	0.9000	1.3155	1.1840
0.5448	1.2000	1.0800	1.4370	1.5520
0.5719	1.4000	1.2600	1.5320	1.9303
0.6008	1.6000	1.4400	1.6597	2.3900
0.6275	1.8000	1.6200	1.8095	2.9314
0.6510	2.0000	1.8000	1.9724	3.5503
0.7287	3.0000	2.7000	2.8666	7.7398

WALL VELOCITIES

TABLE (3.2)

x/H	T	q/U_1	$f(\alpha)$	axisymmetric q/U_1
-0.6399	1.1122	1.0009	1.0005	1.0015
-0.0191	1.1591	1.0432	1.0216	1.0658
-0.0164	1.1598	1.0438	1.0221	1.0669
-0.0125	1.1609	1.0448	1.0227	1.0685
0.0026	1.1653	1.0487	1.0253	1.0753
0.0924	1.2000	1.0800	1.0491	1.1330
0.2353	1.3000	1.1700	1.1286	1.3205
0.3177	1.4000	1.2600	1.2173	1.5338
0.3753	1.5000	1.3500	1.3155	1.7759
0.4243	1.6130	1.4517	1.4370	2.0860
0.4545	1.6995	1.5296	1.5320	2.3433
0.4894	1.8201	1.6381	1.6597	2.7188
0.5233	1.9642	1.7678	1.8095	3.1989
0.5542	2.1246	1.9121	1.9724	3.7714
0.6606	3.0396	2.7356	2.8666	7.8420

CENTRE LINE VELOCITIES

TABLE (3.3)

UPSTREAM RESULTS

x/H 16:1	x/H 6:1	T	$\frac{q}{U_1}\left(\frac{h}{H}\right)$	$f(\alpha)\left(\frac{h}{H}\right)$	axisym. $\frac{q}{U_1}\left(\frac{h}{H}\right)^2$	axisym. q/U_1 16:1	axisym. q/U_1 6:1
0.5862		0.3600	0.3690	0.3833	0.1414	2.2624	
0.6016		0.3800	0.3895	0.4033	0.1571	2.5136	
0.6154		0.4000	0.4100	0.4230	0.1734	2.7744	
0.6660		0.5000	0.5125	0.5143	0.2636	4.2176	
0.6965		0.6000	0.6150	0.5899	0.3628	5.8048	
0.7148	0.6010	0.7000	0.7175	0.6456	0.4632	7.4112	2.7792
0.7250	0.6177	0.8000	0.8200	0.6813	0.5587	8.9392	3.3522
0.7298	0.6255	0.9000	0.9225	0.6999	0.6456	10.3296	3.8736
0.7311	0.6277	1.0000	1.0250	0.7053	0.7229	11.5664	4.3374
0.7481	0.6554	1.0000	1.0250	0.7635	0.7826	12.5216	4.6956
0.7658	0.6830	1.0000	1.0250	0.8110	0.8313	13.3008	4.9878
0.7866	0.7183	1.0000	1.0250	0.8561	0.8775	14.0400	5.2650
0.8576	0.8342	1.0000	1.0250	0.9418	0.9653	15.4448	5.7918
0.9115	0.9222	1.0000	1.0250	0.9831	1.0077	16.1232	6.0462
0.9336	0.9583	1.0000	1.0250	0.9916	1.0164	16.2618	6.0983
0.9573	0.9970	1.0000	1.0250	0.9952	1.0201	16.3211	6.1205
1.0021	1.1183	0.9800	1.0045	0.9984	1.0029	16.0463	6.0173
1.1231	1.2677	0.9758	1.0002	0.9999	1.0001	16.0015	6.0006

WALL VELOCITIES

TABLE (3.4)

x/H 16:1	x/H 6:1	T	$\frac{q}{U_1}\left(\frac{h}{H}\right)$	$f(\alpha)\left(\frac{h}{H}\right)$	axisym. $\frac{q}{U_1}\left(\frac{h}{H}\right)^2$	axisym. q/U_1 16:1	axisym. q/U_1 6:1
0.5030	0.2551	0.3903	0.4001	0.4230	0.1692	2.7072	1.0152
0.5773	0.3764	0.4727	0.4845	0.5143	0.2492	3.9872	1.4952
0.6239	o.4625	0.5398	0.5533	0.5899	0.3264	5.2224	1.9584
0.6534	0.5008	0.5891	0.6038	0.6456	0.3898	6.2368	2.3388
0.6712	0.5298	0.6211	0.6366	0.6813	0.4337	6.9392	2.6022
0.6804	0.5448	0.6380	0.6540	0.6999	0.4577	7.3232	2.7462
0.6830	0.5492	0.6430	0.6591	0.7053	0.4649	7.4384	2.7894
0.7128	0.5978	0.7000	0.7175	0.7635	0.5478	8.7648	3.2868
0.7390	0.6406	0.7500	0.7688	0.8110	0.6234	9.9744	3.7404
0.7669	0.6861	0.8000	0.8200	0.8561	0.7020	11.2320	4.2120
0.8394	0.8045	0.9000	0.9225	0.9418	0.8688	13.9009	5.2128
0.9088	0.9179	0.9500	0.9738	0.9831	0.9573	15.3167	5.7414
0.9371	0.9641	0.9606	0.9846	0.9916	0.9763	15.6208	5.8578
0.9588	0.9995	0.9660	0.9902	0.9952	0.9854	15.7670	5.9126
1.0017	1.0696	0.9719	0.9962	0.9984	0.9946	15.9137	5.9676
1.1228	1.2673	0.9754	0.9998	0.9999	0.9997	15.9956	5.9984

CENTRE LINE VELOCITIES

TABLE (3.5)

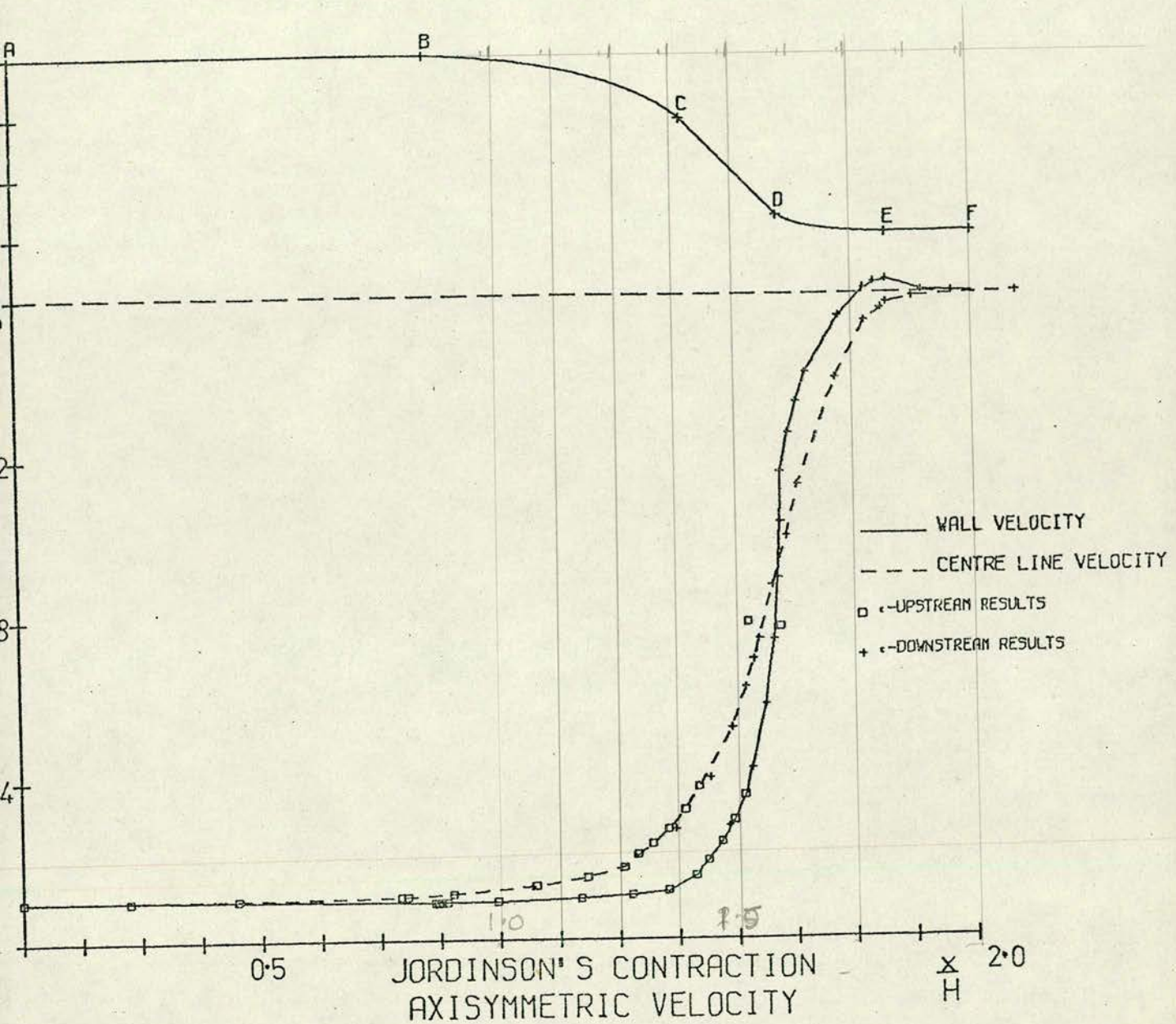
A
B
C
D
E
F
WALL VELOCITY
CENTRE LINE VELOCITY
□ ←UPSTREAM RESULTS
+ ←DOWNSTREAM RESULTS
0·5
1·0
1·5
2·0
X/H
JORDINSON'S CONTRACTION
AXISYMMETRIC VELOCITY

FIGURE (3·2)

Tables (3.2) and (3.3) show the two-dimensional centre line and wall velocity distributions, the value of $f(\alpha)$ and the predicted axisymmetric velocity for the upstream part referred to the distance from the beginning of the contraction. Tables (3.4) and (3.5) show the non-dimensional velocity in the form $\frac{q}{U_1}\left(\frac{h}{H}\right)$, the value of $f(\alpha)$ in the form $f(\alpha)h/H$, the predicted axisymmetric velocity in the form $\frac{q}{U_1}\left(\frac{h}{H}\right)^2$ for the centre line and the wall at the downstream end. In particular, they also show the predicted axisymmetric wall and centre line velocities in the form q/U_1 for axisymmetric contraction ratios of 16:1 and 6:1 referred to distance from the beginning of the contraction. Tables (3.2), (3.3), (3.4) and (3.5) are for the case

$$n = 4 \; ; \quad e^{-\ell_1} = 0{\cdot}9 \; ; \quad e^{\ell_2} = 1{\cdot}025$$

Figure (3.2) show the predicted velocity distribution with respect to the contraction wall for the 16:1 case. A comparison is made in the next chapter between these results and those determined experimentally.

It is interesting to note that when the flow becomes uniform in the downstream end of the contraction in the two-dimensional case, the method predicts that the flow in the corresponding axisymmetric contraction will also be uniform across the same cross section. This follows because the axisymmetric velocity along an α = constant line is obtained by multiplying the two-dimensional velocity at every point of this line by the same constant.

This suggests that a wall shape successfully designed for two-dimensional flow will also be successful as an axisymmetric design /

design because, not only are the adverse pressure gradients decreased and favourable pressure gradients increased, but uniform flow will be obtained in the axisymmetric contraction as quickly as in the two-dimensional contraction.

NOTE

The calculations in this chapter involving Jordinson's approximation have all been applied to the upstream part. The equivalent calculations for the downstream part are almost identical and were performed in the same way.

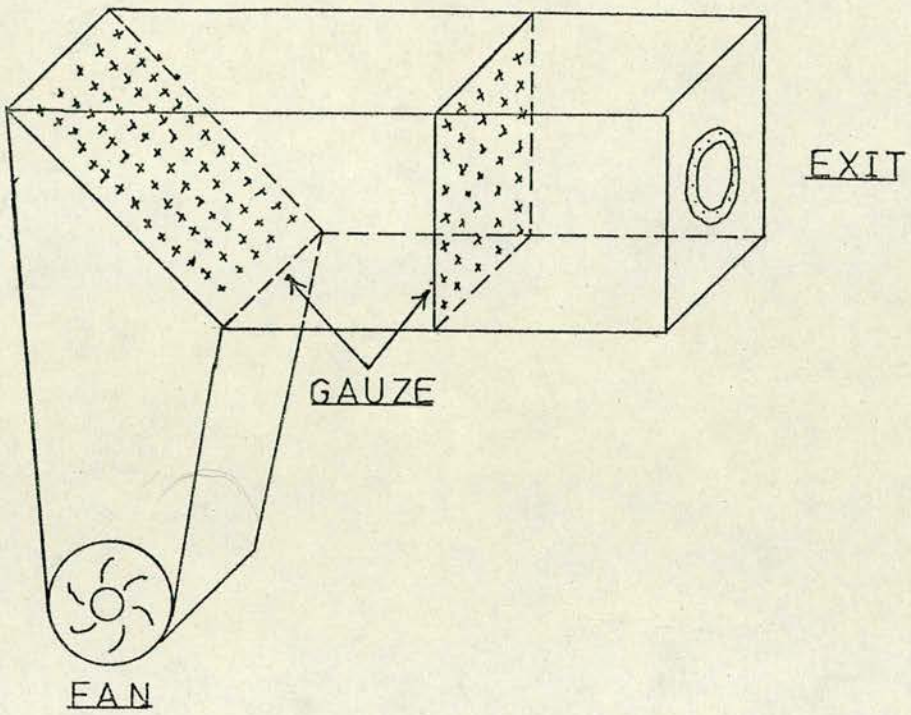

FIGURE (4,1)

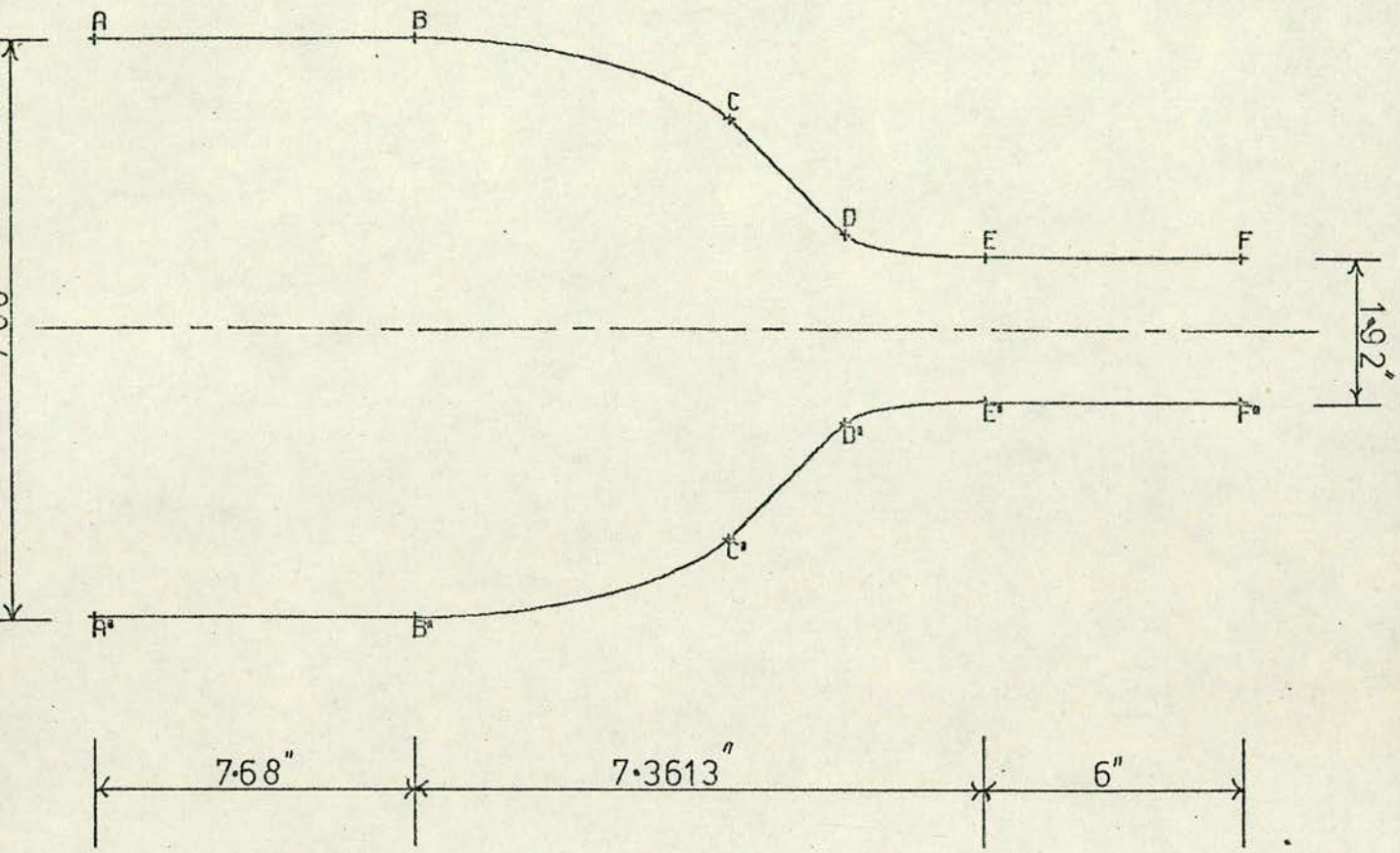

FIGURE (4.2)

CHAPTER 4

EXPERIMENTAL MEASUREMENTS

4.1 INTRODUCTION

An axisymmetric contraction was built according to Jordinson's design for an area contraction ratio of 16:1 and the pressure distribution along the wall was determined. The experimentally determined results are compared with those obtained by applying the method of W.W.W. to Jordinson's approximate solution.

4.2 Description of Model

The model was built of fibreglass in the following way. A solid piece of wood was first turned on a lathe to give the required shape as shown in figure (4.2). This wooden shape was then used as a mould for the fibreglass and the model completed. During this second stage, pressure tappings were inserted at approximately half inch intervals along the length of the model. The work was done and the experiments conducted in the Department of Engineering at the University of Edinburgh where use was made of an existing supply of uniformly moving air. This 'blower' took the form of a centrifugal fan fitted to a diffuser and settling chamber. The settling chamber was rectangular in cross section with a circular exit (figure 4.1). The velocity of the air supplied by the fan could be varied by means of a throttle. The model, whose dimensions are shown in figure (4.2), was built to suit this settling chamber and was attached directly to the chamber exit.

Initially the parallel section downstream of the contraction was 1/4 of the upstream diameter. After a few initial runs it was found /

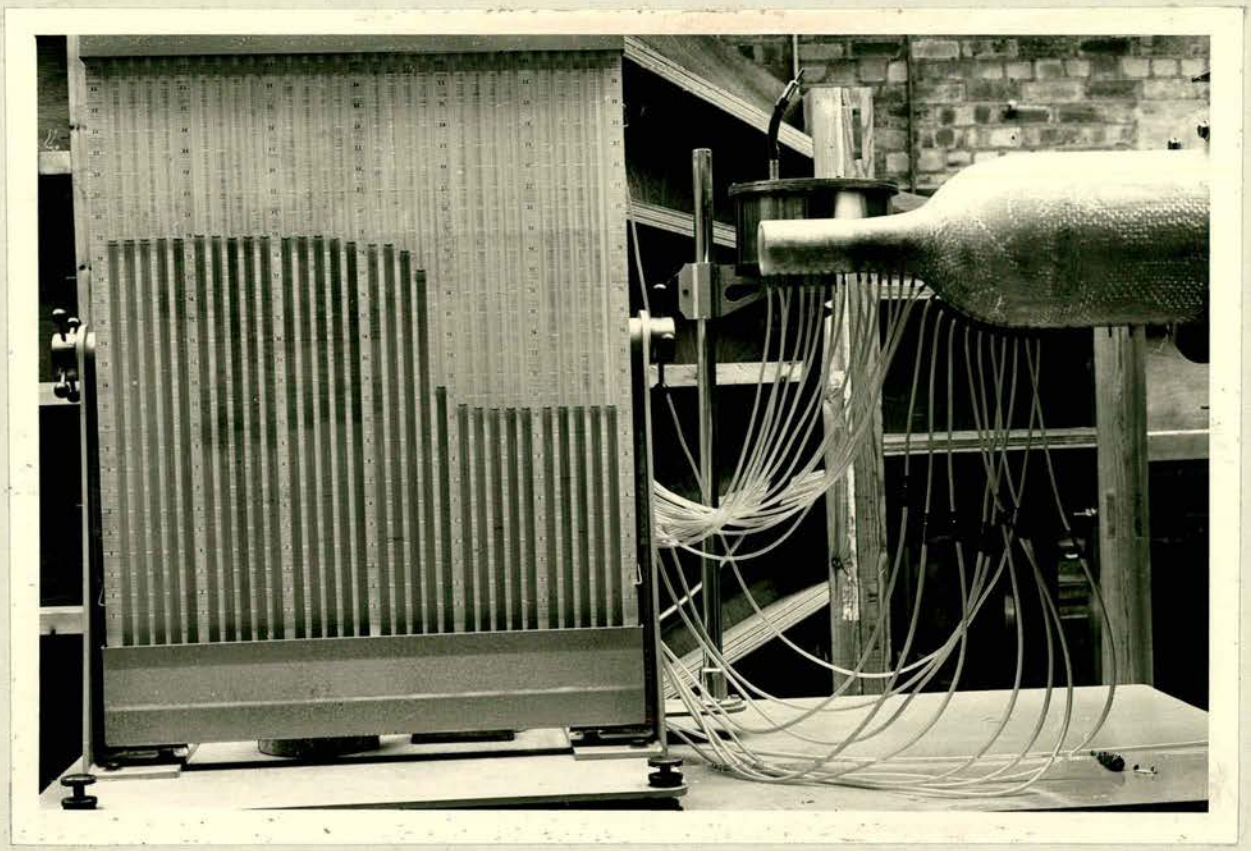

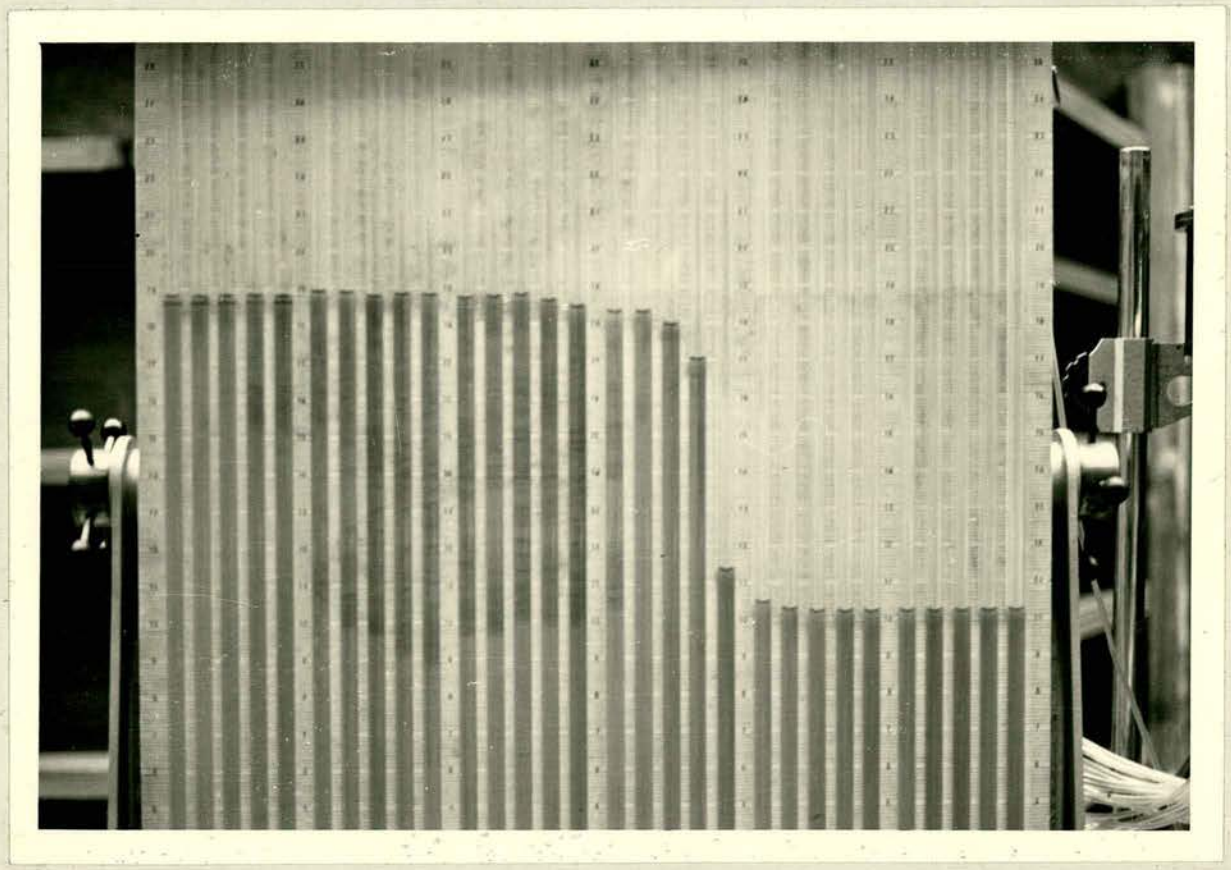

PLATE 1

x/H	C_p 123FT/SEC	C_p 167FT/SEC	C_p 212FT/SEC	C_p MEAN
-0.781	0.0000	0.0000	0.0000	0.0000
0.266	0.0000	0.0000	0.0000	0.0000
0.332	0.0000	0.0006	0.0000	0.0002
0.398	0.0000	0.0016	0.0004	0.0007
0.465	0.0000	0.0016	0.0016	0.0011
0.531	0.0012	0.0026	0.0020	0.0019
0.594	0.0107	0.0103	0.0104	0.0105
0.657	0.0333	0.0322	0.0320	0.0325
0.720	0.1310	0.1374	0.1332	0.1339
0.797	0.7714	0.7806	0.7800	0.7773
0.883	0.8810	0.8839	0.8800	0.8816
0.959	0.9167	0.9354	0.9040	0.9187
1.042	0.9524	0.9484	0.9360	0.9456
1.125	0.9524	0.9484	0.9200	0.9403
1.209	0.9524	0.9677	0.9600	0.9600
1.310	0.9762	0.9871	0.9800	0.9811
1.370	0.9762	0.9806	0.9800	0.9816
1.440	0.9881	0.9741	0.9800	0.9807
1.500	0.9881	0.9871	0.9880	0.9877
1.570	0.9881	0.9871	0.9880	0.9877
1.630	1.0000	0.9871	0.9880	0.9917
1.700	1.0000	0.9871	1.0000	0.9957
1.760	1.0000	1.0000	1.0000	1.0000

TABLE (4.1)

found that the pressure readings at the downstream end varied slightly from those expected for uniform flow. It was assumed that this variation was caused by the moving air exhausting into the atmosphere. To try and reduce the effect this might have on the flow inside the contraction, the length of the downstream parallel section was increased to 0.8H (approximately 6 inches). This modification did improve the flow at the downstream end.

4.3 Description of Experiment and Apparatus

Pressure readings at each tapping point were taken for several different air velocities - from 123 feet/second to 212 feet/second at the exit. Initially the pressure readings were taken on a bank of water manometers as shown in plate 1. However, these were found to be too inaccurate. An electric micromanometer was finally used to measure the pressure difference between the pressure at the beginning of the upstream parallel section and the pressure at all other points. A pitot tube was used to measure the pressure across the exit.

4.4 Results

The results shown in table (4.1) are presented in terms of a pressure coefficient obtained by dividing the pressure drop at each tapping point by the total pressure drop along the length of the model for different wind velocities. The mean pressure coefficient is also shown. The origin for the x-coordinate in the table is taken at the beginning of the contraction.

In /

x/H	q/U_1	C_p
-0.6395	0.9995	0.0000
-0.0015	0.9287	-0.0005
0.0059	0.9199	-0.0006
0.0117	0.9204	-0.0006
0.0234	0.9228	-0.0005
0.1300	0.9442	-0.0004
0.3034	1.0157	0.0001
0.4106	1.0956	0.0007
0.4864	1.1840	0.0016
0.5448	1.5520	0.0055
0.5719	1.9303	0.0107
0.6008	2.3900	0.0185
0.6275	2.9314	0.0298
0.6510	3.5503	0.0455

TABLE (4.2)

UPSTREAM RESULTS

x/H	q/U_1	C_p
0.6965	5.8048	0.1282
0.6660	4.2176	0.0658
0.7148	7.4112	0.2115
0.7250	8.9392	0.3094
0.7298	10.3296	0.4145
0.7311	11.5664	0.5207
0.7481	12.5216	0.6109
0.7658	13.3008	0.6898
0.7866	14.0400	0.7691
0.8576	15.4448	0.9315
0.9115	16.1232	1.0155
0.9336	16.2618	1.0331
0.9573	16.3211	1.0406
1.0316	16.0460	1.0058
1.0947	16.0050	1.0006

TABLE (4.3)

DOWNSTREAM RESULTS

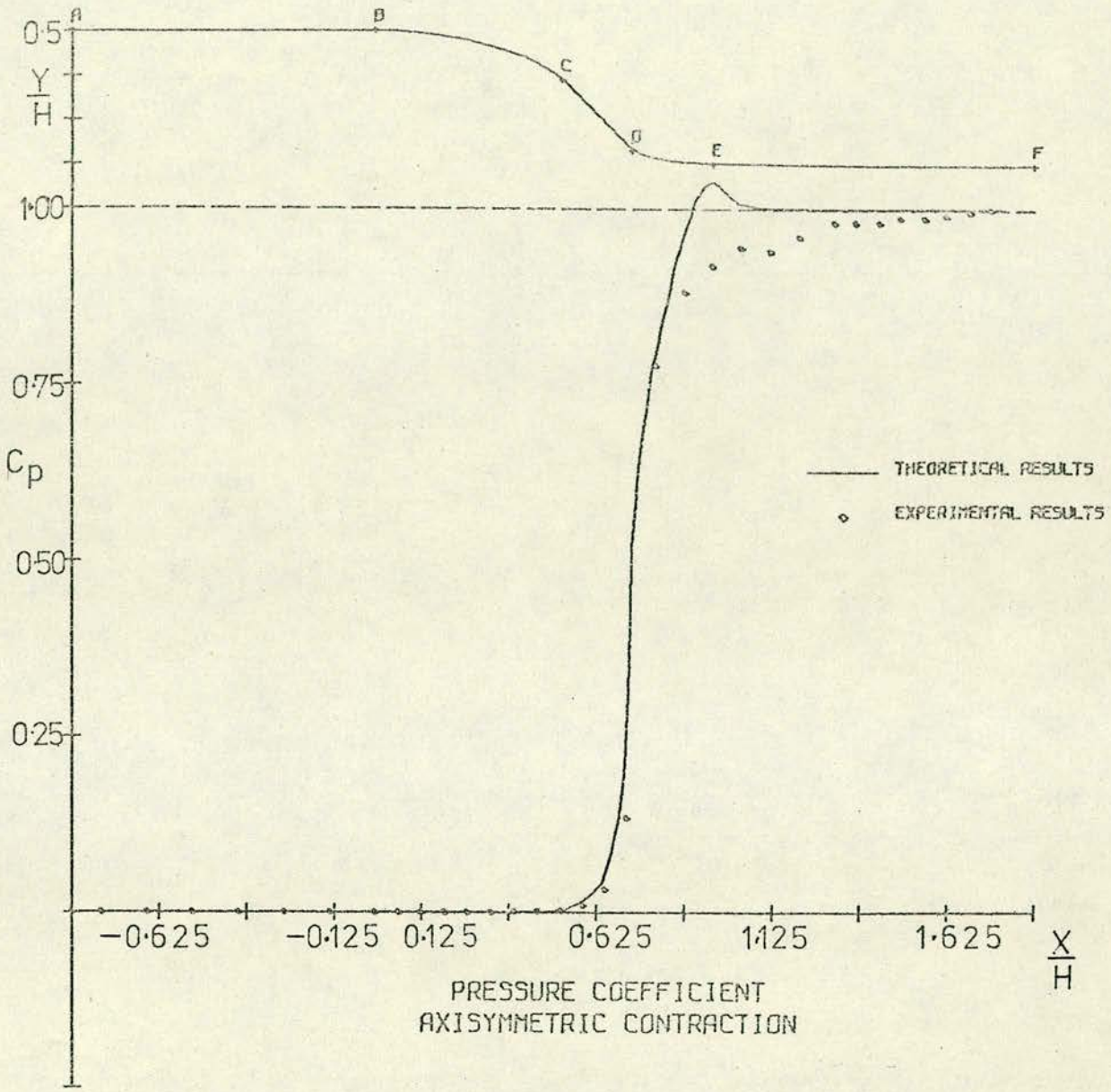
A
B
C
D
E
F
0·5
Y/H
1·00
0·75
Cp
0·50
0·25
−0·625
−0·125
0·125
0·625
1·125
1·625
X/H
THEORETICAL RESULTS
EXPERIMENTAL RESULTS
PRESSURE COEFFICIENT
AXISYMMETRIC CONTRACTION

FIGURE (4·3)

In order to compare the experimental pressure distributions with the theoretical ones of the previous chapter, a pressure coefficient was obtained from the velocities tabulated in tables (3.2) and (3.4). This theoretical pressure coefficient was calculated for each point on the wall using the formula

$$C_p = \frac{U_1^2 - U_p^2}{U_1^2 - U_2^2}$$

where U_p is the velocity at a point on the wall. Tables (4.2) and (4.3) show this theoretical pressure coefficient for the upstream and downstream part. Figure (4.3) shows the mean experimental pressure coefficient and the theoretical pressure coefficient plotted against distance along the contraction.

As can be seen from this graph, agreement between the experimental results and those of theory is, for the most part satisfactory. No adverse pressure gradient was observed at the upstream end and that predicted by W.W.W. method was too small to be observed within the accuracy of the experiment. It is of interest to note that the adverse pressure gradient predicted by W.W.W. method for the axisymmetric case is much less than the original pressure gradient in the two-dimensional case. Similarly, although a measurable adverse pressure gradient is predicted by W.W.W., no adverse pressure gradient was observed at the downstream end. Figure (4.3) indicates how the experimentally observed velocity rises monotonically to the final uniform value. It is stated in W.W.W. and shown in Chapter 3 that the adverse pressure gradients in the axisymmetric case should be less than those in the two-dimensional case. This is confirmed both by experiment and calculation /

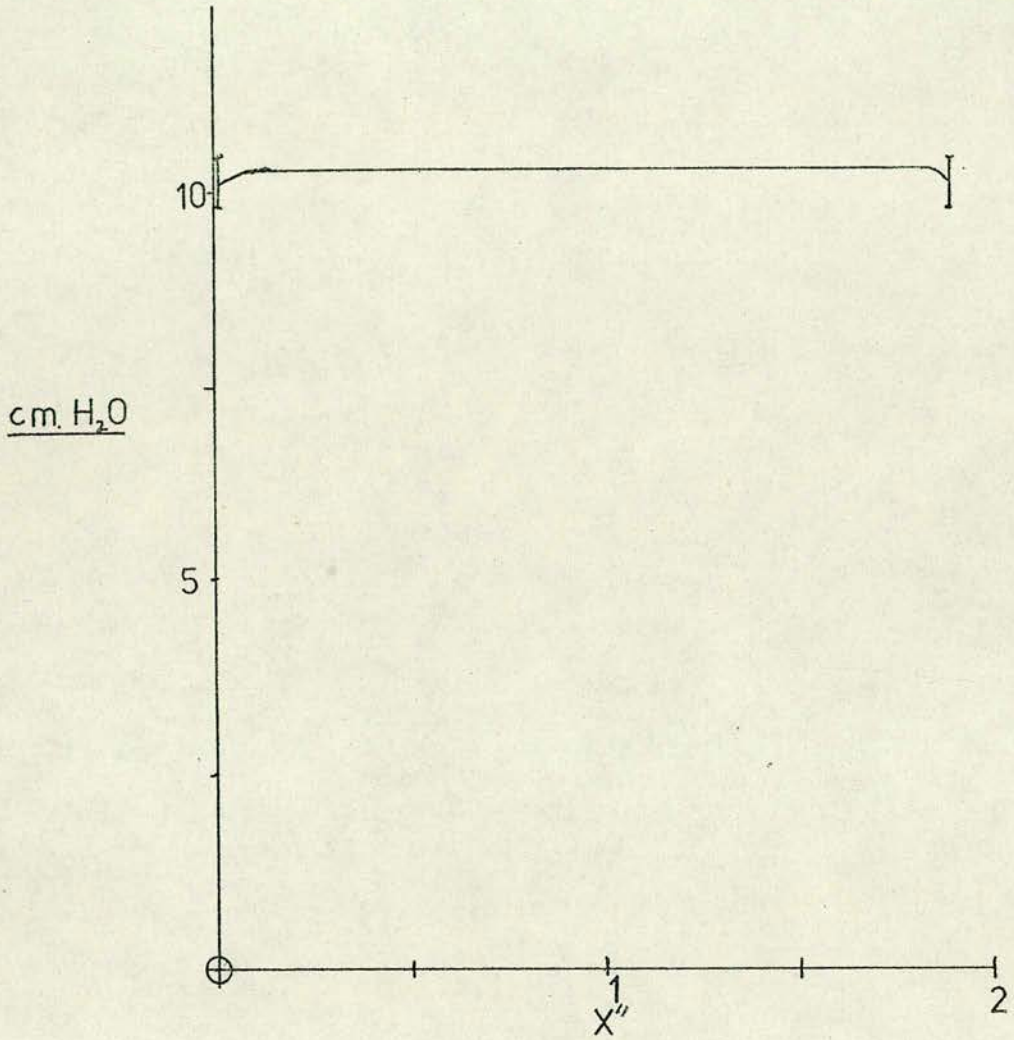

FIGURE (4.4)

calculation for the upstream part of the contraction. However, the departure of the experimental results from the calculated results at the downstream end where an adverse pressure gradient is expected, is probably attributable to the boundary layer which has not been considered in the theory.

The velocity profile at the downstream end was found by measuring the pressure distribution across the end using a pitot tube. The velocity profile was found to be flat and steady except when the pitot tube was very close to the wall (less than 0.1 inches from the wall). In this case the pressure was slightly lower than at other points on the profile and oscillated slightly. The oscillations were fairly slow and of small amplitude and would have been caused by the pitot tube disturbing the boundary layer. A typical velocity profile is shown in figure (4.4).

4.5 Conclusions

The axisymmetric contraction using a wall profile based on a design for a two-dimensional contraction has given very satisfactory results in practice. In addition, in the light of W.W.W.'s results, it seems reasonable to conclude that any axisymmetric contraction built to a satisfactory two-dimensional design will prove successful.

CHAPTER 5

THE SURFACE SINGULARITY METHOD

5.1 INTRODUCTION

In this chapter the method of Smith and Pierce (1958) is described for the calculation of incompressible potential flows. The method is based on the use of a singularity distribution along the surface of a body where this distribution is found numerically as the solution to an integral equation. Hess (1971) states, when discussing incompressible potential flows about two and three-dimensional bodies, that formulation of the problem in this way is an especially efficient procedure. This is because the problem can be solved on the body surface without considering the remainder of the flow field.

In Chapter 6, this method is applied to flows through various two-dimensional and axisymmetric wind tunnel contractions. Before explaining the method however, it is essential to prove that it is soundly based on theory.

5.2 Theoretical Justification

Let ϕ and ϕ' be any two continuously differentiable functions in some closed region R bounded by a surface S and let ϕ and ϕ' have continuous second order derivatives in R, then the result below - sometimes known as Green's Second Identity - can be obtained from Green's theorem.

$$\iiint_R (\phi\nabla^2\phi' - \phi'\nabla^2\phi)\,dV = \iint_S (\phi\nabla\phi' - \phi'\nabla\phi).\underline{n}\,dS \qquad (5.1)$$

If ϕ and ϕ' are harmonic, then the left hand side of (5.1) vanishes /

vanishes giving

$$\iint (\phi \nabla\phi' - \phi' \nabla\phi).\underline{n}\, dS = 0 \qquad (5.2)$$

Writing $\frac{\partial}{\partial n}$ for the derivatives in the direction of the unit normal to the surface gives from (5.2)

$$\iint_S \left(\phi \frac{\partial \phi'}{\partial n} - \phi' \frac{\partial \phi}{\partial n} \right) dS = 0 \qquad (5.3)$$

(Kellog Ch. 8 Theorem VI)

Now, following the analysis given in Lamb, let ϕ be the velocity potential of some fluid motion and let $\phi' = 1/r$ where r is the distance of any point of the fluid from some fixed point P in the fluid. ϕ' will now become infinite at P and so it is necessary to exclude this point from the region R to which the previous equations applied. This can be done by constructing a small spherical surface (S') about the point P as centre and excluding the interior of the sphere from the region of integration. Then, since

$$\nabla^2 \left(\frac{1}{r} \right) = 0$$

equation (5.3) gives

$$\iint_{S'} \phi \frac{\partial}{\partial n}\left(\frac{1}{r}\right) dS' + \iint_S \phi \frac{\partial}{\partial n}\left(\frac{1}{r}\right) dS - \iint_{S'} \frac{1}{r} \frac{\partial \phi}{\partial n}\, dS' - \iint_S \frac{1}{r} \frac{\partial \phi}{\partial n}\, dS = 0 \qquad (5.4)$$

At the surface S', $\frac{\partial}{\partial n}\left(\frac{1}{r}\right) = -1/r^2$ and let $dS' = r^2 d\theta$. Then if r is allowed to decrease to zero, the first integral with respect to S' in (5.4) becomes $-4\pi\phi(p)$ and the second integral with respect to S' vanishes. Hence, from (5.4) a relationship between the /

the velocity potential at the fixed point P in the fluid is obtained in terms of the values of ϕ and $\frac{\partial \phi}{\partial n}$ on the boundaries:

$$\phi(P) = \frac{1}{4\pi} \iint_S \phi \frac{\partial}{\partial n}\left(\frac{1}{r}\right) dS - \frac{1}{4\pi} \iint_S \frac{1}{r} \frac{\partial \phi}{\partial n} dS \qquad (5.5)$$

By a similar argument, if P lies on the surface it can be shown that

$$\phi(P) = \frac{1}{2\pi} \iint_S \phi \frac{\partial}{\partial n}\left(\frac{1}{r}\right) dS - \frac{1}{2\pi} \iint_S \frac{1}{r} \frac{\partial \phi}{\partial n} dS$$

It can be seen from (5.5) that the velocity potential at P is made up of two parts:

(i) The first integral in (5.5) is the velocity potential due to a surface distribution of dipoles of density $\phi/4\pi$ with an axis normal to the surface.

(ii) The second integral in (5.5) is the velocity potential due to a surface distribution of simple sources of density $\frac{1}{4\pi} \frac{\partial \phi}{\partial n}$ per unit area.

As stated in Kellog, a harmonic function continuously differentiable in a closed region (R) may be represented as the sum of the potentials of a simple and a double distribution on the boundary of R. In fact, the velocity potential at any point in a closed region can be expressed in terms of a surface distribution of simple sources or dipoles alone.

Referring to equation (5.3), if P is external to the region R, then $1/r$ is finite throughout the region of integration. So letting $\phi' = 1/r$ in (5.3) gives

$$\iint_S \phi \frac{\partial}{\partial n}\left(\frac{1}{r}\right) dS - \iint_S \frac{1}{r} \frac{\partial \phi}{\partial n} dS = 0 \qquad (5.6)$$

Now if ϕ is the velocity potential in a closed region R with bounding /

bounding surface S, and ϕ'' is the velocity potential for any irrotational fluid motion external to R with the proviso that $\phi'' \to 0$ at infinity, then (5.5) and (5.6) give for some point P contained in R

$$\phi(P) = \frac{1}{4\pi}\iint_S \phi \frac{\partial}{\partial n}\left(\frac{1}{r}\right) dS - \frac{1}{4\pi}\iint_S \frac{1}{r}\frac{\partial \phi}{\partial n}\, dS \tag{5.7}$$

$$0 = \frac{1}{4\pi}\iint_S \phi'' \frac{\partial}{\partial n''}\left(\frac{1}{r}\right) dS - \frac{1}{4\pi}\iint_S \frac{1}{r}\frac{\partial \phi''}{\partial n''}\, dS \tag{5.8}$$

where ∂n and $\partial n''$ are elements of the unit normal drawn inwards for each region of integration so that

$$\frac{\partial}{\partial n} = -\frac{\partial}{\partial n''}$$

Adding (5.7) and (5.8) gives

$$\phi(P) = \frac{1}{4\pi}\iint_S (\phi - \phi'')\frac{\partial}{\partial n}\left(\frac{1}{r}\right) dS - \frac{1}{4\pi}\iint_S \frac{1}{r}\left(\frac{\partial \phi}{\partial n} + \frac{\partial \phi''}{\partial n''}\right) dS \tag{5.9}$$

The value of ϕ'' and its derivatives on the surface have yet to be defined. Therefore, letting $\phi = \phi''$ on the surface eliminates the first integral in (5.9) giving

$$\phi(P) = -\frac{1}{4\pi}\iint_S \frac{1}{r}\left(\frac{\partial \phi}{\partial n} + \frac{\partial \phi''}{\partial n''}\right) dS \tag{5.10}$$

Thus, the velocity potential at any point P is expressed in terms of a surface distribution of simple sources alone of strength $\left(\frac{\partial \phi}{\partial n} + \frac{\partial \phi''}{\partial n''}\right)$. Similarly, if the normal component of velocity is made continuous at the surface so that $\left(\frac{\partial \phi}{\partial n} + \frac{\partial \phi''}{\partial n''}\right)$ vanishes, the velocity potential at P is expressed in terms of a surface distribution of dipoles.

It /

It can be shown that each of these distributions is unique. Kellog states that "no potential due to distributions in regular regions and on regular surfaces finite in number, with continuous densities and moments, can be due to any other distribution of the same character."

5.3 The Method of Smith and Pierce

As previously stated, the potential flow about or within a body is to be calculated by treating the surface of the body as a thin shell over which there is a singularity distribution. A given axisymmetric or two-dimensional body is described by a meridian curve. The coordinate system used in defining this curve is not that of the usual cartesian coordinates because difficulty could be encountered with some multiple valued curves. The surface distance s is therefore used as the fundamental measure of length and no difficulty is encountered when the curve is specified in this (s,y) coordinate system.

The potential at a point P in a region R due to a surface source distribution σ is given by

$$\phi(P) = \iint_S \frac{\sigma(p)}{r}\, dS \qquad (5.11)$$

where as before, r is the distance from the fixed point P to the variable point of integration p on the body surface. In this case P could be either interior or exterior to the surface S and $\sigma(p)$ is the local value of the source strength and is a function of position p on the body surface. In this work, σ is considered constant /

constant on line elements in the two-dimensional case and constant on ring elements round the body in the axisymmetric case.

Differentiation with respect to the coordinates of P is permissable in (5.11) giving

$$\nabla\phi(P) = \iint_S \sigma(p)\nabla\left(\frac{1}{r}\right)dS$$

It can be shown that if '-' refers to an interior region and '+' to an exterior region then the normal velocity at the surface - which is the derivative of the velocity potential in the direction of the normal - due to the singularity distribution is given by the following expressions as stated in Kellog: "If the density σ of the distribution on S is continuous at p, the normal derivative of the potential ϕ approaches limits as P approaches p along the normal to S at p from either side. These limits are

$$\frac{\partial\phi}{\partial n_+} = -2\pi\sigma(p) + \iint_S \sigma(p)\,\frac{\partial}{\partial n}\left(\frac{1}{r}\right)dS \qquad (5.12a)$$

$$\frac{\partial\phi}{\partial n_-} = 2\pi\sigma(p) + \iint_S \sigma(p)\,\frac{\partial}{\partial n}\left(\frac{1}{r}\right)dS \qquad (5.12b)$$

These limits are approached uniformly as to p on any closed portion of S, containing no boundary points of S, on which the density is continuous."

Since the normal velocity and $\frac{\partial}{\partial n}\left(\frac{1}{r}\right)$ are determined by the boundary conditions and the geometry of the body, the singularity distribution $\sigma(p)$ can be found from equations (5.12). Once $\sigma(p)$ is known as a function of the body surface, the velocity potential and its derivatives at any other point in the flow field can be found.

Equations /

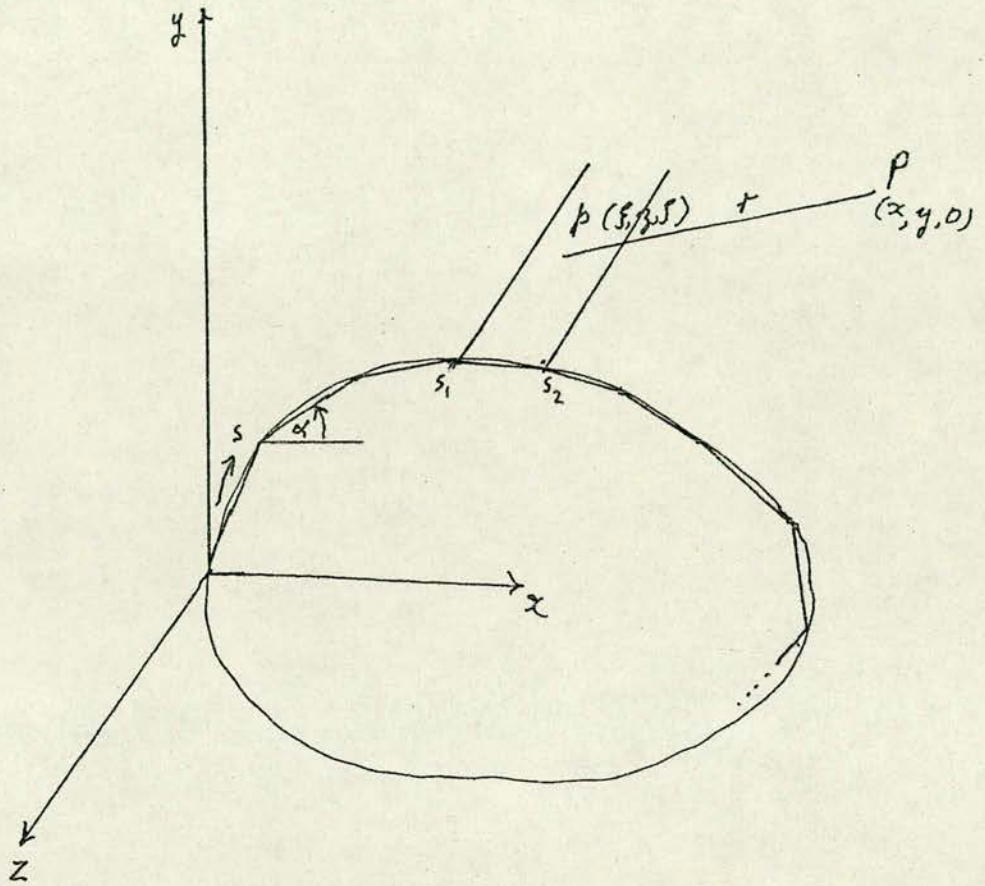

FIGURE (5.1)

Equations (5.12) are Fredholm integral equations of the second kind. The method of solution is to reduce equations (5.12) to a set of linear algebraic equations by dividing the body into n intervals - not necessarily of the same length. The source strength is assumed to be constant on each interval but to vary from interval to interval. That is, the meridian curve is divided into n intervals and approximated by n straight line segments; the body is considered to be constructed of wedges in the two-dimensional case and frusta of cones in the axisymmetric case. The n integrals over each interval in (5.12) can now be evaluated because, if σ is constant on each interval, the integral over the surface reduces to

$$\frac{\partial \phi(P)}{\partial n} = \sum_{i=1}^{n} \sigma_i \iint_{S_i} \frac{\partial}{\partial n_i}\left(\frac{1}{r}\right) dS_i$$

and the value of the integral depends solely on the goemetry of the body. If P is successively taken to be at the centre of each interval, n linear equations in the n values of σ_i are obtained. For a solid body, the induced normal velocity at the surface due to the distribution must be such as to prevent any net flow through the surface and so is known. The problem can now be solved.

The method is essentially the same for two-dimensional and axisymmetric bodies but there are major differences in the analysis. These two cases will therefore be considered separately.

5.4 The Two-dimensional Case

Figure (5.1) illustrates the approximate meridian curve and one of the intervals on a two-dimensional body. The potential at any /

any point P due to the surface source distribution on the strip element bounded by

$$z = -\infty \; ; \quad z = \infty \text{ and } \quad s = s_1 \; ; \quad s = s_2$$

is given by

$$\phi(P) = \iint_S \frac{\sigma}{r} \, dS$$

If P is taken in the plane $z = 0$ the following expression is obtained for r:

$$r = \left[(x-\xi)^2 + (y-\eta)^2 + \zeta^2\right]^{\frac{1}{2}}$$

where (ξ,η,ζ) refers to the variable point of integration. Therefore

$$\phi(P) = \int_{s_1}^{s_2} \int_{-\infty}^{\infty} \frac{\sigma \, d\zeta . ds}{\left[(x-\xi)^2+(y-\eta)^2+\zeta^2\right]^{\frac{1}{2}}}$$

$$= 2 \int_{s_1}^{s_2} \int_{0}^{\infty} \frac{\sigma \, d\zeta . ds}{\left[(x-\xi)^2+(y-\eta)^2+\zeta^2\right]^{\frac{1}{2}}} \qquad (5.13)$$

Equations (5.12) require an expression for the normal derivative of the velocity potential. In addition, once the source distribution has been found, the tangential surface velocity will be of interest. These two velocities - $\frac{\partial \phi}{\partial n}$ and $\frac{\partial \phi}{\partial s}$ - are most conveniently expressed in terms of the directional derivatives $\frac{\partial \phi}{\partial x}$ and $\frac{\partial \phi}{\partial y}$. Therefore, differentiating (5.13) with respect to x and y gives

$$\frac{\partial \phi(P)}{\partial x} = -2 \int_{s_1}^{s_2} \int_{0}^{\infty} \frac{(x-\xi)\sigma d\zeta ds}{\left[(x-\xi)^2+(y-\eta)^2+\zeta^2\right]^{3/2}} \qquad (5.14)$$

$$\frac{\partial \phi(P)}{\partial y} = -2 \int_{s_1}^{s_2} \int_{0}^{\infty} \frac{(y-\eta)\sigma d\zeta ds}{\left[(x-\xi)^2+(y-\eta)^2+\zeta^2\right]^{3/2}} \qquad (5.15)$$

Since σ is constant, the integrals with respect to ζ in (5.14) and /

and (5.15) can be evaluated directly giving

$$\frac{\partial\phi(P)}{\partial x} = -2\int_{s_1}^{s_2} \frac{\sigma(x-\xi)ds}{[(x-\xi)^2+(y-\eta)^2]} \qquad (5.16)$$

$$\frac{\partial\phi(P)}{\partial y} = -2\int_{s_1}^{s_2} \frac{\sigma(y-\eta)ds}{[(x-\xi)^2+(y-\eta)^2]} \qquad (5.17)$$

The denominator in (5.16) and (5.17) is the square of the projection of the distance r onto the plane $z = 0$. If the integrals in (5.16) and (5.17) are to be evaluated exactly, it would be necessary to express this projected distance in terms of s. When P lies at the centre of one of the strips this can be done after making some geometrical constructions and in Smith and Pierce these integrals are evaluated analytically. However, reducing equations (5.16) and (5.17) to an integrable form, integrating them and then evaluating the result requires a more complex computer programme. After some initial tests, it was found that evaluating (5.16) and (5.17) numerically simplified the programming considerably without any significant loss of accuracy or increase in running time. The expressions for the derivatives of ϕ will therefore be left as in (5.16) and (5.17).

If now a complete body is considered to be constructed of n of these strips, the potential and its derivatives at any point will be the sum of the contributions from each strip. Following the notation of Smith and Pierce, the j^{th} interval will be bounded by s_{2j-2} and s_{2j} and its mid-point will be s_{2j-1}. The subscript j will be used in conjunction with ξ and η when referring to the variable of integration and i, x and y will refer to the fixed point of interest. /

interest. Thus the derivatives of the potential at a point $P(x,y)$ due to a body constructed of n intervals will be

$$\frac{\partial\phi(P)}{\partial x} = -2\sum_{j=1}^{n}\sigma_j\int_{s_{2j-2}}^{s_{2j}}\frac{(x-\xi)ds}{[(x-\xi)^2+(y-\eta)^2]} \tag{5.18}$$

$$\frac{\partial\phi(P)}{\partial y} = -2\sum_{j=1}^{n}\sigma_j\int_{s_{2j-2}}^{s_{2j}}\frac{(y-\eta)ds}{[(x-\xi)^2+(y-\eta)^2]} \tag{5.19}$$

If P is taken to be at the mid-point of the i^{th} interval then the above two equations become

$$\frac{\partial\phi(P_{2i-1})}{\partial x} = -2\sum_{j=1}^{n}\int_{s_{2j-2}}^{s_{2j}}\frac{\sigma_j(x_i-\xi)ds}{[(x_i-\xi)^2+(y_i-\eta)^2]} \tag{5.20}$$

$$\frac{\partial\phi(P_{2i-1})}{\partial y} = -2\sum_{j=1}^{n}\int_{s_{2j-2}}^{s_{2j}}\frac{\sigma_j(y_i-\eta)ds}{[(x_i-\xi)^2+(y_i-\eta)^2]} \tag{5.21}$$

The integrals in (5.20) and (5.21) are dependent solely on the geometry of the body and can be written in vector notation as

$$\frac{\partial\phi(P_{2i-1})}{\partial x} = \sum_{j=1}^{n}\sigma_j X_{ij} \tag{5.22}$$

$$\frac{\partial\phi(P_{2i-1})}{\partial y} = \sum_{j=1}^{n}\sigma_j Y_{ij} \tag{5.23}$$

X_{ij} and Y_{ij} will be known as the influence matrices. The normal and tangential derivatives on the surface can now be obtained from (5.22) and (5.23) and are

$$\frac{\partial\phi(P_{2i-1})}{\partial n} \quad /$$

$$\frac{\partial\phi(P_{2i-1})}{\partial n} = \sum_{j=1}^{n} \sigma_j \left(-X_{ij}\sin(\alpha_i) + Y_{ij}\cos(\alpha_i)\right) \qquad (5.24)$$

$$\frac{\partial\phi(P_{2i-1})}{\partial s} = \sum_{j=1}^{n} \sigma_j \left(X_{ij}\cos(\alpha_i) + Y_{ij}\sin(\alpha_i)\right) \qquad (5.25)$$

where α_i is the angle the i^{th} interval makes with the x-axis.

The expressions in (5.24) and (5.25) are not the total normal and tangential velocities. For the case of flow past a body, the contribution from the main stream must be added. Thus the entire normal and tangential velocities are given by

$$-V_\infty\sin(\alpha_i) + \frac{\partial\phi(P_{2i-1})}{\partial n} \qquad (5.26)$$

$$V_\infty\cos(\alpha_i) + \frac{\partial\phi(P_{2i-1})}{\partial s} \qquad (5.27)$$

respectively.

For a solid surface, the total normal velocity must be zero. Therefore using (5.24) and (5.26) gives the final equation to be solved for the source distribution:

$$V_\infty\sin(\alpha_i) = \sum_{j=1}^{n} \sigma_j \{-X_{ij}\sin(\alpha_i) + Y_{ij}\cos(\alpha_i)\} \qquad (5.28)$$

Having found all the σ_j, the tangential surface velocity can be found from (5.27) and the velocity at any point in the flow field from (5.18) and (5.19).

It should be noted that when the point P coincides with the point p, the integrals when $i = j$ in (5.16) and (5.17) have a singularity at one point in the range of integration. When the integrals in (5.16) and (5.17) are evaluated analytically, Smith and /

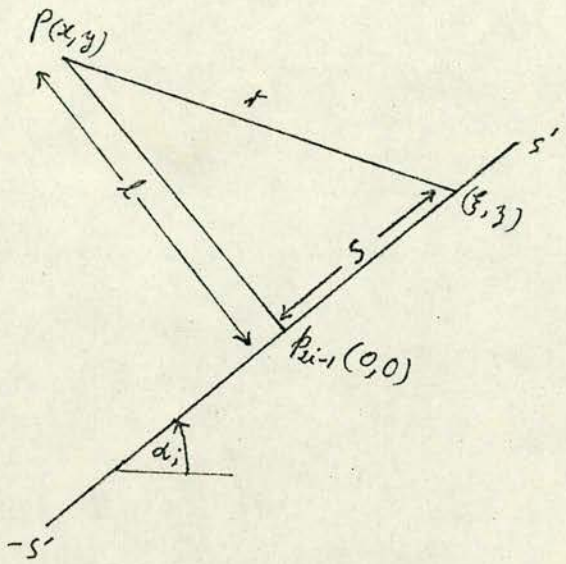

FIGURE (5.2)

and Pierce show that when P coincides with the mid-point of the interval of interest, the quantities X_{ij} and Y_{ij} have the following limiting values

$$X_{ii} \to 2\pi\sin(\alpha_i) \quad ; \quad Y_{ii} \to -2\pi\cos(\alpha_i)$$

Using (5.24), the normal derivative has the limit

$$\frac{\partial\phi(P_{2i-1})}{\partial n} = [-2\pi\sin^2(\alpha_i) - 2\pi\cos^2(\alpha_i)]\sigma_i = -2\pi\sigma_i$$

which is the result anticipated by theory. However, this result can also be easily demonstrated. Referring to figure (5.2) and considering the terms in equations (5.16) and (5.17) it can be seen that

$$(x-\xi) = -\left(\ell\sin(\alpha_i) + s\cos(\alpha_i)\right)$$

$$(y-\eta) = \left(\ell\cos(\alpha_i) - s\sin(\alpha_i)\right)$$

Therefore, from (5.16), taking origin at the mid-point of the interval

$$\frac{\partial\phi(P)}{\partial x} = 2\int_{-s'}^{s'} \frac{\sigma_i.\ell\sin(\alpha_i)+s\cos(\alpha_i)}{\ell^2 + s^2}\, ds$$

$$= [4\sin(\alpha_i)\tan^{-1}\left(\frac{s'}{\ell}\right) + \cos\alpha_i\ \ell og(1)]\sigma_i$$

$$\frac{\partial\phi(P)}{\partial y} = -2\int_{-s'}^{s'} \frac{\sigma_i.\ell\cos(\alpha_i)-s\sin(\alpha_i)}{\ell^2 + s^2}\, ds$$

$$= [-4\cos(\alpha_i)\tan^{-1}\left(\frac{s}{\ell}\right) + \sin(\alpha_i)\ \ell og(1)]\sigma_i$$

In /

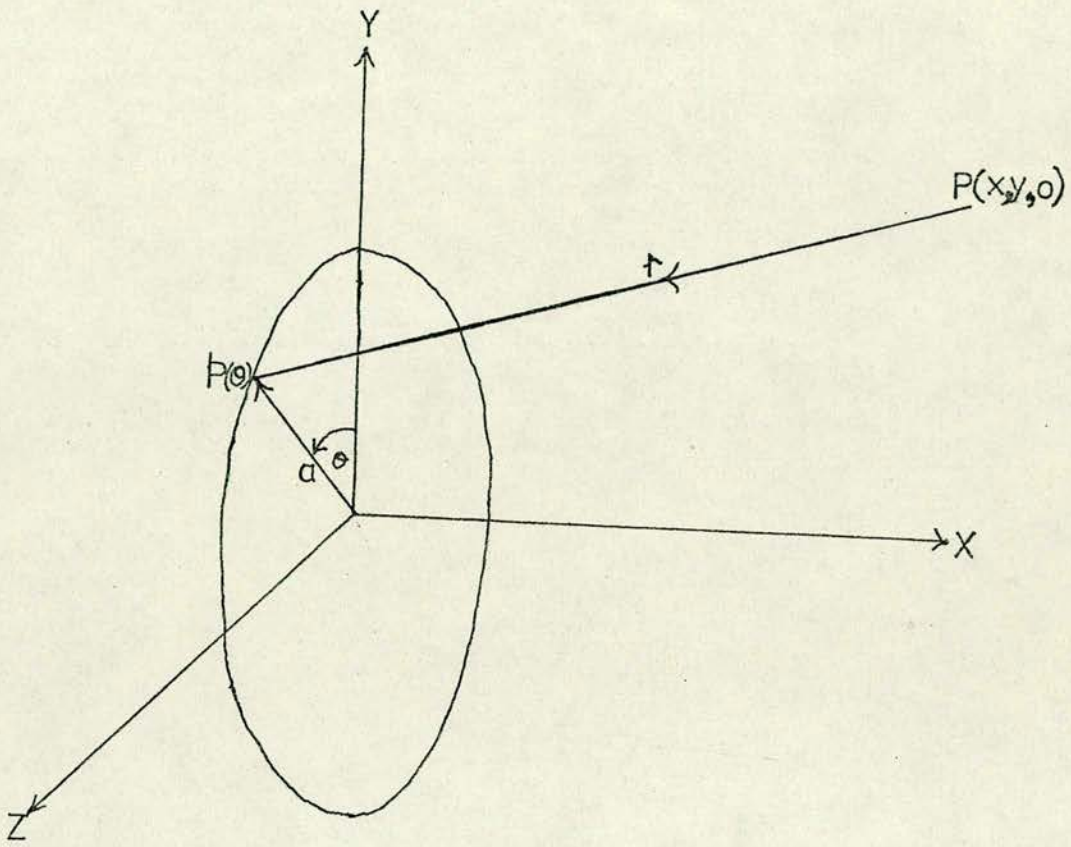

FIGURE (5.3)

In the limit as $l \to 0$, it can be seen that as $P \to p_{2i-1}$

$$\frac{\partial \phi(p_{2i-1})}{\partial x} \to 2\pi \sin(\alpha_i)\sigma_i \; ; \; \frac{\partial \phi(p_{2i-1})}{\partial y} \to -2\pi \cos(\alpha_i)\sigma_i \quad .$$

Knowing this result, the programming of the problem can be eased by simply assigning the values $2\pi\sin(\alpha_i)$ and $-2\pi\cos(\alpha_i)$ to the matrix elements X_{ii} and Y_{ii} respectively.

5.5 The Axisymmetric Case

As in the two-dimensional case, the meridian curve of the body is approximated by a number of straight lines. However, in this case the body is assumed to be constructed of frusta of cones on which the source strength is constant. The integrals involved can no longer be evaluated analytically and the treatment of the singular element - when P coincides with p - is more difficult and is given separate consideration.

The element of integration is an infinitely thin ring. The potential due to a uniform constant source distribution on a ring at a general point P will therefore be considered first. Following the analysis of Smith and Pierce, consider a ring of radius a lying in the zy plane, centred at the origin. A general point P is taken in the xy plane at a distance r from the variable point of integration $p(\theta)$ on the ring (figure 5.3). The distance r can be written as

$$r = \{x^2+(y-a\cos(\theta)^2 + a^2\sin^2(\theta)\}^{\frac{1}{2}}$$

$$= \{x^2+y^2+a^2-2ay\cos(\theta)\}^{\frac{1}{2}} \qquad (5.29)$$

If the constant source density on the ring has value σ, then the potential at P can be written down as

$$\phi(P) = /$$

$$\phi(P) = \int_0^{2\pi a} \frac{\sigma\, ds}{r} = 2a\sigma \int_0^{\pi} \frac{d\theta}{r}$$

Using (5.29) gives

$$\phi(P) = 2a\sigma \int_0^{\pi} \frac{d\theta}{\{x^2+y^2+a^2-2ay\cos\theta\}^{\frac{1}{2}}} \tag{5.30}$$

As before, differentiating through the integral with respect to the coordinates of P is permissable giving, from (5.30)

$$\frac{\partial\phi(P)}{\partial x} = -2\sigma a \int_0^{\pi} \frac{x\, d\theta}{\{x^2+y^2+a^2-2ay\cos\theta\}^{3/2}} \tag{5.31}$$

$$\frac{\partial\phi(P)}{\partial y} = -2\sigma a \int_0^{\pi} \frac{(y-a\cos\theta)\, d\theta}{\{x^2+y^2+a^2-2ay\cos\theta\}^{3/2}} \tag{5.32}$$

Equations (5.31) and (5.32) involve elliptic integrals and can be reduced to standard form by expressing the distance r in terms of its maximum value b and its minimum value c . That is

$$b^2 = x^2 + (y+a)^2$$

$$c^2 = x^2 + (y-a)^2 \quad .$$

r can now be written as

$$r^2 = \frac{b^2+c^2}{2} - \frac{b^2-c^2}{2}\cos(\theta) = b^2\sin^2\left(\frac{\theta}{2}\right) + c^2\cos^2\left(\frac{\theta}{2}\right)$$

So that (5.31) and (5.32) can now be written as

$$\frac{\partial\phi(P)}{\partial x} = -2\sigma a \int_0^{\pi} \frac{x\, d\theta}{\{b^2\sin^2\left(\frac{\theta}{2}\right) + c^2\cos^2\left(\frac{\theta}{2}\right)\}^{3/2}} = -\frac{2\sigma a}{b^3} \int_0^{\pi} \frac{x\, d\theta}{\{1-\frac{b^2-c^2}{b^2}\cos^2\left(\frac{\theta}{2}\right)\}^{3/2}}$$

$$\frac{\partial\phi(P)}{\partial y} = -2\sigma a \int_0^{\pi} \frac{(y-a\cos(\theta))\, d\theta}{\{b^2\sin^2\left(\frac{\theta}{2}\right) + c^2\cos^2\left(\frac{\theta}{2}\right)\}^{3/2}} = -\frac{2a\sigma}{b^3} \int_0^{\pi} \frac{(y-a\cos(\theta))\, d\theta}{\{1-\frac{b^2-c^2}{b^2}\cos^2\left(\frac{\theta}{2}\right)\}^{3/2}}$$

Introduce /

Introduce the constant k where

$$k^2 = \frac{b^2-c^2}{b^2} = \frac{4ay}{x^2+(y+a)^2}$$

After some manipulation the following two relations are obtained for the derivatives of the velocity potential when b and c are eliminated

$$\frac{\partial\phi(P)}{\partial x} = \frac{-4a\sigma x \; E(k)}{\sqrt{(y+a)^2+x^2}\;[(y-a)^2+x^2]} \tag{5.33}$$

$$\frac{\partial\phi(P)}{\partial y} = \frac{-2a\sigma}{y\sqrt{(y+a)^2+x^2}}\left[K(k) + \frac{y^2-a^2-x^2}{(y-a)^2+x^2}E(k)\right] \tag{5.34}$$

where $K(k)$ and $E(k)$ are the complete elliptic integrals of the first and second kind respectively.

Equations (5.33) and (5.34) give the directional derivatives of the velocity potential at the fixed point P due to a uniform source distribution on a ring of radius 'a' centred at the origin. The corresponding expressions for a constant source distribution on a frustum of a cone can be obtained by considering the frustum to be constructed of infinitely many rings and integrating over the frustum. As before, let (x,y,z) and P refer to the fixed point and (ξ,η,ζ) and p to the variable point of integration. Then noting that each infinitesimal ring is now centred at the point $(\xi,0,0)$ and of radius η, the results for a frustum of a cone are from (5.33) and (5.34)

$$\frac{\partial\phi(P)}{\partial x} = \int_{S_1}^{S_2} \frac{-4\eta(x-\xi)\sigma \; E(k)\; ds}{\sqrt{(y+\eta)^2+(x-\xi)^2}\;[(y-\eta)^2+(x-\xi)^2]} \tag{5.35}$$

$$\frac{\partial\phi(P)}{\partial y} = \int_{S_1}^{S_2} \frac{-2\eta\sigma}{y\sqrt{(y+\eta)^2+(x-\xi)^2}}\left[K(k) + \frac{y^2-\eta^2-(x-\xi)^2}{(y-\eta)^2+(x-\xi)^2}E(k)\right]ds \tag{5.36}$$

where /

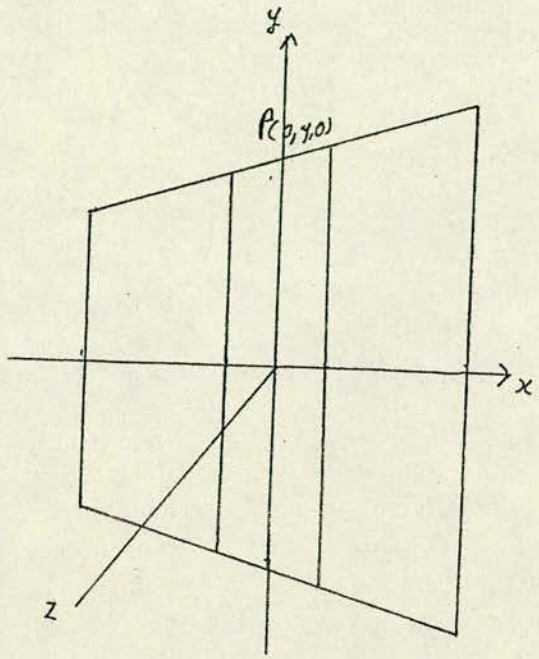

FIGURE (5.4)

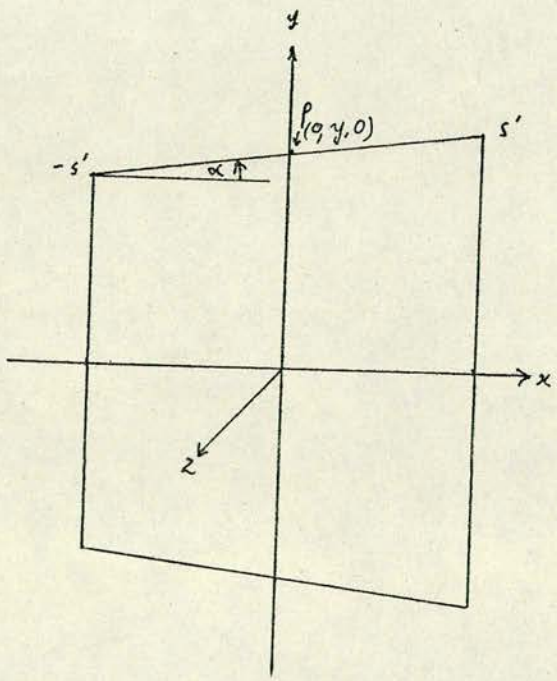

FIGURE (5.5)

where

$$k^2 = \frac{4\eta y}{(y+\eta)^2 + (x-\xi)^2}$$

Equations (5.35) and (5.36) are valid provided P does not lie on the surface of the frustum of the cone. In this case the integrals in (5.35) and (5.36) must be treated differently. Referring to figure (5.4), when P lies on the surface of a frustum, the frustum is divided into three subelements and the effect of a source distribution on this frustum is taken to be the sum of the effects of each subelement. The two ordinary subelements are treated in the ordinary way using equations (5.35) and (5.36). The singular subelement - that is, the one on which P lies - requires special treatment and attention is now given to this case.

An enlarged diagram of the singular subelement is shown in figure (5.5). Following the analysis of Smith and Pierce, the element is of slant height $2s'$ and the sides are at an angle α to the x-axis. The point P is at the mid-point of the surface at $(0,y,0)$. In this respect the analysis to follow differs from that for the two-dimensional case and from the theoretical result where the normal derivative of the potential at the surface was obtained by finding this derivative at a general point and allowing the point to approach the surface along the normal. Thus, the factor $2\pi\sigma(p)$ which is present when a proper limiting procedure is used is absent in the numerical treatment. However, in a more general treatment, Smith and Pierce showed this term to be present. In any case, since it has already been proved in section 5.3, equation (5.12) that the term $2\pi\sigma$ is present, no additional proof will be given. The contribution to the derivatives /

derivatives of ϕ with respect to x and y excluding the term $2\pi\sigma$ will be defined as $\left(\frac{\partial\phi}{\partial x}\right)'$ and $\left(\frac{\partial\phi}{\partial y}\right)'$ respectively.

From figure (5.5) it can be seen that the terms in equations (5.35) and (5.36) are given by

$$x = 0 \; ; \quad y = \text{a constant} \; ; \quad \xi = s\cos(\alpha) \; ; \quad \eta = y + s\sin(\alpha)$$

On the singular subelement therefore, equations (5.35) and (5.36) can be written as

$$\left(\frac{\partial\phi(P)}{\partial x}\right)' = \int_{-s'}^{s'} \frac{4\sigma\left(y+s\sin(\alpha)\right)\cos(\alpha)E(k)}{\sqrt{4y^2+4sy\sin(\alpha)+s^2}}\,\frac{ds}{s}$$

$$\left(\frac{\partial\phi(P)}{\partial y}\right)' = \int_{-s'}^{s'} \frac{-2\sigma(y+s\sin\alpha)}{y\sqrt{4y^2+4sy\sin(\alpha)+s^2}}\left[K(k) + \frac{-(s^2+2ys\sin\alpha)}{s^2}E(k)\right]ds$$

Changing the variable of integration to $S = s/y$ and using the fact that both σ and α are constant yields

$$\left(\frac{\partial\phi(P)}{\partial x}\right)' = 4\sigma\cos\alpha\int_{-S'}^{S'} \frac{\left(1+S\sin(\alpha)\right)E(k)}{\sqrt{4+4S\sin(\alpha)+S^2}}\,\frac{ds}{S} \qquad (5.37)$$

$$\left(\frac{\partial\phi(P)}{\partial y}\right)' = -2\sigma\int_{-S'}^{S'} \frac{1+S\sin(\alpha)}{\sqrt{4+4S\sin(\alpha)+S^2}}\left[K(k) - \frac{S+2\sin(\alpha)}{S}E(k)\right]ds \qquad (5.38)$$

where

$$k^2 = \frac{4\left(1+S\sin(\alpha)\right)}{4+4S\sin(\alpha)+S^2} \qquad (5.39)$$

S is small - usually less than $0{\cdot}001$ - and so to evaluate the integrals in (5.37) and (5.38) the integrands are expanded in a power series in S. When S is small, $k \simeq 1$. The complementary modulus k' must therefore be small. The complete elliptic integrals are expanded in a power series in S by first expressing them as a series in the complementary /

complementary modulus as given in Jahnke and Emde. The complementary modulus can then be written as a power series in S using (5.39) as

$$\left.\begin{aligned} k'^2 = 1 - k^2 = 1 - \frac{4\{1+S\sin(\alpha)\}}{4+4S\sin(\alpha)+S^2} &= \frac{\frac{1}{4}S^2}{1+(S\sin(\alpha)+\frac{S^2}{4}} \\ = \tfrac{1}{4}S^2\Big[1-S\sin(\alpha) &+ \left(\sin^2(\alpha)-\tfrac{1}{4}\right)S^2 + \tfrac{1}{2}\left(\sin(\alpha)-\sin^3(\alpha)\right)S^3 \\ + \left(\frac{1}{16}-\frac{3}{4}\sin^2(\alpha)+\sin^4(\alpha)\right)S^4 &+ \ldots\ldots\Big] \end{aligned}\right\} \quad (5.40)$$

Hence, substituting (5.40) into the series for $K(k)$ and $E(k)$ gives

$$\left.\begin{aligned} E(k) = 1 + \left(\frac{1}{8}\log(8)-\frac{1}{16}\right)S^2 &+ \left(\frac{1}{8}-\frac{1}{8}\log(8)\right)\sin(\alpha)S^3 + \ldots\ldots \\ - \tfrac{1}{2}\left(\log(S^2)\right)\Big[\frac{1}{8}S^2 &- \frac{1}{8}\sin(\alpha)\,S^3 + \ldots\Big] \end{aligned}\right\}$$

$$\left.\begin{aligned} K(k) = \log(8) + \tfrac{1}{2}\sin(\alpha)S + \left(\frac{1}{16}+\frac{1}{16}\log(8)-\tfrac{1}{4}\sin^2(\alpha)S^2\right. &+ \ldots\ldots \\ - \tfrac{1}{2}\left(\log(S^2)\right)\Big[1+\frac{1}{16}S^2 &- \frac{1}{16}\sin(\alpha)S^3 + \ldots\Big] \end{aligned}\right\}$$

The remaining factor $\left(4+4S\sin(\alpha)+S^2\right)^{-\frac{1}{2}}$ in (5.37) and (5.38) is easily expanded in a series in S. The integrals in (5.37) and (5.38) can now be written entirely as a series in S which involves only terms of the form S^n and $S^n\log(S)$. The integration is then straight forward giving

$$\left(\frac{\partial\phi(P)}{\partial x}\right)' = \sigma\sin(\alpha)\cos(\alpha)\left[2S'+\left(\frac{13}{72}+\frac{1}{12}\log\left(\frac{S'}{8}\right)+\frac{1}{12}\sin^2(\alpha)\right)S'^3 + \ldots\right] \quad (5.41)$$

$$\left.\begin{aligned} \left(\frac{\partial\phi(P)}{\partial y}\right)' = \sigma\Big[\left(2\sin^2(\alpha)+2\log\left(\frac{S'}{8}\right)\right)S' &- \frac{1}{24}\left(3+3\log\left(\frac{S'}{8}\right)\right. \\ - \quad 3\sin^2(\alpha)-2\sin^4(\alpha)\Big)S'^3 &+ \ldots\Big] \end{aligned}\right\} \quad (5.42)$$

Therefore, /

Therefore, when P lies on the frustum of the cone, the velocities induced in the x and y directions due to the complete frustum are given by

$$\frac{\partial\phi(p)}{\partial x_+} = 2\pi\sigma_+ \sin(\alpha) + \left(\frac{\partial\phi}{\partial x}\right)^* \tag{5.43a}$$

$$\frac{\partial\phi(p)}{\partial y_+} = -2\pi\sigma_+ \cos(\alpha) + \left(\frac{\partial\phi}{\partial y}\right)^* \tag{5.43b}$$

for external flow and

$$\frac{\partial\phi(p)}{\partial x_-} = -2\pi\sigma_- \sin(\alpha) + \left(\frac{\partial\phi}{\partial x}\right)^* \tag{5.44a}$$

$$\frac{\partial\phi(p)}{\partial y_-} = 2\pi\sigma_- \cos(\alpha) + \left(\frac{\partial\phi}{\partial y}\right)^* \tag{5.44b}$$

for internal flow where $\left(\frac{\partial\phi}{\partial x}\right)^*$ and $\left(\frac{\partial\phi}{\partial y}\right)^*$ include the contributions from the singular subelement and from both ordinary subelements obtained from (5.35) and (5.36).

Using the same notation as in the two-dimensional case, let the body be considered to be constructed entirely of frusta of cones, n in number. The source density of the j^{th} frustum therefore makes the following contributions to the directional derivatives of ϕ at the mid-point of the i^{th} frustum for $i \neq j$ from (5.35) and (5.36).

$$\left.\begin{aligned}\frac{\partial\phi(P_{2i-1})}{\partial x} &= -4\int_{s_{2j-2}}^{s_{2j}} \frac{\eta_j (x_{2i-1}-\xi_j)\sigma_j\, E(k)ds}{\sqrt{(y_{2i-1}+\eta_j)^2+(x_{2i-1}-\xi_j)^2}\left[(y_{2i-1}-\eta_j)^2+(x_{2i-1}-\xi_j)^2\right]} \\ &= \sigma_j X_{ij}\end{aligned}\right\} \tag{5.45}$$

$$\frac{\partial\phi(P_{2i-1})}{\partial y} = /$$

$$\left.\begin{aligned}\frac{\partial\phi(P_{2i-1})}{\partial y} &= -2\int_{s_{2j-2}}^{s_{2j}} \frac{\sigma_j\,\eta_j}{y_{2i-1}\sqrt{(y_{2i-1}+\eta_j)^2+(x_{2i-1}-\xi_j)^2}} \\ &\left[K(k) + \frac{y_{2i-1}^2-\eta_j^2-(x_{2i-1}-\xi_j)^2}{(y_{2i-1}-\eta_j)^2+(x_{2i-1}-\xi_j)^2}\,E(k)\right]ds = \sigma_j\,Y_{ij}\end{aligned}\right\} \quad (5.46)$$

When $i = j$ the following expressions are obtained for X_{ii} and Y_{ii} from (5.35), (5.36), (5.41) and (5.42) where the term $2\pi\sigma_i$ has been omitted

$$\left.\begin{aligned}X_{ii} &= \sin(\alpha_i)\cos(\alpha_i)\left[2S_i+\left(\frac{13}{72}+\frac{1}{12}\log\left(\frac{S_i}{8}\right)+\frac{1}{12}\sin^2(\alpha_i)\right)S_i^3+\ldots\right] \\ &- 4\int_{s_{2i-2}}^{s_{2i-1}-S_iy_{2i-1}} \frac{\eta_i(x_{2i-1}-\xi_i)\,E(k)\,ds}{\sqrt{(y_{2i-1}+\eta_i)^2+(x_{2i-1}-\xi_i)^2}\left[(y_{2i-1}-\eta_i)^2+(x_{2i-1}-\xi_i)^2\right]} \\ &- 4\int_{s_{2i-1}+S_iy_{2i-1}}^{s_{2i}} \frac{\eta_i(x_{2i-1}-\xi_i)\,E(k)\,ds}{\sqrt{(y_{2i-1}+\eta_i)^2+(x_{2i-1}-\xi_i)^2}\left[(y_{2i-1}-\eta_i)^2+(x_{2i-1}-\xi_i)^2\right]}\end{aligned}\right\} \quad (5.47)$$

$$\left.\begin{aligned}Y_{ii} &= \left(2\sin^2(\alpha_i)+2\log\left(\frac{S_i}{8}\right)\right)S_i - \frac{1}{24}\left(3+3\log\left(\frac{S_i}{8}\right)-3\sin^2(\alpha_i)-2\sin^4(\alpha_i)\right)S_i^3+\ldots \\ &-2\int_{s_{2i-2}}^{s_{2i-1}-S_iy_{2i-1}} \frac{\eta_i}{y_{2i-1}\sqrt{(y_{2i-1}+\eta_i)^2+(x_{2i-1}-\xi_i)^2}}\left[K(k)+\frac{y_{2i-1}^2-\eta_i^2-(x_{2i-1}-\xi_i)^2}{(y_{2i-1}-\eta_i)^2+(x_{2i-1}-\xi_i)^2}\,E(k)\right]ds \\ &-2\int_{s_{2i-1}+S_iy_{2i-1}}^{s_{2i}} \frac{\eta_i}{y_{2i-1}\sqrt{(y_{2i-1}+\eta_i)^2+(x_{2i-1}-\xi_i)^2}}\left[K(k)+\frac{y_{2i-1}^2-\eta_i^2-(x_{2i-1}-\xi_i)^2}{(y_{2i-1}-\eta_i)^2+(x_{2i-1}-\xi_i)^2}\,E(k)\right]ds\end{aligned}\right\} \quad (5.48)$$

As /

As for the two-dimensional case, the system of equations to be solved for external flows can now be formulated as

$$\frac{\partial\phi(P_{2i-1})}{\partial n} = -2\pi\sigma_i - \sin(\alpha_i) \sum_{j=1}^{n} \sigma_j X_{ij} + \cos(\alpha_i) \sum_{j=1}^{n} \sigma_j Y_{ij} \qquad (5.49)$$

and for internal flows as

$$\frac{\partial\phi(P_{2i-1})}{\partial n} = 2\pi\sigma_i - \sin(\alpha_i) \sum_{j=1}^{n} \sigma_j X_{ij} + \cos(\alpha_i) \sum_{j=1}^{n} \sigma_j Y_{ij} \qquad (5.50)$$

In fact, if in (5.50) the positive direction of the normal is taken towards the inside of the surface and α_i is replaced by $(\alpha_i + \pi)$, equation (5.50) becomes

$$-\frac{\partial\phi(P_{2i-1})}{\partial n} = 2\pi\sigma_i + \sin(\alpha_i) \sum_{j=1}^{n} \sigma_j X_{ij} - \cos(\alpha_i) \sum_{j=1}^{n} \sigma_j Y_{ij} \qquad (5.51)$$

It can be seen that (5.51) and (5.49) are identical. Thus one equation suffices for both external and internal flows. The different results for each flow are obtained by traversing the body contour in opposite directions. Smith and Pierce make this point by stating that if the flow field lies to the left as the body contour is traversed then

$$\frac{\partial\phi(P_{2i-1})}{\partial n} = -2\pi\sigma_i - \sin(\alpha_i) \sum_{j=1}^{n} \sigma_j X_{ij} + \cos(\alpha_i) \sum_{j=1}^{n} \sigma_j Y_{ij} \qquad (5.52)$$

and

$$\frac{\partial\phi(P_{2i-1})}{\partial s} = \cos(\alpha_i) \sum_{j=1}^{n} \sigma_j X_{ij} + \sin(\alpha_i) \sum_{j=1}^{n} \sigma_j Y_{ij} \qquad (5.53)$$

are /

are valid for both internal and external flows.

Knowing the normal velocity at any point on the body surface means that equation (5.52) constitutes n linear equations in the n unknown values of σ. As in the two-dimensional case for flow past a solid body, for example, the total normal velocity at the surface must be zero. Thus, if the body is placed in a uniform stream, velocity V_∞ at infinity, then equation (5.52) to determine σ becomes

$$V_\infty \sin(\alpha_i) = -2\pi\sigma_i - \sin(\alpha_i) \sum_{j=1}^{n} \sigma_j X_{ij} + \cos(\alpha_i) \sum_{j=1}^{n} \sigma_j Y_{ij} \qquad (5.54)$$

Equation (5.54) is almost the same as the corresponding equation for the two-dimensional case although it must be remembered that the matrix elements X_{ij} and Y_{ij} have different formulae in each case. Once the source distribution has been found, the tangential velocity on the surface can be determined using (5.53) where again the main stream velocity must be added. In the same way, by application of equations (5.35) and (5.36) only, the velocity at any other point in the flow field can be determined since no singular integral then exists.

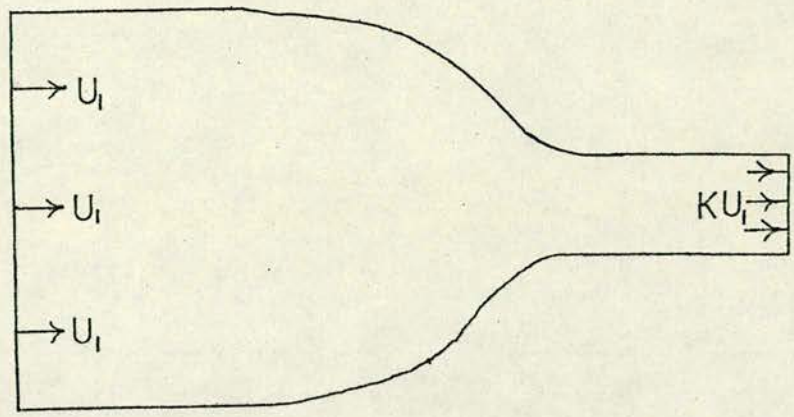

FIGURE (6.1)

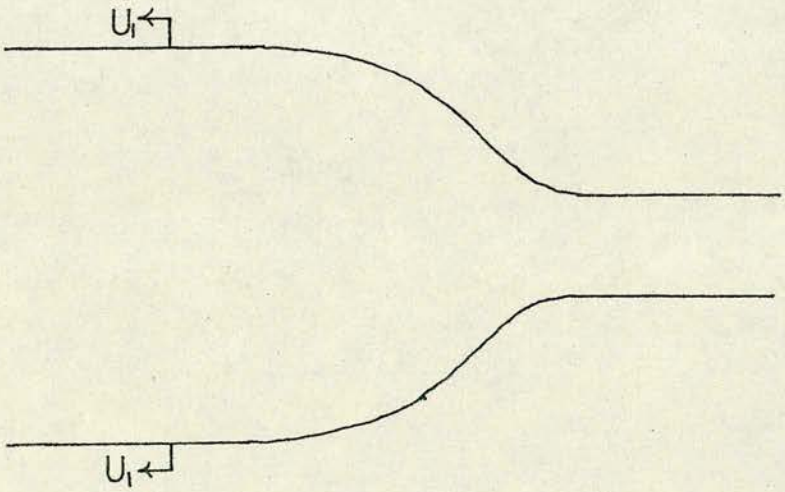

FIGURE (6.2)

CHAPTER 6

APPLICATION OF THE SURFACE SINGULARITY METHOD TO WIND TUNNEL CONTRACTIONS

6.1 INTRODUCTION

In section (5.2) the theoretical justification for the surface singularity method was presented for flow either inside or outside closed bodies. Wind tunnel contractions, however, are not closed bodies but are open at each end. The duct could be made closed by constructing planes upstream and downstream of the contraction across the stream. The boundary conditions on these planes would then be that the velocities on each plane should be normal to the plane and should satisfy the equation of conservation of mass. That is, on the upstream plane

$$\frac{\partial \phi}{\partial n} = U_1$$

and on the downstream plane

$$\frac{\partial \phi}{\partial n} = -U_2 = -KU_1$$

(see figure 6.1). These boundary conditions are equivalent to imposing a uniform flow upstream and downstream of the contraction. In theory, this would mean that the planes are at $+\infty$ and $-\infty$ and that the duct is infinitely long.

An alternative approach is to consider the duct to be open at each end and to be moving with constant velocity through an infinite bath of fluid at rest (figure 6.2). (This eases the computation by eliminating the sharp corners and reducing the number of surfaces.) This /

DUCT NUMBER	LENGTH OF UPSTREAM PARALLEL SECTION	LENGTH OF DOWNSTREAM PARALLEL SECTION	TOTAL LENGTH OF DUCT
1	4.5H	3.5H	9.0H
2	3.5H	2.4H	6.9H
3	2.3H	1.3H	4.6H
4	1.3H	0.3H	2.6H
5	0.48H	0.25H	1.72H

TABLE (6.1)

This still has the effect of imposing a uniform flow upstream of the contraction and does not change the analysis for the rest of the duct. This alternative method was used to calculate the flows through several two-dimensional and axisymmetric contractions.

6.2 The Parallel Sections

Before calculating the flow through the contractions, it is necessary to construct parallel sections upstream and downstream of the contraction and there is no way of deciding 'a priori' how long these parallel sections should be. The duct is thought of as being infinite in length and so these parallel lengths should be long enough to be considered infinite as far as the numerical analysis is concerned. The calculated flow near the open ends of the duct is therefore inaccurate and there must be sufficient length of parallel section to allow the flow to settle down. That is, the parallel sections must be sufficiently long to prevent the end effects from disturbing the flow in the contraction. These end effects arise from the method of analysis in which, because the duct is not infinite in length, the source distribution does not decrease to zero at each end of the duct as might be expected but still has a small finite value.

Flow calculations were run on a two-dimensional 4:1 contraction for the conditions shown in table (6.1). It was found that although the end effects were small, it required a distance of about H to 2H for the flow to settle down at the upstream end of the duct. At the downstream end, the end effects were noticeable within a distance of H to 1.5H from the end of the duct. The results from /

from ducts (1) and (2) in table (6.1) were better than those from the other ducts and it was decided that for all further calculations, the parallel sections as used in duct (1) rather than (2) would be employed. These longer parallel sections helped give a better overall picture not only of the flow in the contraction but also along the parallel sections adjacent to the contraction.

Similar calculations were performed for axisymmetric contractions and again, parallel sections as in (1) table (6.1) were chosen for all further calculations.

For either two-dimensional or axisymmetric contractions, using parallel sections longer than in (1) table (6.1) would be of little advantage and in fact, the dimensions of (1) table (6.1) are probably slightly longer than absolutely necessary.

6.3 Distribution of Body Elements

It was stated in section (5.3) that the meridian curve is approximated by a series of straight lines and that the body or, in this case, the duct is to be constructed of flat elements. There is no way of predetermining the best distribution of body elements. The total number of elements and the length of each element required to give a good solution can only be determined by experience and trial and error. A guide to the distribution of elements is given by Hess (1972) who states that no element should differ in length from its nearest neighbour by more than 50%. In regions of high curvature, the elements should be shorter and more highly concentrated than in regions of more uniform flow. A poor distribution of elements results /

results in a large amount of the fluid 'leaking' through the solid surface and therefore, in an inaccurate solution. More will be said of this leakage later.

Using the parallel sections of (1) table (6.1), after a few initial calculations it was found that a 112 element duct gave very good results in the two-dimensional case. The length of the elements varied from 0.4H at each end of the duct to an almost uniform length of 0.025H over the contraction itself. Increasing the number of elements to over 112 and reducing their length might yield some improvement but, since the results obtained were very good, the extra computing time was not warranted.

After some initial testing the same distribution of elements was used for the axisymmetric ducts. In this case the results obtained were not so good as those for the two-dimensional ducts and the leakage was greater. In an attempt to improve these results a modification of the method of Smith and Pierce was tried; further reference to this is made in section (6.6) .

6.4 Two-Dimensional Ducts

Using the parallel sections of (1) table (6.1) and 112 intervals as described in the previous section, the influence matrices X_{ij} and Y_{ij} were calculated using equations (5.20) and (5.21) for several contractions. The contractions were assumed to be moving with unit velocity ($U_1 = 1$ in figure 6.2). The source density distribution was then calculated using equations (5.28) where $V_\infty = 1$. Then, using this source distribution, the tangential wall velocity, the centre line velocity and the velocity profile /

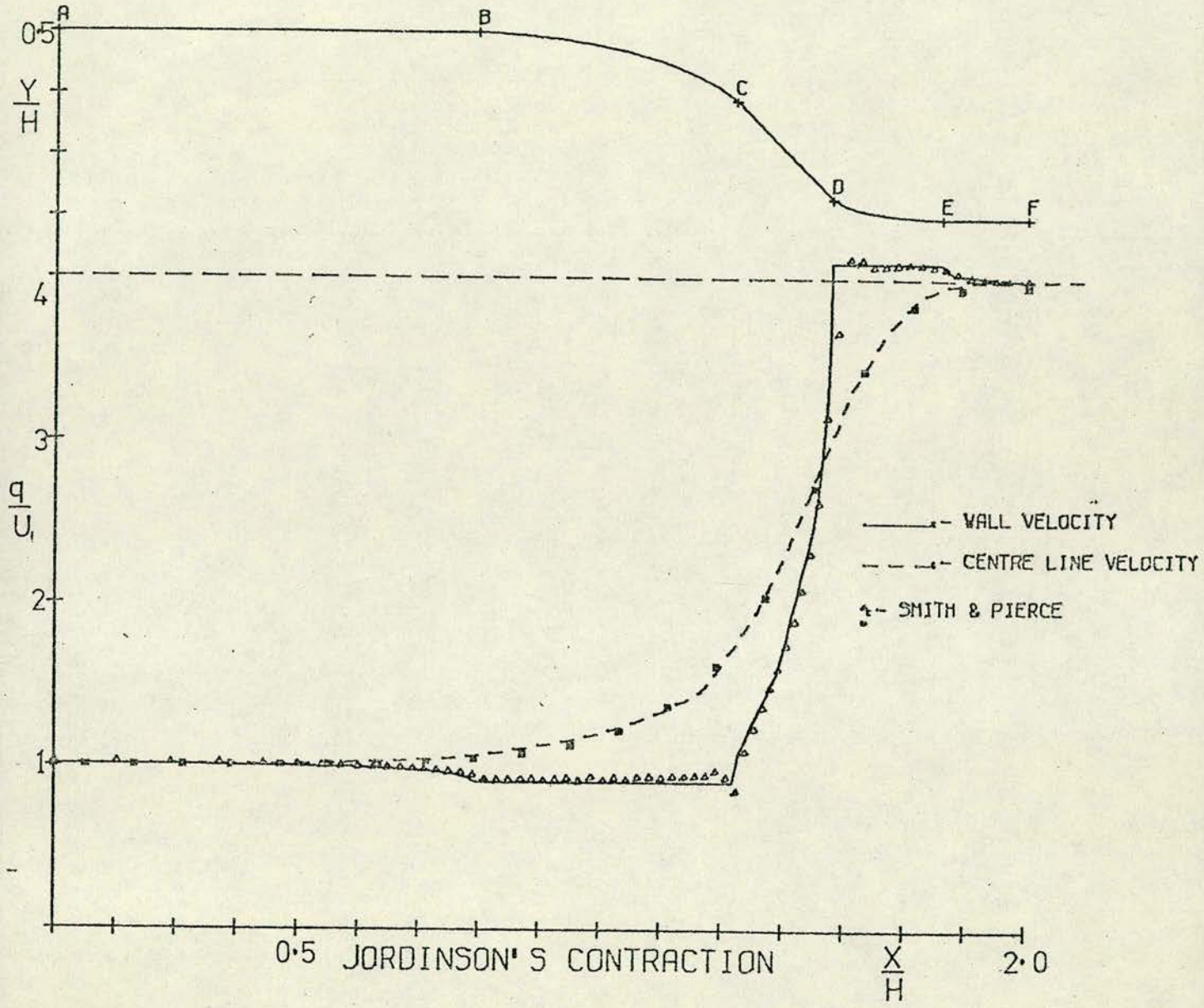
A
B
C
D
E
F
0·5
Y/H
4
3
q/U₁
2
1
WALL VELOCITY
CENTRE LINE VELOCITY
SMITH & PIERCE
0·5
JORDINSON'S CONTRACTION
X/H
2·0

FIGURE (6.3)

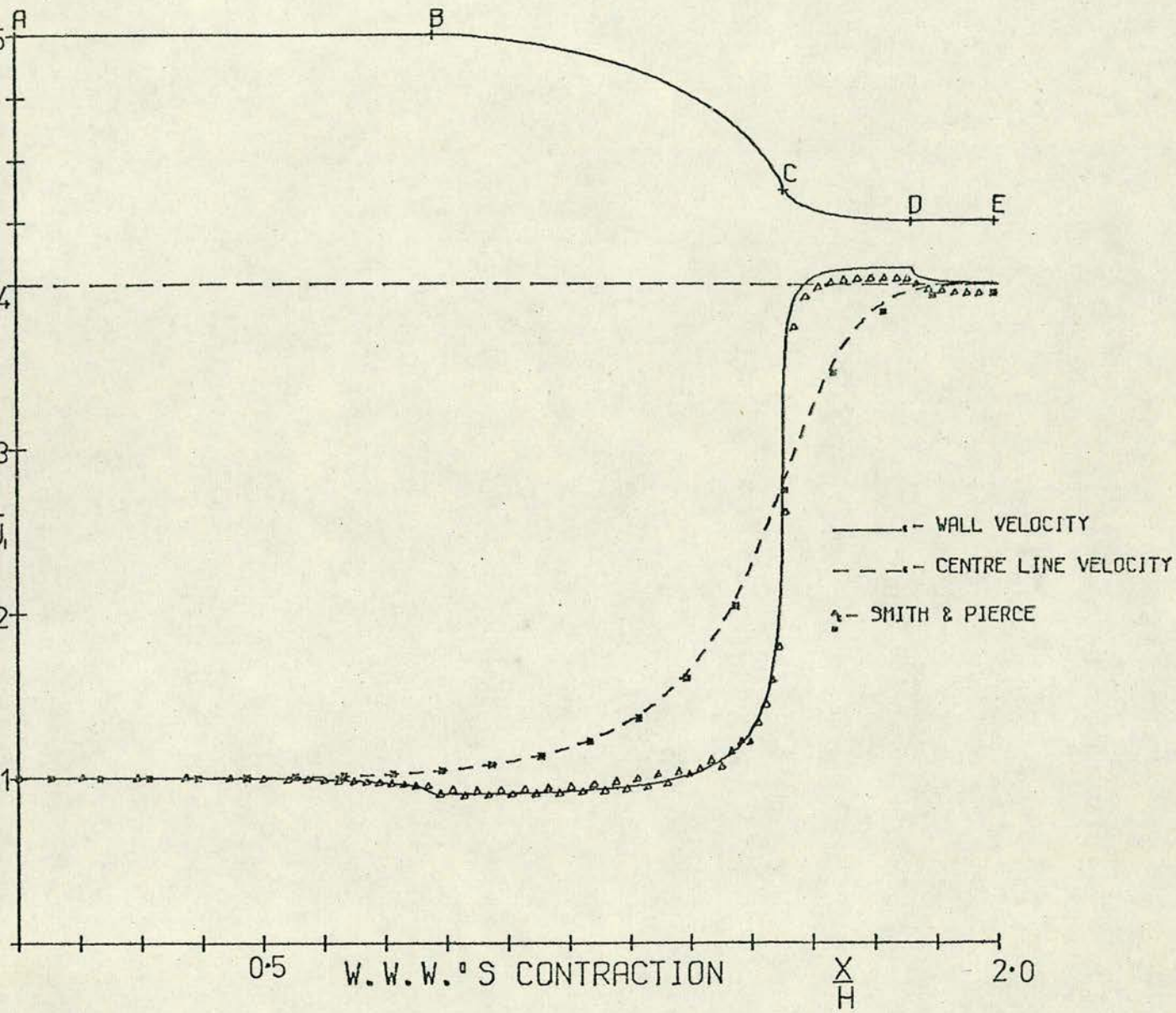
A
B
C
D
E
WALL VELOCITY
CENTRE LINE VELOCITY
SMITH & PIERCE
0·5
W.W.W.'S CONTRACTION
X/H
2·0

FIGURE (64)

$\frac{x}{H}$	$\frac{y}{H}$	WALL VELOCITY $\frac{q}{U_1}$
0.0000	0.5000	1.0029
0.2125	0.5000	1.0025
0.3725	0.5000	0.9973
0.4625	0.5000	0.9920
0.5275	0.5000	0.9860
0.5833	0.5000	0.9783
0.6333	0.5000	0.9683
0.6833	0.5000	0.9513
0.7333	0.4997	0.9164
0.7832	0.4970	0.9189
0.8330	0.4926	0.9188
0.8827	0.4869	0.9139
0.9322	0.4795	0.9165
0.9813	0.4705	0.9252
1.0301	0.4594	0.9325
1.0789	0.4461	0.9400
1.1263	0.4303	0.9605
1.1725	0.4113	0.9812
1.2168	0.3882	1.0246
1.2567	0.3584	1.0826
1.2932	0.3242	1.6829
1.3366	0.3001	1.9541
1.3840	0.2842	1.9966
1.4328	0.2732	2.0202
1.4821	0.2653	2.0286
1.5318	0.2598	2.0292
1.5816	0.2559	2.0318
1.6313	0.2530	2.0418
1.6810	0.2514	2.0282
1.7309	0.2503	2.0340
1.7824	0.2500	2.0166
1.8340	0.2500	2.0036
1.8840	0.2500	1.9986
1.9334	0.2500	1.9960
1.9909	0.2500	1.9945
2.0509	0.2500	1.9938

$\frac{x}{H}$	CENTRE LINE VELOCITY $\frac{q}{U_1}$
0.0000	1.0009
0.1375	1.0016
0.2375	1.0027
0.3375	1.0046
0.4375	1.0083
0.5375	1.0149
0.6375	1.0265
0.7375	1.0463
0.8375	1.0784
0.9375	1.1287
1.0375	1.2046
1.1375	1.3139
1.2375	1.4575
1.3375	1.6185
1.4375	1.7646
1.5375	1.8718
1.6375	1.9377
1.7375	1.9720
1.8375	1.9866
1.9375	1.9917
2.0375	1.9932
2.1375	1.9935

TABLE 6.2

$\frac{x}{H}$	$\frac{y}{H}$	WALL VELOCITY $\frac{q}{U_1}$
0.0000	0.5000	1.0043
0.2125	0.5000	1.0028
0.3725	0.5000	0.9970
0.4625	0.5000	0.9915
0.5275	0.5000	0.9852
0.5833	0.5000	0.9773
0.6333	0.5000	0.9673
0.6833	0.5000	0.9506
0.7325	0.4997	0.9149
0.7817	0.4971	0.9181
0.8315	0.4928	0.9154
0.8764	0.4878	0.9039
0.9259	0.4805	0.9166
0.9751	0.4717	0.9239
1.0239	0.4610	0.9285
1.0722	0.4481	0.9326
1.1196	0.4328	0.9416
1.1679	0.4134	0.9531
1.2124	0.3908	0.9884
1.2550	0.3599	0.9791
1.2906	0.3248	1.3776
1.3284	0.2895	1.9412
1.3745	0.2651	2.2281
1.4225	0.2507	2.2489
1.4716	0.2410	2.2614
1.5216	0.2342	2.2766
1.5734	0.2296	2.2828
1.6257	0.2265	2.2728
1.6780	0.2248	2.2629
1.7227	0.2238	2.2754
1.7673	0.2236	2.2490
1.8189	0.2236	2.2345
1.8704	0.2236	2.2289
1.9204	0.2236	2.2264
1.9699	0.2236	2.2252
2.0274	0.2236	2.2242

$\frac{x}{H}$	CENTRE LINE VELOCITY $\frac{q}{U_1}$
0.0000	1.0006
0.1375	1.0009
0.2375	1.0020
0.3375	1.0040
0.4375	1.0077
0.5375	1.0145
0.6375	1.0265
0.7375	1.0470
0.8375	1.0807
0.9375	1.1344
1.0375	1.2179
1.1375	1.3436
1.2375	1.5197
1.3375	1.7314
1.4375	1.9317
1.5375	2.0777
1.6375	2.1630
1.7375	2.2036
1.8375	2.2187
1.9375	2.2231
2.0375	2.2241

TABLE 6.3

$\frac{x}{H}$	$\frac{y}{H}$	WALL VELOCITY $\frac{q}{U_1}$
0.0000	0.5000	1.0050
0.2125	0.5000	1.0036
0.3725	0.5000	0.9975
0.4625	0.5000	0.9918
0.5275	0.5000	0.9854
0.5833	0.5000	0.9774
0.6333	0.5000	0.9675
0.6833	0.5000	0.9511
0.7333	0.4996	0.9157
0.7832	0.4970	0.9186
0.8330	0.4926	0.9156
0.8827	0.4869	0.9062
0.9322	0.4795	0.9086
0.9813	0.4705	0.9162
1.0301	0.4594	0.9196
1.0789	0.4461	0.9222
1.1263	0.4303	0.9371
1.1725	0.4113	0.9462
1.2168	0.3882	0.9728
1.2567	0.3584	0.9480
1.2922	0.3231	1.3174
1.3276	0.2878	1.6783
1.3664	0.2554	2.3994
1.4125	0.2363	2.4611
1.4609	0.2242	2.4763
1.5103	0.2162	2.4853
1.5600	0.2110	2.4872
1.6099	0.2077	2.4780
1.6598	0.2055	2.4918
1.7086	0.2044	2.4830
1.7573	0.2041	2.4600
1.8105	0.2041	2.4440
1.8605	0.2041	2.4385
1.9102	0.2041	2.4360
1.9624	0.2041	2.4346
2.0224	0.2041	2.4340

$\frac{x}{H}$	CENTRE LINE VELOCITY $\frac{q}{U_1}$
0.0000	1.0003
0.1375	1.0009
0.2375	1.0019
0.3375	1.0039
0.4375	1.0076
0.5375	1.0145
0.6375	1.0267
0.7375	1.0476
0.8375	1.0822
0.9375	1.1379
1.0375	1.2261
1.1375	1.3626
1.2375	1.5632
1.3375	1.8200
1.4375	2.0753
1.5375	2.2624
1.6375	2.3677
1.7375	2.4142
1.8375	2.4296
1.9375	2.4334
2.0375	2.4341

TABLE 6.4

profile across the flow at several stations were calculated for each contraction.

Figure (6.3) shows the wall and centre line velocities plotted against distance along the contraction together with the theoretical results obtained using Jordinson's approximate method for a contraction with parameters $n=4$, $e^{-\ell_1}= 0.9$, $e^{\ell_2} = 1.025$ and contraction ratio of 4:1 . From this graph it can be seen that the results agree well with the theoretical velocity distributions. Using the same lengths of parallel sections, and approximately the same distribution of elements, the flow through the contraction designed using W.W.W.'s method (section 2.3; figure 2.5) was calculated. Figure (6.4) shows the results obtained, using the method of this chapter, for the wall and centre line velocities compared with the exact results. Again the agreement is very good. The flows through several other contractions designed using Jordinson's method with the same parameters as the above 4:1 contraction were calculated for contraction ratios of 2:1, $\sqrt{5}$:1 and $\sqrt{6}$:1. The results are shown in tables (6.2), (6.3) and (6.4).

In order to obtain another estimate of the accuracy of the method, the flux across the inlet and outlet planes of the contraction was calculated. The flux was found by calculating the velocity at several points in a plane across the stream using equations (5.18) and (5.19) and integrating the velocity with respect to distance across the stream. For all the two-dimensional contractions tested, the flux at the downstream end of the contraction was always better than /

x = 0.7208H	
$\frac{y}{H}$	$\frac{q}{U_1}$
0.00	1.0422
0.05	1.0408
0.10	1.0366
0.15	1.0297
0.20	1.0203
0.25	1.0087
0.30	0.9952
0.35	0.9800
0.40	0.9632
0.45	0.9438
0.50	0.9251
Flux = 1.000	

BEGINNING OF THE CONTRACTION

x = 1.7433H	
$\frac{y}{H}$	$\frac{q}{U_1}$
0.000	1.9732
0.025	1.9738
0.050	1.9756
0.075	1.9786
0.100	1.9826
0.125	1.9878
0.150	1.9941
0.175	2.0016
0.200	2.0106
0.225	2.0232
0.250	2.0298
Flux = 0.996	

END OF THE CONTRACTION

x = 2.7375H	
$\frac{y}{H}$	$\frac{q}{U_1}$
0.000	1.9927
0.025	1.9927
0.050	1.9927
0.075	1.9927
0.100	1.9927
0.125	1.9927
0.150	1.9928
0.175	1.9928
0.200	1.9929
0.225	1.9935
0.250	1.9935
Flux = 0.996	

TABLE 6.5

x = 0.7208H	
$\frac{y}{H}$	$\frac{q}{U_1}$
0.00	1.0428
0.05	1.0413
0.10	1.0368
0.15	1.0295
0.20	1.0197
0.25	1.0076
0.30	0.9938
0.35	0.9783
0.40	0.9612
0.45	0.9418
0.50	0.9234
Flux = 1.000	

BEGINNING OF THE CONTRACTION

x = 1.7298H	
$\frac{y}{H}$	$\frac{q}{U_1}$
0.0000	2.2016
0.0224	2.2023
0.0447	2.2043
0.0671	2.2076
0.0894	2.2121
0.1118	2.2180
0.1342	2.2251
0.1565	2.2335
0.1789	2.2426
0.2012	2.2576
0.2236	2.2711
Flux = 0.995	

END OF THE CONTRACTION

x = 2.2375H	
$\frac{y}{H}$	$\frac{q}{U_1}$
0.0000	2.2240
0.0224	2.2240
0.0447	2.2241
0.0671	2.2241
0.0894	2.2241
0.1118	2.2241
0.1342	2.2241
0.1565	2.2241
0.1789	2.2242
0.2012	2.2242
0.2236	2.2242
Flux = 0.995	

TABLE 6.6

x = 0.7208H	
$\frac{y}{H}$	$\frac{q}{U_1}$
0.00	1.0433
0.05	1.0418
0.10	1.0372
0.15	1.0297
0.20	1.0196
0.25	1.0073
0.30	0.9932
0.35	0.9777
0.40	0.9606
0.45	0.9413
0.50	0.9391
Flux = 1.0000	

BEGINNING OF THE CONTRACTION

x = 1.7198H	
$\frac{y}{H}$	$\frac{q}{U_1}$
0.0000	2.4090
0.0204	2.4097
0.0408	2.4119
0.0612	2.4155
0.0816	2.4206
0.1021	2.4270
0.1225	2.4349
0.1429	2.4442
0.1633	2.4554
0.1837	2.4709
0.2041	2.4830
Flux = 0.9935	

END OF THE CONTRACTION

x = 2.7375H	
$\frac{y}{H}$	$\frac{q}{U_1}$
0.0000	2.4325
0.0204	2.4325
0.0408	2.4325
0.0612	2.4325
0.0816	2.4325
0.1021	2.4325
0.1225	2.4325
0.1429	2.4326
0.1633	2.4329
0.1837	2.4338
0.2041	2.4340
Flux = 0.9931	

TABLE 6.7

x = 0.7208H	
$\frac{y}{H}$	$\frac{q}{U_1}$
0.00	1.0400
0.05	1.0385
0.10	1.0341
0.15	1.0270
0.20	1.0176
0.25	1.0062
0.30	0.9932
0.35	0.9792
0.40	0.9643
0.45	0.9491
0.50	0.9416
Flux = 1.000	

BEGINNING OF THE CONTRACTION

x = 1.7149H	
$\frac{y}{H}$	$\frac{q}{U_1}$
0.0000	3.9301
0.0125	3.9311
0.0250	3.9339
0.0375	3.9386
0.0500	3.9451
0.0625	3.9532
0.0750	3.9629
0.0875	3.9740
0.1000	3.9863
0.1125	3.9991
0.1250	3.9997
Flux = 0.9897	

END OF THE CONTRACTION

x = 2.2375H	
$\frac{y}{H}$	$\frac{q}{U_1}$
0.0000	3.9478
0.0125	3.9578
0.0250	3.9578
0.0375	3.9578
0.0500	3.9579
0.0625	3.9579
0.0750	3.9579
0.0875	3.9579
0.1000	3.9580
0.1125	3.9580
0.1250	3.9580
Flux = 0.9895	

TABLE 6.8

than 98·5% of the flux at the entrance to the contraction and, except for Jordinson's 4:1 contraction, better than 99% . Tables (6.5), (6.6), (6.7) and (6.8) show the velocity profile across the entrances and at various distances downstream of Jordinson's 2:1, $\sqrt{5}$:1, $\sqrt{6}$:1 and 4:1 contractions with the percentage flux across each plane. It can be seen that the flow becomes uniform very quickly at the downstream ends of these contractions which is an important requirement for any practical design.

6.5 Leakage and the Higher Order Solution

From these last results it can be seen that a small amount of flux has been lost. This is the leakage referred to in section (6.3). This leakage - which can be quite large for a poor distribution of elements - exists because of errors inherent in the method. The method assumes that the source strength is constant on each element and that each element is flat. Also, when reducing the integral equations to a set of linear algebraic equations, the normal velocity is only evaluated at one point on each element. Thus, if the direction of the normal changes over an interval, there could be a net flow through the interval. Hess (1972) found that the errors inherent in this method are greatest for interior flows and for flows about bodies with regions concave to the flow. In fact, for exterior flows about convex bodies he found that there tends to be a cancellation of errors.

The element distribution affects the amount of leakage as also does the total number of elements. This can be seen from the following example. For Jordinson's 4:1 contraction described in the /

the previous section, a 56 interval solution resulted in only 95% of the upstream flux being calculated at the downstream end compared with 98·5% for the 112 interval solution. Increasing the number of intervals to over 112 might yield some improvement but, since the results shown in figures (6.3) and (6.4) are very good, the extra computing time is not warranted.

Instead of increasing the number of elements in an attempt to improve the results, increased accuracy could be obtained by using the higher order method of Hess (1972). In this improvement on the basic method of Smith and Pierce, the source strength is allowed to vary over each element and is expressed as a polynomial in the distance s across each element. The elements are no longer flat but are arcs of circles whose radii are calculated to give a good fit to the original meridian curve. It is found that the best results are obtained using these curved elements and a linearly varying source density. The contributions from a higher order variation in the source density are found to be negligibly small. In addition Hess shows that it is mathematically inconsistent to use either flat elements and linearly varying source densities or constant source densities and curved elements since the correction obtained from each improvement is of the same magnitude. Hence, using this higher order method, the accuracy obtained in the solution for a given number of intervals is much better in general than that obtained from the base method for the same number of intervals. Alternatively, the same degree of accuracy as that of the base method could be obtained by using the higher order method and fewer intervals. The system of equations to be solved remains essentially the same and so /

so reducing the number of intervals would reduce the computing time required to solve these equations. The expressions for the equivalent of the influence matrices are, however, more complex in the higher order method and so the time required to calculate these matrices for a given number of intervals will be greater than in the base method. It is not always certain therefore, that using fewer elements and the higher order solution will result in an overall reduction of computing time for a given degree of accuracy.

When calculating the flows through the two-dimensional ducts the base method only was used for the following reasons. Firstly, the results obtained from the base method were very good and, since the greater part of the meridian curve of the duct consisted of straight lines, using the higher order solution might not, in any case, increase the accuracy of the 112 interval solution obtained using the base method. Secondly, the c.p.u. time required to calculate the source density distribution and the tangential wall velocity for 112 intervals was only 4 minutes (160 seconds to calculate the influence matrices X_{ij} and Y_{ij} and 80 seconds to calculate the source distribution and the tangential wall velocity).

Thus, the base method of Smith and Pierce has proved very successful in calculating the flows through ducts in two-dimensions. The calculation of flows through axisymmetric ducts using this method was not, however, quite so successful.

6.6 Axisymmetric Ducts

The flows through several axisymmetric contractions with the same /

same meridian curves as the two-dimensional contractions described in the previous section were calculated. That is, for contractions designed using Jordinson's method for parameters $n = 4$, $e^{-\ell_1} = 0.9$, $e^{\ell_2} = 1.025$ and contraction ratios of 16:1, 6:1, 5:1 and 4:1 by area. The problem of leakage in axisymmetric ducts is much greater than in the two-dimensional case and, because of the more complicated expressions for the coefficients in the influence matrices, no higher order solution has yet been developed. Charles W. Dawson of the Naval Ship Research and Development Centre, U.S. Department of the Navy, is at present working on a higher order solution but as yet without good results. For an area contraction ratio of 4:1, the results were quite acceptable with a total of 95% of the flux flowing through the contraction. As the contraction ratio is increased, the amount of leakage increases. For area contraction ratios of 5:1 and 6:1 the percentages of the upstream flux calculated at the downstream end of the contraction were 93% and 91% respectively. For an area contraction ratio of 16:1 the figure calculated was at best 78% for 112 intervals. In an attempt to improve this figure without just increasing the number of intervals the following modification of the base method was used.

The coefficient X_{ij} in the influence matrix is the velocity induced in the x-direction at the mid-point of the i^{th} element by a unit source distribution over the j^{th} interval; the physical interpretation of the coefficients Y_{ij} is identical. The modification consisted of finding the velocity induced at several points on the i^{th} element due to the source distribution on the j^{th} element /

element and taking the average of the results over the i^{th} element. Thus the matrix elements X_{ij} and Y_{ij} are the average effect on the i^{th} element due to a source distribution on the j^{th} element. It was hoped that a more accurate solution could be obtained for the same number of intervals by overcoming one of the causes of leakage described in section (6.5). In fact, with these new averaged influence matrices, solving equation (5.54) is equivalent to calculating the total flux through each element and equating the result to zero. The results obtained using this averaging procedure were slightly better with 82% of the upstream flux being calculated at the downstream end of Jordinson's 16:1 contraction.

The initial reluctance to increase the number of intervals to improve on the 112 interval solution was not only because of the computer time required to calculate the influence matrices but also because of the amount of storage required. The modified method just described only requires the same amount of store as the base 112 interval solution and the equations to be solved for the source distribution remain the same. A 224 interval solution was contemplated in an attempt to improve the accuracy of the solution. The c.p.u. time required to calculate the diagonal elements only of the matrices X_{ij} and Y_{ij} was approximately 23 minutes and the time required to calculate the rest of the influence matrices was approximately the same. In addition, the space required for each of these matrices was about half a megabyte - over 400,000 bytes - which exceeded the available core in the computer. It is desirable that any solution, in addition to being accurate, should not require an excessive amount of computer time and so be reasonably inexpensive to /

$\frac{x}{H}$	$\frac{y}{H}$	WALL VELOCITY $\frac{q}{U_1}$
0.0000	0.5000	1.0281
0.2125	0.5000	1.0261
0.3725	0.5000	1.0121
0.4625	0.5000	1.0050
0.5275	0.5000	0.9991
0.5833	0.5000	0.9940
0.6333	0.5000	0.9921
0.6833	0.5000	0.9911
0.7333	0.4997	0.9576
0.7832	0.4970	0.9827
0.8330	0.4926	0.9585
0.8827	0.4869	0.9282
0.9322	0.4795	0.9538
0.9813	0.4705	0.9980
1.0301	0.4594	1.0172
1.0789	0.4461	1.0492
1.1263	0.4303	1.1202
1.1725	0.4113	1.1679
1.2168	0.3882	1.2743
1.2567	0.3584	1.3623
1.2932	0.3242	2.1619
1.3366	0.3001	2.9842
1.3840	0.2842	3.2390
1.4328	0.2732	3.4453
1.4821	0.2653	3.5542
1.5318	0.2598	3.6541
1.5816	0.2559	3.7708
1.6313	0.2530	3.7816
1.6810	0.2514	3.8396
1.7309	0.2503	3.8425
1.7824	0.2500	3.8561
1.8340	0.2500	3.8306
1.8840	0.2500	3.8225
1.9334	0.2500	3.8189
1.9909	0.2500	3.8157
2.0509	0.2500	3.8145

$\frac{x}{H}$	CENTRE LINE VELOCITY $\frac{q}{U_1}$
0.0000	0.9990
0.1375	0.9982
0.2375	0.9982
0.3375	0.9992
0.4375	1.0026
0.5375	1.0104
0.6375	1.0266
0.7375	1.0579
0.8375	1.1147
0.9375	1.2134
1.0375	1.3795
1.1375	1.6493
1.2375	2.0511
1.3375	2.5518
1.4375	3.0374
1.5375	3.4060
1.6375	3.6353
1.7375	3.7532
1.8375	3.8003
1.9375	3.8144
2.0375	3.8178
2.1375	3.8183

4 : 1 CONTRACTION

TABLE 6.9a

x = 0.7208H	
$\frac{y}{H}$	$\frac{q}{U_1}$
0.00	1.0527
0.05	1.0498
0.10	1.0456
0.15	1.0387
0.20	1.0295
0.25	1.0182
0.30	1.0053
0.35	0.9911
0.40	0.9758
0.45	0.9596
0.50	0.9423
Flux = 0.992	

BEGINNING OF THE CONTRACTION

x = 1.7433H	
$\frac{y}{H}$	$\frac{q}{U_1}$
0.000	3.7572
0.025	3.7585
0.050	3.7617
0.075	3.7670
0.100	3.7744
0.125	3.7840
0.150	3.7958
0.175	3.8099
0.200	3.8272
0.225	3.8513
0.250	3.8737
Flux = 0.953	

END OF THE CONTRACTION

x = 2.7375H	
$\frac{y}{H}$	$\frac{q}{U_1}$
0.000	3.8117
0.025	3.8117
0.050	3.8117
0.075	3.8117
0.100	3.8117
0.125	3.8117
0.150	3.8118
0.175	3.8123
0.200	3.8139
0.225	3.8207
0.250	3.8262
Flux = 0.953	

4 : 1 CONTRACTION

TABLE 6.9b

$\frac{x}{H}$	$\frac{y}{H}$	WALL VELOCITY $\frac{q}{U_1}$
0.0000	0.5000	1.0378
0.2125	0.5000	1.0356
0.3725	0.5000	1.0187
0.4625	0.5000	1.0105
0.5275	0.5000	1.0040
0.5833	0.5000	0.9988
0.6333	0.5000	0.9984
0.6833	0.5000	1.0006
0.7325	0.4997	0.9704
0.7817	0.4971	0.9925
0.8315	0.4928	0.9514
0.8764	0.4878	0.9044
0.9259	0.4805	0.9835
0.9751	0.4717	1.0324
1.0239	0.4610	1.0457
1.0722	0.4481	1.0578
1.1196	0.4328	1.1148
1.1679	0.4134	1.1436
1.2124	0.3908	1.2724
1.2550	0.3599	1.2820
1.2906	0.3248	1.6799
1.3284	0.2895	2.7463
1.3745	0.2651	3.7851
1.4225	0.2507	4.0771
1.4716	0.2410	4.3137
1.5216	0.2342	4.5363
1.5734	0.2296	4.6460
1.6257	0.2265	4.6386
1.6780	0.2248	4.7215
1.7727	0.2238	4.7304
1.7673	0.2236	4.7373
1.8189	0.2236	4.7072
1.8704	0.2236	4.6967
1.9204	0.2236	4.6923
1.9699	0.2236	4.6903
2.0274	0.2236	4.6871

$\frac{x}{H}$	CENTRE LINE VELOCITY $\frac{q}{U_1}$
0.0000	1.0017
0.1375	1.0005
0.2375	1.0002
0.3375	1.0011
0.4375	1.0041
0.5375	1.0115
0.6375	1.0274
0.7375	1.0584
0.8375	1.1156
0.9375	1.2171
1.0375	1.3943
1.1375	1.6999
1.2375	2.1980
1.3375	2.8851
1.4375	3.5992
1.5375	4.1458
1.6375	4.4716
1.7375	4.6249
1.8375	4.6776
1.9375	4.6903
2.0375	4.6926

5 : 1 CONTRACTION

TABLE 6.10a

x = 0.7208H	
$\frac{y}{H}$	$\frac{q}{U_1}$
0.00	1.0521
0.05	1.0503
0.10	1.0460
0.15	1.0391
0.20	1.0297
0.25	1.0185
0.30	1.0057
0.35	0.9917
0.40	0.9768
0.45	0.9614
0.50	0.9477
Flux = 0.993	

BEGINNING OF THE CONTRACTION

x = 1.7298H	
$\frac{y}{H}$	$\frac{q}{U_1}$
0.0000	4.6173
0.0224	4.6190
0.0447	4.6229
0.0671	4.6295
0.0894	4.6387
0.1118	4.6506
0.1342	4.6652
0.1565	4.6827
0.1789	4.7041
0.2012	4.7338
0.2236	4.7925
Flux = 0.938	

END OF THE CONTRACTION

x = 2.2375H	
$\frac{y}{H}$	$\frac{q}{U_1}$
0.0000	4.6924
0.0224	4.6924
0.0447	4.6924
0.0671	4.6925
0.0894	4.6926
0.1118	4.6926
0.1342	4.6927
0.1565	4.6929
0.1789	4.6931
0.2012	4.6934
0.2236	4.6937
Flux = 0.938	

5 : 1 CONTRACTION

TABLE 6.10b

$\frac{x}{H}$	$\frac{y}{H}$	WALL VELOCITY $\frac{q}{U_1}$
0.0000	0.5000	1.0417
0.2125	0.5000	1.0392
0.3725	0.5000	1.0186
0.4625	0.5000	1.0091
0.5275	0.5000	1.0019
0.5833	0.5000	0.9969
0.6333	0.5000	0.9986
0.6833	0.5000	1.0055
0.7333	0.4996	0.9710
0.7832	0.4970	1.0056
0.8330	0.4926	0.9610
0.8827	0.4869	0.9081
0.9322	0.4795	0.9376
0.9813	0.4705	0.9914
1.0301	0.4594	1.0025
1.0789	0.4461	1.0305
1.1263	0.4303	1.1088
1.1725	0.4113	1.1414
1.2168	0.3882	1.2488
1.2567	0.3584	1.2053
1.2922	0.3231	1.5693
1.3276	0.2878	2.1853
1.3664	0.2554	4.0694
1.4125	0.2363	4.5711
1.4609	0.2242	4.9022
1.5103	0.2162	5.1304
1.5600	0.2110	5.2895
1.6099	0.2077	5.3860
1.6598	0.2055	5.5572
1.7086	0.2044	5.4960
1.7573	0.2041	5.5201
1.8105	0.2041	5.4826
1.8605	0.2041	5.4713
1.9102	0.2041	5.4660
1.9629	0.2041	5.4619
2.0224	0.2041	5.4595

$\frac{x}{H}$	CENTRE LINE VELOCITY $\frac{q}{U_1}$
0.0000	0.9966
0.1375	0.9950
0.2375	0.9944
0.3375	0.9947
0.4375	0.9972
0.5375	1.0038
0.6375	1.0185
0.7375	1.0478
0.8375	1.1027
0.9375	1.2018
1.0375	1.3792
1.1375	1.6981
1.2375	2.2545
1.3375	3.0958
1.4375	4.0408
1.5375	4.7805
1.6375	5.2082
1.7375	5.3958
1.8375	5.4522
1.9375	5.4634
2.0375	5.4651
2.1375	5.4650

6 : 1 CONTRACTION

TABLE 6.11a

x = 0.7208H	
$\frac{y}{H}$	$\frac{q}{U_1}$
0.00	1.0429
0.05	1.0401
0.10	1.0354
0.15	1.0292
0.20	1.0202
0.25	1.0094
0.30	0.9972
0.35	0.9840
0.40	0.9701
0.45	0.9565
0.50	0.9455
Flux = 0.986	

BEGINNING OF THE CONTRACTION

x = 1.7198H	
$\frac{y}{H}$	$\frac{q}{U_1}$
0.0000	5.3626
2.0204	5.3768
0.0408	5.3814
0.0612	5.3893
0.0816	5.4001
0.1021	5.4141
0.1225	5.4314
0.1429	5.4521
0.1633	5.4774
0.1837	5.5122
0.2041	5.5810
Flux = 0.910	

END OF THE CONTRACTION

x = 2.7375H	
$\frac{y}{H}$	$\frac{q}{U1}$
0.0000	5.4500
0.0204	5.4500
0.0408	5.4500
0.0612	5.4500
0.0816	5.4501
0.1021	5.4502
0.1225	5.4508
0.1429	5.4522
0.1633	5.4566
0.1837	5.4700
0.2041	5.4995
Flux = 0.910	

6 : 1 CONTRACTION

TABLE 6.11b

$\frac{x}{H}$	$\frac{y}{H}$	WALL VELOCITY $\frac{q}{U_1}$
0.0000	0.5000	1.1128
0.2125	0.5000	1.0910
0.3725	0.5000	1.0423
0.4625	0.5000	1.0279
0.5275	0.5000	1.0171
0.5833	0.5000	1.0100
0.6333	0.5000	1.0150
0.6833	0.5000	1.0229
0.7333	0.4999	1.0847
0.7833	0.4980	0.9358
0.8331	0.4942	0.9544
0.8799	0.4893	0.9263
0.9294	0.4826	1.0517
0.9787	0.4742	1.0991
1.0277	0.4640	1.0887
1.0761	0.4517	1.0820
1.1239	0.4370	1.0794
1.1715	0.4190	1.0828
1.2153	0.3984	1.6488
1.2570	0.3722	1.9895
1.2949	0.3371	1.0924
1.3313	0.3007	1.7128
1.3638	0.2682	2.2768
1.3963	0.2357	3.0329
1.4288	0.2032	4.1768
1.4622	0.1716	6.8161
1.5051	0.1460	11.3488
1.5543	0.1346	12.2156
1.6032	0.1289	12.9045
1.6524	0.1261	13.3159
1.7024	0.1251	13.3899
1.7539	0.1250	13.1824
1.8056	0.1250	13.0955
1.8556	0.1250	13.0467
1.9050	0.1250	13.0094
1.9625	0.1250	12.9496
2.0225	0.1250	12.8953

$\frac{x}{H}$	CENTRE LINE VELOCITY $\frac{q}{U_1}$
0.0000	1.0690
0.1375	1.0643
0.2375	1.0610
0.3375	1.0581
0.4375	1.0566
0.5375	1.0577
0.6375	1.0636
0.7375	1.0789
0.8375	1.1115
0.9375	1.1756
1.0375	1.2999
1.1375	1.5513
1.2375	2.0981
1.3375	3.3468
1.4375	6.0427
1.5375	9.8290
1.6375	12.1741
1.7375	12.8662
1.8375	12.5009
1.9375	12.9485
2.0375	12.9473

16 : 1 CONTRACTION - AVERAGED COEFFICIENT

TABLE 6.12a

x = 0.7208H	
$\frac{y}{H}$	$\frac{q}{U_1}$
0.00	1.0539
0.05	1.0518
0.10	1.0469
0.15	1.0390
0.20	1.0285
0.25	1.0160
0.30	1.0018
0.35	0.9862
0.40	0.9689
0.45	0.9469
0.50	0.9261
Flux = 0.985	

BEGINNING OF THE CONTRACTION

x = 1.7149H	
$\frac{y}{H}$	$\frac{q}{U_1}$
0.0000	13.0046
0.0125	13.0082
0.0250	13.0171
0.0375	13.0319
0.0500	13.0525
0.0625	13.0787
0.0750	13.1104
0.0875	13.1476
0.1000	13.1900
0.1125	13.2326
0.1250	13.2751
Flux = 0.822	

END OF THE CONTRACTION

x = 2.2375H	
$\frac{y}{H}$	$\frac{q}{U_1}$
0.0000	12.7279
0.0125	12.7280
0.0250	12.7285
0.0375	12.7292
0.0500	12.7303
0.0625	12.7316
0.0750	12.7333
0.0875	12.7353
0.1000	12.7375
0.1125	12.7384
0.1250	12.7396
Flux = 0.796	

16 : 1 CONTRACTION - AVERAGED COEFFICIENTS

TABLE 6.12b

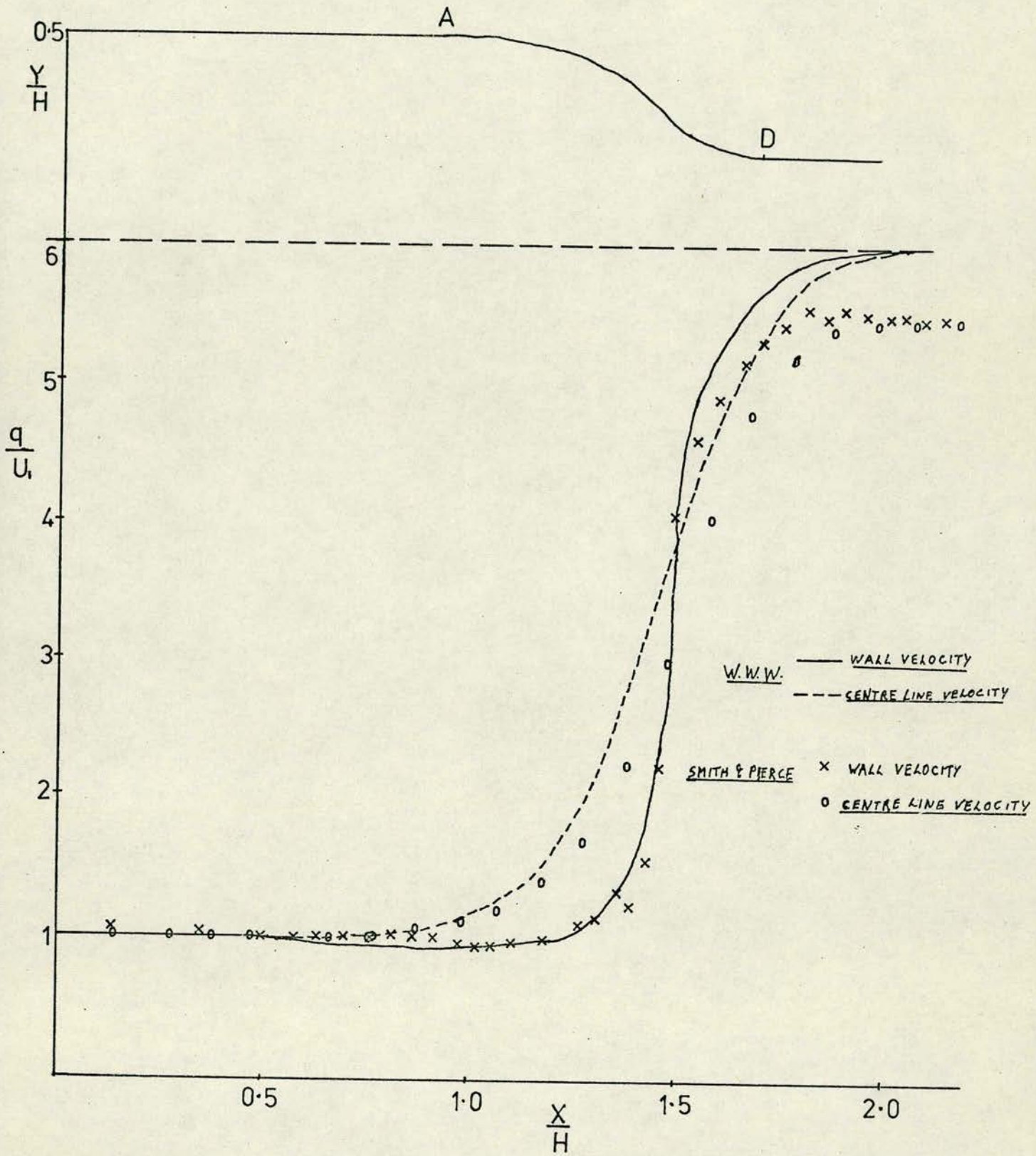
A
D
0·5
Y/H
6
5
4
3
2
1
q/U₁
0·5
1·0
1·5
2·0
X/H
W.W.W.
WALL VELOCITY
CENTRE LINE VELOCITY
SMITH & PIERCE
WALL VELOCITY
CENTRE LINE VELOCITY

FIGURE (6.5)

to obtain. From previous experiments using different numbers of intervals, it was not thought that the 224 interval solution would improve the accuracy significantly enough to justify the extra computer work and that the problem of leakage would need to be solved in some other more efficient way - possibly by the development of a higher order solution as in the two-dimensional case. The 224 interval solution was thus abandoned.

Calculating the flux through the contraction is only of limited value as a check on the accuracy of the solution since, just as there is leakage from the duct, there is a certain small amount of leakage from the outside of the contraction into the internal flow. Using the results from the averaged method for Jordinson's 16:1 contraction, the flux across planes passing through B, C, and E in figure (6.3) was 98.5%, 80% and 82% respectively. From these results it can be seen that most of the flux is lost on the surface BC which is concave to the flow while a small amount of fluid is gained - or created - on the surface CE which is convex to the flow.

The results obtained for the various axisymmetric contractions are shown in tables (6.9), (6.10), (6.11), (6.12). Figure (6.5) shows the centre line and wall velocity obtained using this method for a contraction ratio of 6:1 compared with the results obtained using W.W.W.'s method.

6.7 The Calculated Source Distribution

For flow inside or outside closed bodies, an essential condition on the surface distribution of singularities is that the integral of the source strength over the body surface must be zero. This statement of /

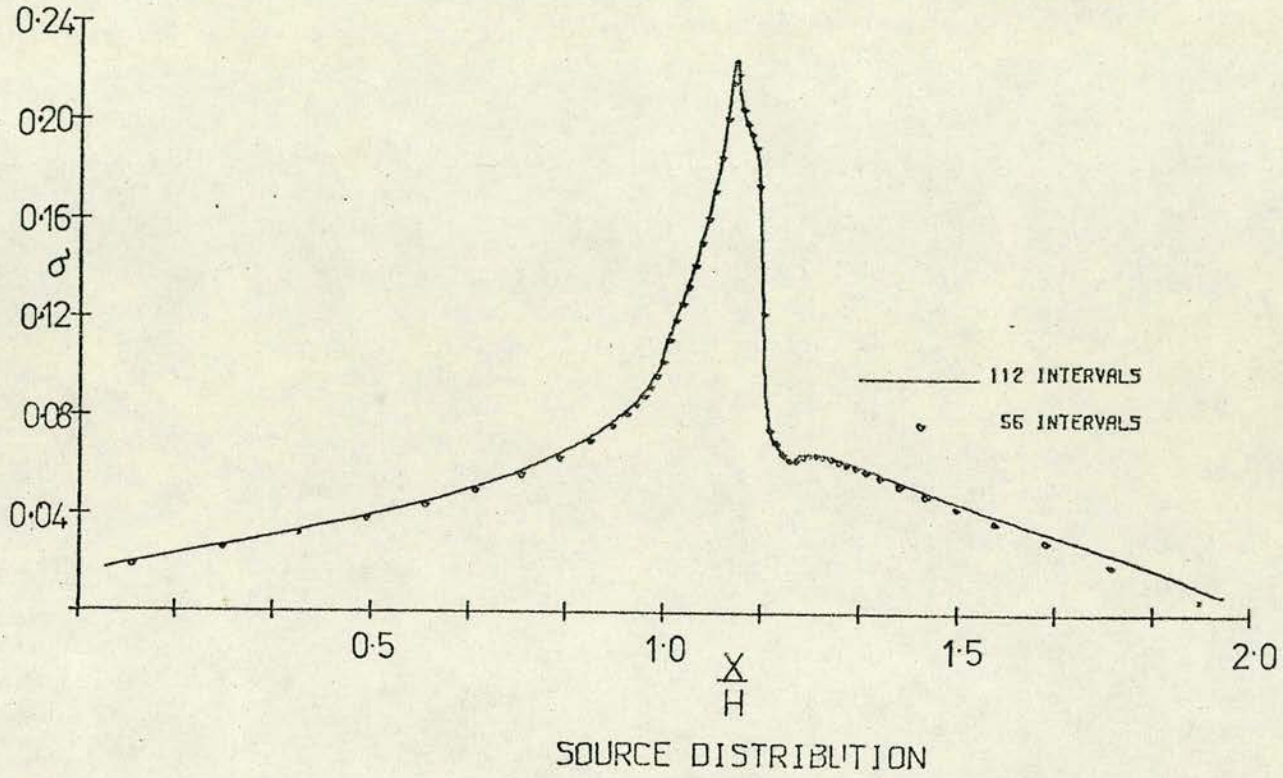
0·24
0·20
0·16
σ
0·12
0·08
0·04
0·5
1·0
X/H
1·5
2·0
112 INTERVALS
56 INTERVALS
SOURCE DISTRIBUTION

FIGURE (6.6)

of mass conservation is also given by Kellog as "the Neumann problem is solvable under the essential condition that the integral over the bounding surface of the values assigned to the normal derivative vanishes". Therefore, for flows concerning closed bodies divided into a finite number of intervals, the condition

$$\sum_{i=1}^{n} \sigma_i = 0 \qquad (6.1)$$

provides either a useful check on the accuracy of the solution or, alternatively, another equation from which the source distribution can be determined. For open bodies such as ducts or when only part of a body surface is used, there may be a net flow leaving the body and going to ∞ . Thus, as previously stated, the duct must be thought of as being infinite in length and equation (6.1) no longer holds. The singularity distributions calculated for all the ducts - two-dimensional and axisymmetric - was found to consist entirely of sources.

The source distribution was most sensitive to length of parallel section and not so sensitive to the variation of interval length. For example, figure (6.6) illustrates the source distribution calculated for the same length of parallel sections but for 112 interval and 56 interval solutions for Jordinson's two-dimensional 4:1 contraction. It can be seen that the source distributions for both solutions are very similar as might be expected since this source distribution should be unique for any given surface.

6.8 Computing

All programmes were written in IMP - a development of Atlas Autocode - /

Autocode - and were run at the Edinburgh Regional Computing Centre. Initially the computers used were an IBM 365/50 and an ICL 4/70. Later work including that of this chapter was done on an ICL 4/75 using the Edinburgh Multi-Access System. In addition, most of the graphs in this thesis were drawn by a graph plotter attached to an IBM 370/158.

As previously mentioned, the same lengths of parallel section with the same distribution of elements were used for all contractions. In order to obtain the boundary points for a complete duct, a programme was written which, when given the coordinates of the contraction, used linear interpolation and an iterative procedure to divide the contraction into intervals of equal curve length (approximately 0·025H in all cases). Linear interpolation was sufficiently accurate since the contraction coordinates were initially obtained at very small intervals. The programme then added the parallel sections at each end and returned the boundary points for the complete duct. The different contractions varied only slightly in length and initially it was convenient to adjust the length of the parallel sections by a small amount to obtain a total of 113 boundary points for a 112 interval solution. Because of the time required to calculate the influence matrices X_{ij} and Y_{ij} - especially in the axisymmetric case - it was convenient to split the computation of the source distribution into two parts. In the two-dimensional case, the first programme calculated the influence matrices X_{ij} and Y_{ij} and mapped each onto a file. In the axisymmetric case, because of time restrictions placed on programmes, two programmes were used to calculate X_{ij} and Y_{ij}. One calculated the diagonal elements X_{ii} and Y_{ii} and the other calculated the remaining elements in the influence matrices. /

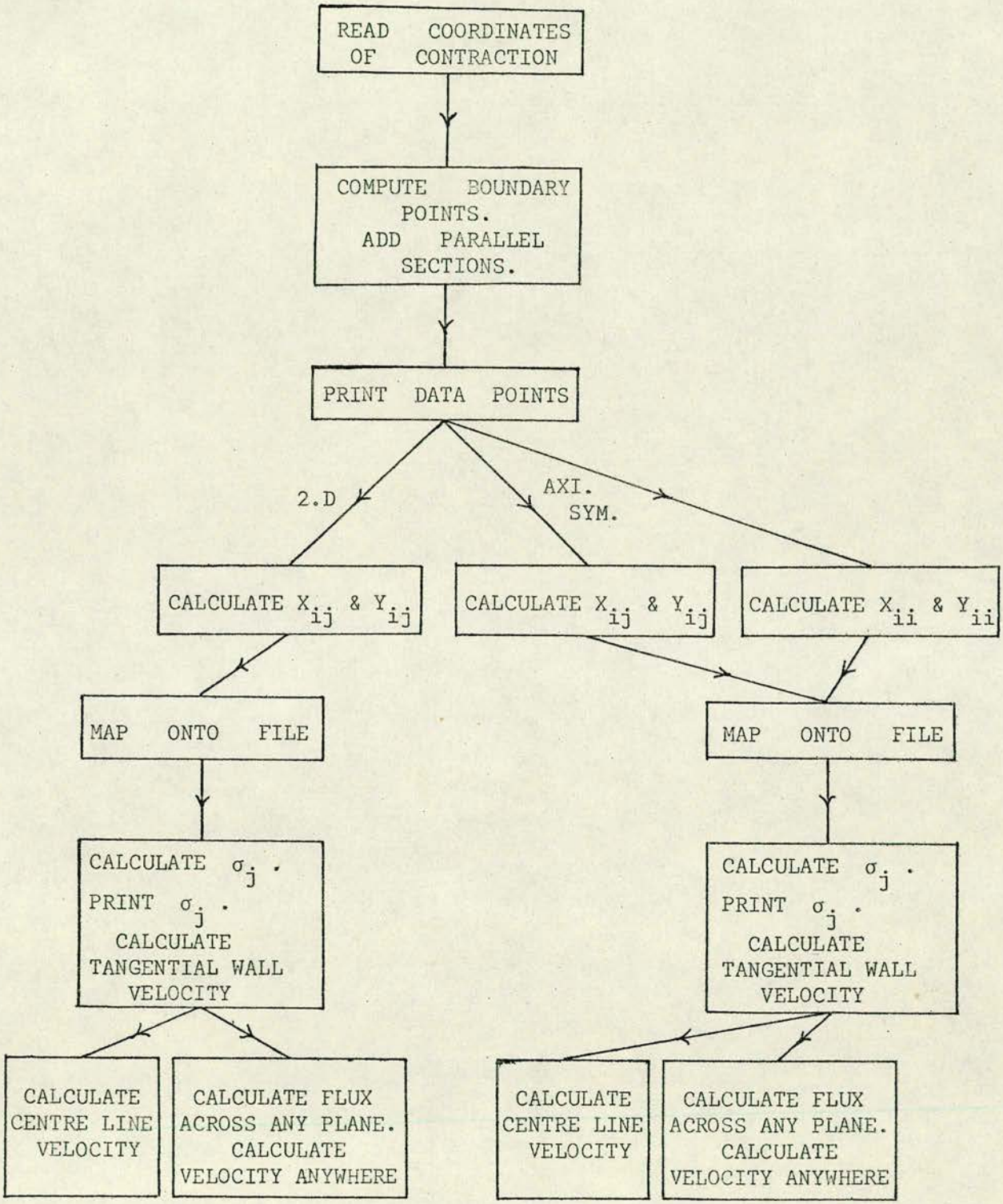
READ COORDINATES OF CONTRACTION
COMPUTE BOUNDARY POINTS. ADD PARALLEL SECTIONS.
PRINT DATA POINTS
2.D
AXI. SYM.
CALCULATE X_{ij} & Y_{ij}
CALCULATE X_{ij} & Y_{ij}
CALCULATE X_{ii} & Y_{ii}
MAP ONTO FILE
MAP ONTO FILE
CALCULATE σ_j .
PRINT σ_j .
CALCULATE TANGENTIAL WALL VELOCITY
CALCULATE σ_j .
PRINT σ_j .
CALCULATE TANGENTIAL WALL VELOCITY
CALCULATE CENTRE LINE VELOCITY
CALCULATE FLUX ACROSS ANY PLANE. CALCULATE VELOCITY ANYWHERE
CALCULATE CENTRE LINE VELOCITY
CALCULATE FLUX ACROSS ANY PLANE. CALCULATE VELOCITY ANYWHERE

FIGURE (6.7)

matrices. Both of these programmes mapped the matrix elements onto the same file. In this way, a permanent record of the influence matrices was kept. Mapping the elements of the matrices onto a file in this way was more efficient than using input and output streams and allowed any element to be accessed at any time and as often as required in a programme in the same way as an element of an array declared in a programme. Thus, it was not necessary to have the matrices X_{ij} and Y_{ij} stored in arrays in any of the programmes. A further programme in each case then calculated the source density distribution and the tangential wall velocity. From the source distribution, the centre line velocity and the velocity at any point in the stream - including the flux across any plane - were calculated using a further two programmes in each case. The programme chart in figure (6.7) illustrates how the programmes were used.

It should be noted that a boundary of 113 points gives 112 intervals on the meridian curve and therefore 112 linear equations to be solved in the axisymmetric case. In the two-dimensional case, however, there are two separate curves to the duct - above and below the centre line - and so there are in fact 224 intervals. The programme made use of the symmetry in the latter case and still obtained 112 equations to be solved for the 112 different values of the source strength because if σ_i is the source strength on the i^{th} element then

$$\sigma_i = \sigma_{225-i} \qquad i = 1, 2, \ldots, 224 \quad .$$

Thus, the calculation of each of the matrices X_{ij} and Y_{ij} required (112×112) calculations in the axisymmetric case and (112×224-112) in the two-dimensional case. (In the latter case, the value of the diagonal elements X_{ii} and Y_{ii} are known - see section (5.4) - and can be mapped directly onto the file.) In addition, from the symmetry

$$X_{ij} = /$$

$$X_{ij} = X_{225-j,\ 225-j}$$

$$Y_{ij} = -Y_{225-j,\ 225-j}$$

for

$$i = 1, 2, 3, \ldots 224 \quad \text{and} \quad j = 1, 2, 3, \ldots 224 \quad .$$

In the two-dimensional case, the equations to be solved for the source distribution (5.28) can be written

$$V_\infty \sin(\alpha_i) = A_{ij}\ \sigma_j$$

where

$$A_{ij} = -X_{ij} \sin(\alpha_i) + Y_{ij} \cos(\alpha_i) \quad .$$

Similarly, in the axisymmetric case, equations (5.54) can be written as

$$V_\infty \sin(\alpha_i) = A_{ij}\ \sigma_j$$

where

$$A_{ij} = -X_{ij} \sin(\alpha_i) + Y_{ij} \cos(\alpha_i)$$

for $i \neq j$ and

$$A_{ii} = -X_{ii} \sin(\alpha_i) + Y_{ii} \cos(\alpha_i) - 2\pi \quad .$$

In both cases, the matrix A_{ij} is diagonally dominant which helps to give a fast solution using an IMP library routine. The routine - called IMP DLEQSP - solves in double precision, a system of linear equations by first scaling the matrix of coefficients so that the maximum of the modulii of the elements in each row and column is 1 . The routine then performs Gaussian elimination with complete pivoting to produce the required triangular forms from which the solution is obtained by rescaling and back substitution. This routine required approximately 80 seconds to solve 112 equations.

Most /

Most of the numerical integrations in the earlier chapters were performed by a routine which used Simpson's rule successively increasing the number of nodal points until two results agreed to within a specified accuracy. For the integrations of this chapter, however, a second library routine - called IMP DGALEG - evaluated in double precision the integral of a function of one variable over a closed bounded interval to a specified accuracy (ε) using Gaussian quadrature. The routine calculated five and six point approximations I5 and I6. If

$$|I5 - I6| < \varepsilon$$

the value of I6 was returned as the result. If not, the interval was halved and the method applied to each half. The accuracy test was then applied to the sum of the contributions from each half. This process continued until either the required accuracy was achieved or, failing that, until a specified number of subintervals had been constructed when the routine stopped, returning I6 together with an estimate of the accuracy. A warning message was also printed in this second case.

The complete elliptic integrals required in the calculation of the axisymmetric influence matrices were evaluated using the library routines DCEL1 and DCEL2 . These double precision routines were written in FORTRAN but calling them from an IMP programme presented no additional difficulties.

It has already been stated that the calculation of the two-dimensional influence matrices required approximately 160 seconds of c.p.u. time on the ICL 4/75 for 112 intervals. The time required for the axisymmetric influence matrices was considerably longer being approximately 22 minutes for the diagonal elements and 15 minutes for the remainder of the elements for a 112 interval solution. The time required to calculate /

calculate the centre line velocity at 89 points was 37 seconds in the two-dimensional case and 137 seconds in the axisymmetric case.

6.9 CONCLUSIONS

The calculation of flows through two-dimensional contractions using the method of Smith and Pierce has proved very successful, providing an accurate as well as efficient way of calculating two-dimensional duct flow. Thus, given the boundary curve of a contraction, the wall and centre line velocities and the velocity profile can be obtained quickly using relatively short programmes. The method for the calculation of axisymmetric duct flow, although fairly successful for the smaller contraction ratios, would not provide a reliable or accurate solution to general contraction calculations. The modification of the method of Smith and Pierce described in section (6.6) increased the accuracy for Jordinson's 16:1 contraction by about 5% and, if applied to the smaller contraction ratio ducts, could possibly improve the accuracy to that achieved for the two-dimensional ducts. This is still not a satisfactory method for general axisymmetric contractions. The problem of leakage in the axisymmetric case is severe and the method requires improving probably by the development of a higher order solution as in the two-dimensional case.

It was hoped that using this method together with an iterative procedure, an axisymmetric contraction could be designed with a specified wall velocity. Even neglecting the problem of leakage, the computing time for such a programme could be prohibitive.

CHAPTER 7

CONCLUSIONS

When designing a wind tunnel contraction - either two-dimensional or axisymmetric - it should be decided whether to design a contraction of finite or infinite length. At the expense of increased length, the errors introduced by truncating an infinite contraction and adding parallel sections could be made quite small but, since in practice contractions are finite in length, it is more accurate and more satisfying to design a contraction of finite length from the start. The methods of designing contractions of finite length are not numerous and have been considered already. The two-dimensional contraction described by Gibbings and Dixon and Jordinson has already proved satisfactory in practice for certain contraction ratios and adverse pressure gradients. From a practical point of view, since the velocity distribution inside a contraction is quite sensitive to wall shape, this contraction could simplify an accurate construction since it is basically two curved walls joined by a straight section at a fixed angle to the axis. Building such a contraction should therefore be easier than building one with a more elaborate continuous curve for a wall shape (cf. W.W.W. figure (2.7)) .

Jordinson's treatment of the contraction suggests that it is possible to build and match several downstream parts to one upstream part to vary either the contraction ratio or the adverse pressure gradient at the downstream end or vice versa. Thus, for a two-dimensional finite length contraction, Jordinson's design proves to be quite /

quite versatile. In the light of the results of Chapter 3, it can be seen that Jordinson's design proves equally versatile as an axisymmetric contraction. For, using the method of W.W.W., the axisymmetric velocity distribution in the upstream part for a given adverse pressure gradient and any contraction ratio can be found. The axisymmetric velocity distribution in the downstream part for a given adverse pressure gradient can be tabulated in terms of the variable h/H. Thus, when a contraction ratio (K = H/h) has been chosen, the predicted axisymmetric velocity distribution in the downstream part can be found from the table. By performing a few calculations for different adverse pressure gradients at each end, it is now possible to prepare a few tables such that the predicted axisymmetric velocity distribution can be found for various upstream and downstream conditions and infinitely many contraction ratios by simply consulting the tables and matching different upstream and downstream parts. For example, tables (3.2) and (3.3) are for the upstream part for one adverse pressure gradient and tables (3.4) and (3.5) show the velocities for the downstream part for a given adverse pressure gradient and any contraction ratio H/h. In particular, they show the results for contraction ratios of 16:1 and 6:1 by area.

The method of Smith and Pierce described in Chapters 5 and 6 provides an accurate and easily obtainable solution to the flow through a given contraction in two-dimensions. It should be noted that although the calculation of the wall velocity distribution was split into two parts for convenience in this work, the complete problem could have been solved using one programme.

Previously, /

Previously, after designing a contraction to behave in a certain way, the boundary coordinates were often displaced by the estimated boundary layer thickness in an attempt to make the constructed contraction behave as closely as possible to the design conditions. However, from recent work in boundary layer development, it is now possible to calculate the approximate boundary layer growth once the wall velocity is known. One method of calculating the boundary layer growth iterates between the potential and boundary layer solutions and the method of Smith and Pierce is very suitable for obtaining the potential flow solution.

Nothing has been said so far of the effect of compressibility. An estimate of the effect of the compressibility of air on the results obtained from the methods of this thesis could be made by using a transformation such as the Karman-Tsien rule. However, the magnitudes of the velocities arising in low speed contractions are such as to make any compressibility effect negligibly small.

SUGGESTIONS FOR FURTHER RESEARCH

The inaccuracies in the method of Smith and Pierce for calculating flows through axisymmetric contractions have already been described. The development of a more accurate higher order solution could, however, provide a powerful method of obtaining the solution to duct flow and it is hoped that more work will be done in this field.

The calculation of the boundary layer development in contractions also requires further attention - especially in the axisymmetric case - and, perhaps using the method of Smith and Pierce to obtain the potential flow solution, it is hoped that further work will simplify the /

the calculation of the boundary layer development.

In conclusion, it is hoped that this thesis has eliminated some of the magic involved in the design of contractions and that use will be made of the method and tables of Chapter 3 to build axisymmetric contractions of finite length with a known wall and centre line velocity distribution.

REFERENCES

1. Bradshaw, P. and R.C. Pankhurst "The design of low speed wind tunnels". NPL Aero. Report No. 1039.

2. Dawson, C.W. and J.S. Dean "The XYZ potential flow program". Dept. of the Navy, Naval Ship Research and Development Centre, Report No. 3892, June 1972.

3. Gibbings, J.C. and J.R. Dixon "Two Dimensional Contracting Duct Flow". Quart. Journ. Mech. and Applied Math., Vol. 10, pt. 1, 1957.

4. Hess, J.L. "Numerical Solution of the Integral Equation for the Neumann Problem with Application to Aircraft and Ships". Douglas Aircraft Co., Engineering Paper No. 5987, 1971.

5. Hess, J.L. "High Order Numerical Solution of the Integral Equation for the Two-Dimensional Neumann Problem". Computer Methods in Applied Mech. and Eng., 2, 1973.

6. Hughes, N.J.S. "Two-Dimensional Constant Velocity Ducts". A.R.C. R. & M. No. 2089, Dec. 1944.

7. Jahnke, J. and Emde F. "Tables of Functions with formulae and Curves". (American Ed.) 1943.

8. Jeppson, R.W. "Inverse Formulation and Finite Difference Solution for Flow from a Circular Orifice". Journ. Fluid Mech. 1970, Vol. 40, pt. 1.

9. Jordinson, R. "Design of Wind Tunnel Contractions". Air. Eng. 33, 299 (1961).

10. Kellog, O.D. "Foundations of Potential Theory". Frederick Ungar Publ. Co. (1929).

11. Lamb, H. "Hydrodynamics". Cambridge University Press (1932).

12. Lighthill, M.J. "A New Method of Two-Dimensional Aerodynamic Design" A.R.C. R. & M. 2112 (1945).

13. Milne-Thomson, L.M. "Theoretical Hydrodynamics". 2nd Edition, 1949.

14. Mooljee, N.K. "Numerical Verification of an exact solution in the design of a Two-Dimensional Wind Tunnel Contraction". Thesis submitted for Post-graduate Diploma in Fluid Dynamics, University of Edinburgh, (1971).

15. Smith, A.M.O. and J. Pierce "Exact Solution of the Neumann Problem Calculation of Non-circulatory Plane and Axially Symmetric Flows About or Within Arbitrary Boundaries". Douglas Aircraft Co. Report No. ES 26988, April 1958.

16. Schlichting, H. "Boundary Layer Theory". McGraw-Hill Publ. (1960).

17. /

17. Thwaites, B. "On the Design of Contractions for Wind Tunnels". A.R.C. R. & M. No. 2279, March 1946.

18. Tsein, H.S. "On the Design of the Contraction Cone for a Wind Tunnel". Journ, Aero. Sciences, 10, (2), 1943.

19. Whitehead, L.G., L.Y. Wu and M.H.L. Waters "Contracting Ducts of Finite Length". Aero. Quart. Feb. 1951.

20. Wooding, R.A. "An Approximate Transformation for Plane and Axisymmetric Potential Flows". Australian Journ. Applied Sciences, 1964, 15.

LIST OF SYMBOLS

(R,θ)	Polar coordinates
(X,Y,Z)	Cartesian coordinates
(ξ,η,ζ)	Cartesian coordinates of variable point of integration
Y	Distance perpendicular to x-axis
r	Distance between two points
S	Distance measured along a surface
U_1	Velocity upstream of contraction
U_2	Velocity downstream of contraction
U_P	Velocity of a point P
V_A	Axisymmetric velocity
V_T	Two-dimensional velocity
V_∞	Uniform velocity at infinity
(U,V)	Velocity components
$q = U-iV$	Complex velocity
q	Magnitude of the velocity
ℓ_1,ℓ_2	Constants
$T = qe^{\ell_1}/U_1$	Non-dimensional velocity
$Z = X+IY$	Complex variable
α	Two-dimensional velocity potential
β	Two-dimensional stream function
ϕ	Axisymmetric velocity potential
ψ	Axisymmetric stream function
$W = \alpha+i\beta$	Complex velocity potential
$\zeta = \log\left(\frac{dW}{dZ}\right)$	Logarithmic hodograph plane
A_{ij},X_{ij},Y_{ij}	Influence matrices
H	Width of contraction at the upstream end
h	Width of contraction at the downstream end
K	Contraction ratio
k	Modulus of the complete elliptic integrals
$K(k)$ /	

$K(k)$	The complete elliptic integral of the first kind
$E(k)$	The complete elliptic integral of the second kind
m	Source strength
σ	Surface source density
θ, α	Angular measures
C_p	Pressure coefficient
b, c	Constants defined in Chapter 5
i, j, n	Integers
$\frac{\partial}{\partial n}$	Derivative in the direction of the normal to a surface

ON AN APPROXIMATION TO THE FLOW THROUGH AXI-SYMMETRIC CONTRACTING DUCTS

R. JORDINSON AND J.G. RODGER

(Department of Mathematics, University of Edinburgh)

(Hydraulics Research Station, Wallingford, Berks)

Reprinted from THE AERONAUTICAL QUARTERLY VOL.XXXII FEBRUARY 1981

Printed by Technical Editing and Reproduction Ltd, Harford House, 7-9 Charlotte St, London, W1P 1HD, and Published by the Royal Aeronautical Society, 4 Hamilton Place, London, W1V 0BQ

ON AN APPROXIMATION TO THE FLOW THROUGH AXI-SYMMETRIC CONTRACTING DUCTS

R. JORDINSON AND J.G. RODGER

(Department of Mathematics, University of Edinburgh) *(Hydraulics Research Station, Wallingford, Berks)*

Summary: A method is given for the calculation of incompressible, inviscid flow through an axi-symmetric contracting duct for which the two dimensional flow with the same meridianal boundaries is known. The method, which is based on Whitehead, Wu and Waters original proposal, assumes that the contraction consists of two separate portions, upstream and downstream respectively. The flow in each portion is calculated and the two portions matched to produce a contraction of given area ratio with preassigned values of the two dimensional 'overshoot' and 'undershoot' parameters. It is worth emphasizing that in practice it is only necessary to do the calculations once to predict wall velocities for a family of contraction shapes with different area ratios provided they share a common upstream or downstream portion. The results given here show reasonable agreement with the pressure coefficients obtained in experiment for the upstream end of a small scale contraction of area ratio 16:1. There is however a discrepancy between theory and experiment at the downstream end and a qualitative explanation is advanced for this.

1. Introduction

The recent paper by Laidler & Walkden[1] prompts the present authors to describe an alternative, though approximate method of designing an axisymmetric contraction which is possibly simpler to apply in practice. The basis of this method is to treat the flows in the upstream and downstream portions of the contraction as separate and to match the portions appropriately to define a contraction of given inlet/exit area ratio. This method has been successfully applied to two dimensional contractions (see Jordinson[2]) and it seems reasonable to extend this to the axisymmetric case.

To obtain the flows through the two separate axisymmetric portions from the equivalent two dimensional contraction the well known method of Whitehead, Wu and Waters[3] is used. The basis of this method is an approximation to the equation which relates the two dimensional and axisymmetric flows through a duct with the same meridianal shape. This equation is

$$\frac{\partial}{\partial\alpha}\left\{\frac{1}{y}\frac{\partial\psi}{\partial\alpha}\right\}+\frac{\partial}{\partial\beta}\left\{\frac{1}{y}\frac{\partial\psi}{\partial\beta}\right\}=0 \qquad (1)$$

Received December 1979; revision received August 1980

where ψ is the axisymmetric stream function and α,β the velocity potential and stream function respectively for the plane flow. Whitehead, Wu and Waters argue that since the streamlines of the two flows do not differ greatly in shape, derivatives of ψ with respect to α will be much smaller than those with respect to β. Thus (1) reduces to

$$\frac{\partial}{\partial\beta}\left\{\frac{1}{y}\frac{\partial\psi}{\partial\beta}\right\} = 0, \text{ so that } \frac{1}{y}\frac{\partial\psi}{\partial\beta} = f(\alpha).$$

Applying the same approximation to the relation between the two dimensional and axisymmetric velocities q_T and q_A respectively leads to the relation

$$\frac{q_A}{q_T} = f(\alpha) = \frac{1}{y}\frac{\partial\psi}{\partial\beta} \tag{2}$$

where $f(\alpha)$ is a function to be determined.

Hence, according to this approximation, on an equipotential line q_A is a constant multiple of q_T, so that given the two dimensional velocity distribution the axisymmetric one can be calculated, provided $f(\alpha)$ is known. From (2), integrating on an equipotential line gives

$$\frac{U_1H^2}{8} = f(\alpha)\int_{-U_1H/2}^{0} y\,d\beta \tag{3}$$

where the duct has upstream width H. It has been assumed that $\psi = 0$, $\beta = 0$ on the wall, the values on the centre line being $-U_1H^2/8$ and $-U_1H/2$ respectively.

2. Notation

H	diameter of upstream parallel section
h	diameter of downstream parallel section
$e^{-\ell_1}$	undershoot parameter on two dimensional upstream curved section BC ($\ell_1 > 0$)
e^{ℓ_2}	overshoot parameter on two dimensional downstream curved section DE ($\ell_2 > 0$)
m	source strength in hodograph solution ($= U_1H/2\pi$)
n	π/n angle of inclination of straight section to axis
q_A	axisymmetric fluid speed at a point
q_T	two dimensional fluid speed at the same point
s	arcual distance along an equipotential α = constant
U_1	speed at infinity in upstream parallel section
U_2	speed at infinity in downstream parallel section
x,y	coordinates for two dimensional and axisymmetric flows

$x_i (i=1(1)4)$	local coordinates for curved sections
C_p	non dimensional pressure coefficient $= \dfrac{q_A^2 - U_1^2}{U_2^2 - U_1^2}$
α, β	velocity potential, stream function for two dimensional flow
ψ	axisymmetric stream function
θ	angle of inclination of a streamline in two dimensions
η	$= q_T e^{\ell_1}/U_1$ - dimensionless speed in upstream portion
ξ	$= q_T e^{-\ell_2}/U_2$ - dimensionless speed in downstream portion
ζ	logarithmic hodograph variable

3. Calculation of f(α)

To find f(α) the solution for the two dimensional contraction given by Jordinson (op cit) has been used. The independent upstream and downstream portions of the contraction are shown in figures 1a and 1b, the solution in each being found by working in the hodograph plane.

($\zeta = \ell n \dfrac{U_r}{q_T} + i\theta$, where r = 1,2 respectively for upstream and downstream portions). The curved sections in both upstream and downstream portions are designed to have constant velocities along them. The velocity ratios $e^{-\ell_1}$ and e^{ℓ_2} determine the magnitude of the adverse pressure gradients (near the inlet and exit planes) which are bound to be present in any finite length contraction. The choice of ℓ_1 and ℓ_2 implies some control over the 'undershoot' and 'overshoot' (the usual terms for these adverse pressure gradients). The table given later shows how the two dimensional constant velocities are modified in the axisymmetric case.

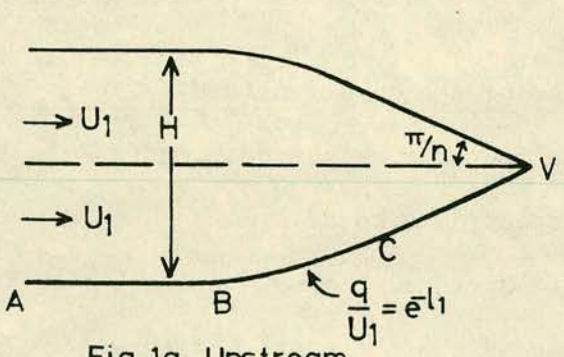

Fig.1a Upstream

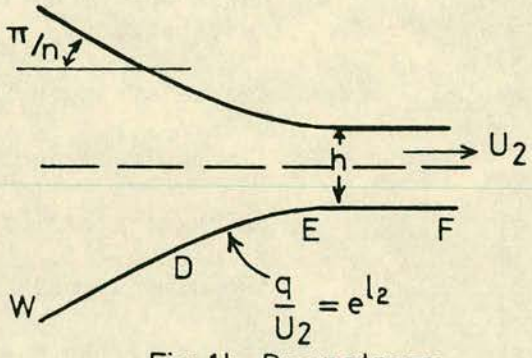

Fig.1b Downstream

In the solution for the upstream portion α and β are found to be given by

$$e^{\frac{\alpha + i\beta}{m}} = \sinh^2 \frac{n\ell_1}{2} - \sinh^2 \left\{ \frac{n(\ell_1 - \zeta)}{2} \right\} \qquad (4)$$

where $U_1 e^{-\ell_1}$ is the velocity on the curved portion ($\ell_1 > 0$), π/n the acute angle of inclination of the straight portion to the axis, m the source strength in the hodograph plane ($= U_1 H/2\pi$) and $\zeta = \ell n\, U_1/q_T + i\theta$. Separating (4) into real and imaginary parts gives

$$e^{\alpha/m} \cos \beta/m = \cosh(n\ell_1/2) - (\eta^n + \eta^{-n})\cos(n\theta)/4 \qquad (5)$$

and

$$e^{\alpha/m} \sin \beta/m = (\eta^n - \eta^{-n}) \sin(n\theta)/4 \qquad (6)$$

where $\eta = q_T\, e^{\ell_1}/U_1$, is the dimensionless velocity upstream. To evaluate the integral in (3) y must be known as a function of β and this can be achieved by differentiating (5) and (6) with respect to s, the distance along an equipotential line, keeping α fixed. In the resulting pair of equations, the elimination of $d\theta/ds$ followed by the use of the equations $dy/ds = \cos\theta$ (on an equipotential) and $d\beta/ds = q_T = U_1 \eta e^{-\ell_1}$ gives

$$\frac{1}{H}\int_o^y dy = \frac{n e^{\ell_1 - \alpha/m}}{8\pi} \int_{\eta_o}^{\eta} \frac{(\eta^{2n} + \eta^{-2n} - 2\cos 2n\theta)\cos\theta\, d\eta}{\eta^2\{\eta^n \sin(n\theta + \beta/m) + \eta^{-n}\sin(n\theta - \beta/m)\}} \qquad (7)$$

where $\eta = \eta_o$ on the centre line. The integral on the rhs of (7) can be evaluated on an equipotential line since both θ and β/m are known functions of η from (5) and (6). The integrand contains a singularity on the centre line where $\theta = 0$ and $\beta = -m\pi$ which is to be expected from the symmetry of the velocity distribution. It is however possible to show that the singularity is an integrable one of the form $(\eta - \eta_o)^{-\frac{1}{2}}$ as $\eta \to \eta_o$; in practice it is avoided by using an appropriate limiting procedure in the numerical integration.

The results corresponding to (5) and (6) for the downstream portion are

$$e^{-\alpha/m}\cos \beta/m = \cosh(n\ell_2/2) - (\xi^n + \xi^{-n})\cos(n\theta)/4 \qquad (8)$$

$$e^{-\alpha/m}\sin \beta/m = -(\xi^n - \xi^{-n})\sin(n\theta)/4 \qquad (9)$$

where $\xi = q_T\, e^{-\ell_2}/U_2$ ($\ell_2 > 0$). After the necessary analysis the downstream equation derived from (3), corresponding to (7) is

$$\frac{1}{h}\int_o^h dy = \frac{n e^{-\ell_2 + \alpha/m}}{8\pi} \int_{\xi_o}^{\xi} \frac{(\xi^{2n} + \xi^{-2n} - 2\cos 2n\theta)\cos\theta\, d\xi}{\xi^2\{\xi^n \sin(n\theta - \beta/m) + \xi^{-n}\sin(n\theta + \beta/m)\}} \qquad (10)$$

where $\xi = \xi_o$ on the centre line. As for the upstream case, θ and β/m are known functions of ξ for a given value of α, from (8) and (9), and there is a corresponding qualification over the nature of the integrand at the centre line.

In (7) and (10) the upper limit of the integral on the rhs is the value of the non-dimensional velocity on the wall of the contraction. Hence for each value of this parameter - known for the two dimensional case - $f(\alpha)$ can be calculated from (3) and the value of q_A obtained using (2). Over the curved portions the two dimensional velocities are constant so it remains to specify

the two dimensional velocity distributions on the straight sections to complete the calculation of q_A. Note that in the formulae quoted below the x-direction is taken positive in the downstream direction. On the upstream parallel section AB, with the origin at B and taking x_1 as the local coordinate,

$$\frac{x_1}{H} = \frac{ne^{\ell_1}}{2\pi} \int_1^{\eta_u} \frac{\eta^{2n} - 1}{\eta^2(\eta^{2n} - 2\eta^n \cosh n\ell_1 + 1)}\, d\eta, \quad 1 \leqslant \eta_u \leqslant e^{\ell_1};$$

on the inclined section CV, with the origin at C, taking x_2 as the local co-ordinate,

$$\frac{x_2}{H} = \frac{ne^{\ell_1}}{2\pi} \cos\left(\frac{\pi}{n}\right) \int_1^{\eta_u} \frac{\eta^{2n} - 1}{\eta^2(\eta^{2n} + 2\eta^n \cosh n\ell_1 + 1)}\, d\eta, \quad \eta_u \geqslant 1.$$

For the downstream portion, the velocity distribution on the inclined portion WD, taking D as origin and taking x_3 as the local coordinate, is

$$\frac{x_3}{h} = \frac{ne^{-\ell_2}}{2\pi} \cos\left(\frac{\pi}{n}\right) \int_1^{\xi_u} \frac{\xi^{2n} - 1}{\xi^2(\xi^{2n} + 2\xi^n \cosh n\ell_2 + 1)}\, d\xi, \quad 0 < \xi_u \leqslant 1;$$

on the parallel section EF, taking E as origin and taking x_4 as local co-ordinate,

$$\frac{x_4}{h} = \frac{ne^{-\ell_2}}{2\pi} \int_1^{\xi_u} \frac{\xi^{2n} - 1}{\xi^2(\xi^{2n} - 2\xi^n \cosh n\ell_2 + 1)}\, d\xi, \quad 1 \geqslant \xi > e^{-\ell_2}.$$

4. Practical Use of the Method

In practice the two dimensional contraction (H/h) is chosen with suitable values for H,h and the angle of inclination (π/n) of the straight section. By selecting suitable values of ℓ_1 and ℓ_2 the coordinates of the curved sections can be found (see Jordinson[2]) and the lengths of the straight sections are then chosen to fit in with the required value of H/h. The present method gives the predicted velocity distributions for flow through an axisymmetric contraction with the same wall shape and area ratio $(H/h)^2$.

5. Results

With the present day easy availability of computer routines for integration it is unnecessary to produce sets of tables showing velocity distributions etc. for different values of ℓ_1, ℓ_2 and n. Instead it seems reasonable to present just one table for each of the upstream and downstream portions, the chosen values being $e^{-\ell_1} = 0.9$, $e^{\ell_2} = 1.025$ and $n = 4$. These values were used some time ago in the design of a successful two dimensional contraction and, more recently, to predict the flow through an experimental axisymmetric contraction of area ratio 16:1. The latter was fitted with pressure tappings thus affording a useful comparison between theory and experiment.

The upstream results for $f(\alpha)$ are consistent with its expected behaviour, namely a monotonic increase from a value of unity far upstream to a value without limit as the source on the axis is approached. The column for q_A/U_1

TABLE

Wall Velocity Distributions for Two Dimensional and Axisymmetric Flows

Upstream Portion $e^{-\ell_1} = 0.9$: origin at B					Downstream Portion $e^{\ell_2} = 1.025$: origin at E				
x/H	y/H	q_T/U_1	f(α)	q_A/U_1	x/h	y/h	q_T/U_2	f(α)	q_A/U_2
-0.1263	0	0.972	1.0099	0.9817	-1.0481	.2922	.6150	.5900	.3629
-0.0613	0	0.954	1.0150	0.9683	- .9750	.2192	.7175	.6457	.4633
-0.0254	0	0.936	1.0187	0.9535	- .9341	.1783	.8200	.6814	.5587
-0.0062	0	0.918	1.0211	0.9373	- .9148	.1589	.9225	.7000	.6457
0	0	0.900	1.0219	0.9197	- .9096	.1537	1.025	.7053	.7230
0.2002	.0184	0.900	1.0739	0.9665	- .8975	.1440	1.025	.7173	.7353
.3760	.0593	0.900	1.1836	1.0652	- .8546	.1183	1.025	.7537	.7725
.4714	.0980	0.900	1.2928	1.1635	- .7632	.0813	1.025	.8157	.8361
.5177	.1257	0.900	1.3707	1.2336	- .5716	.0373	1.025	.9043	.9270
.5309	.1364	0.900	1.3986	1.2588	- .3723	.0146	1.025	.9570	.9809
.6510	.2564	1.800	1.9725	3.5504	0	0	1.025	.9952	1.0201
.7287	.3342	2.700	2.8676	7.7425	.0042	0	1.0209	.9953	1.0161
.7697	.3752	3.600	3.8103	13.7171	.0174	0	1.0168	.9958	1.0125
.7946	.4000	4.500	4.7474	21.3632	.0427	0	1.0127	.9965	1.0092
.8112	.4167	5.400	5.6937	30.7459	.0873	0	1.0086	.9976	1.0061

shows clearly the presence of 'undershoot' as the inlet is approached, i.e. a velocity minimum near the inlet plane. The value of q_A increases over the curved section in contrast to the prescribed constant two dimensional velocity q_T.

For the downstream portion, as expected, $f(\alpha)$ increases from zero far upstream to a value of unity far downstream in the parallel section. q_A again rises over the curved section rising to a maximum close to the exit plane. It is however clear that for both upstream and downstream portions the resulting axisymmetric adverse pressure gradients are less than those in the two dimensional flow - as suggested by Whitehead, Wu and Waters.

The shape of the axisymmetric experimental contraction is shown in figure 2 along with the predicted wall velocity distributions for both upstream and downstream portions. For convenience the latter results are plotted using U_1 as reference velocity. There are two sets of data, one for each of the separate portions which give a reasonable match over the inclined straight portion of the wall. The centre line velocities can easily be deduced from the preceding analysis and these are also shown on figure 2 with satisfactory matching over the straight portion. Superimposed on both pairs of curves are points taken from a numerical solution kindly supplied by Dr. T. Morel (private communication). His method of solution, which applied to the whole contraction, is referred to in Morel[4] and used the wall coordinates of the experimental contraction as data. There is satisfactory agreement between the current analytical method and the numerical solution which gives confidence in the approximation used in the former.

Figure 3 shows the pressure coefficient C_p plotted against length for the solution where $C_p = \dfrac{U_1^2 - q_A^2}{U_1^2 - U_2^2}$. The overshoot shows clearly at the downstream end where the value of C_p rises to a maximum of 1.08 approximately and then falls to unity after a distance of about one exit plane radius. The experimental points are superimposed and these lie fairly close to the upstream curve almost as far as the downstream end of the inclined straight portion. On the downstream curved section DE the experimental points lie below the theoretical curve and indeed exhibit no obvious overshoot.

The experimental values have been carefully checked so that the discrepancy between theory and experiment is most likely due to the neglect of viscous effects. It is possible to advance a partial explanation in qualitative terms as follows. The adverse pressure gradient downstream of E must produce a thickening of the boundary layer so reducing the effective diameter of the downstream parallel section. If this diameter diminishes with distance downstream thus producing a convergence of the potential flow, the overshoot could well be eliminated and/or displaced downstream; the arrowed experimental point may just indicate the latter possibility. It is clear that further investigation of the flow at the downstream end is needed from both theoretical and experimental points of view, the former to include boundary layer effects. In connection with the latter it is worth observing that there seems to be a dearth of published experimental data on pressure distributions on the walls of axisymmetric contracting ducts.

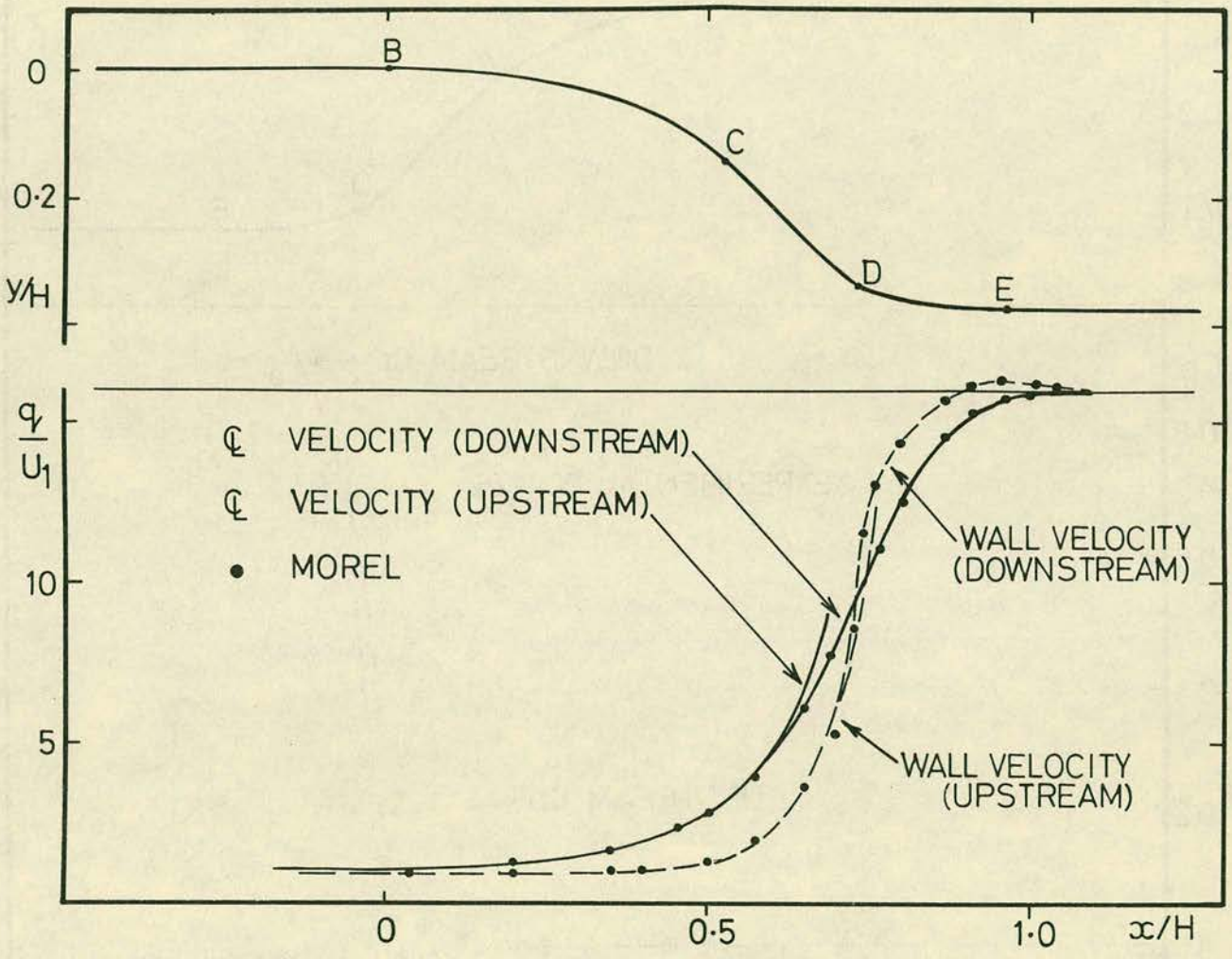

Fig. 2. Axisymmetric velocity distributions and contraction shape

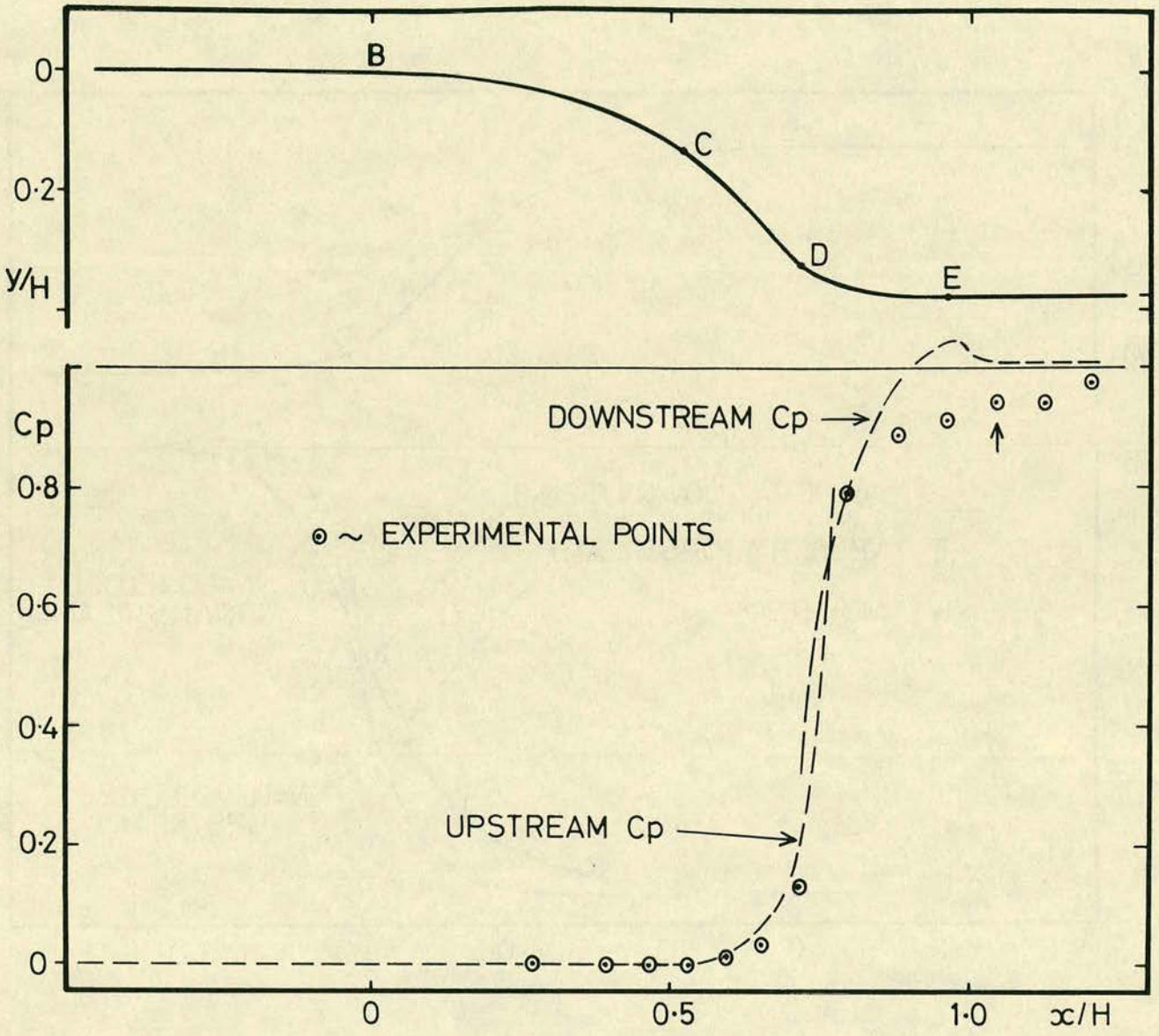

Fig. 3. Comparison of theoretical and experimental pressure coefficients

6. Concluding Remarks

The method described here is based on the assumption that each end of the contraction is independent of the other and can be considered separately. Thus, using one upstream portion, several downstream ones could be matched to give different area ratios or different values of 'overshoot' and 'undershoot' and vice-versa. In particular it is worth emphasising that keeping ℓ_1, ℓ_2 and n fixed it is only necessary to make *one* application of the method to predict axisymmetric velocity distributions in several contractions of different area ratios, provided they share a common upstream or downstream portion. The only additional calculation required for each contraction is to refer the results to the same origin. This is easily done once the dimensions of the contraction are fixed as described above.

Finally, it is of interest to note that nozzles for use with high speed water jets have been designed using the present method. These are showing satisfactory results when tested and it is hoped to report on this development in due course.

Authors' Note

The work described in this paper was carried out at Edinburgh University and formed part of a Ph.D. thesis submitted by J.G.R.[5]

References

1 Laidler, P. and Walkden, F. — The design of axisymmetric ducts for incompressible flow. *Aeronautical Quarterly*, Vol. 28, p 21, February 1977

2 Jordinson, R. — Design of wind tunnel contractions. *Aircraft Engineering*, p 294, October 1961

3 Whitehead, L.G., Wu, L.Y. and Waters, M.H.L. — Contracting ducts of finite length. *Aeronautical Quarterly*, Vol. 2, p 254, February 1951

4 Morel, T. — Comprehensive design of axisymmetric wind tunnel contractions. *Journal of Fluids Engineering*, p 225, June 1975

5 Rodger, J.G. — Design of wind tunnel contractions. Ph.D. thesis. Edinburgh University, 1976.